Energy and moisture exchange processes over heterogeneous land-surfaces in a weather prediction model

Dissertation
zur
Erlangung des Doktorgrades (Dr. rer. nat.)
der
Mathematisch Naturwissenschaftlichen Fakultät
der
Rheinischen Friedrich-Wilhelms-Universität Bonn

vorgelegt von
Felix Ament
aus
Frankfurt am Main

Februar 2006

Angefertig mit Genehmigung der Mathematisch-Naturwissenschaftlichen Fakultät
der Rheinischen Friedrich-Wilhelms-Universität.

1. Referent: Prof. Dr. C. Simmer
2. Referentin: Prof. Dr. S. Crewell
3. Referent: Prof. Dr. A. A. M. Holtslag

Abstract

Land-surfaces exhibit significant variablity at very small scales - in contrast to the atmosphere, where horizontal diffusion reduces small scale fluctuations effectively. It is a challenging task for numerical weather prediction (NWP) to account for these different characteristics while calculating exchange fluxes between these two systems: Surface processes need to be considered with higher spatial resolution than atmospheric effects and high resolution initial conditions and parameters of the surface are required. This study evaluates methods to solve these surface heterogeneity problems on the basis of integrations of the non-hydrostatic weather prediction model Lokal-Modell (LM) both in a NWP configuration (grid spacing of 7 km) and in a regional climate model set up (grid spacing of 21 km). The runs are performed for the 30-day periode of the LITFASS-2003 experiment.

Two heterogeneity parameterisation schemes, the mosaic and tile approach, have been implemented into LM. Both methods decompose the surface within one atmospheric grid box into several patches to resolve subgrid scale variability. The mosaic approach utilises an explicit, geographical sub-grid, whereas the tile approach subdivides the surface according to a certain criteria, e.g. land-use. In general, the tile method requires less computational time since fewer patches are used. However, the mosaic technique is more flexible since it takes multivariate heterogeneity into account.

Two major model enhancements are needed to simulate the observed exchange fluxes during LITFASS-2003 successfully: land-use dependent stomatal resistance parameters and vegetation albedo, and the use of accurate soil moisture data for initialisation. The latter is obtained by multi-year assimilation runs of the soil module of LM driven exclusively by observations. This technique ensures a balanced model state and allows to capture heterogeneity effects due to soil moisture variations induced by inhomogeneous rainfall.

The flux predictions of all integrations using these enhancements agree well with the observations within the range of measurement uncertainty independently from the representation of heterogeneity. The impact of improved surface fluxes on forecasts of atmospheric state variables is beneficial. Using high resolution integrations (e.g. grid spacing of 1 km) as reference, a clear ranking of parameterisation schemes can be established: The mosaic approach leads to very accurate flux predictions, followed by the tile approach, and the operational homogeneous approach. The deviations in forecasted surface fluxes of all methods decay significantly, if averages over larger scales are considered. The ranking of the methods can be explained by analysing the small scale variance of high resolution runs: The variance of surface quantities is by far larger than those of corresponding atmospheric quantities. This supports the assumption inherent to the mosaic and tile approach to refine the surface only. During LITFASS-2003, a considerable fraction of flux variability is explained by soil moisture variations which are not correlated with land-use. These subgrid scale heterogeneities can only be resolved by the mosaic approach and not by a tile scheme.

Zusammenfassung

Landoberflächen zeichnen sich durch eine hohe Variabilität auf kleinen Skalen aus - im Gegensatz zur Atmosphäre, in der horizontale Diffusion kleinskalige Fluktuationen effektiv reduziert. Diese unterschiedlichen Eigenschaften bei der Berechnung der Austauschflüsse von Energie und Feuchte zwischen beiden Systemen zu berücksichtigen, ist eine schwierige Aufgabe für die numerische Wettervorhersage: Oberflächenprozesse erfordern eine höhere räumliche Auflösung als atmosphärische Effekte und entsprechend werden hochaufgelöste Anfangsbedingungen und Parameter der Oberfläche benötigt. Diese Studie erprobt Methoden zur Lösung dieser Heterogenitätsprobleme auf der Basis von Rechnungen mit dem nicht-hydrostatischen Wettervorhersagemodell Lokal-Modell (LM) sowohl in einer Konfiguration zur Wettervorhersage (Gitterweite 7 km) als auch in einer Einstellung, die einem regionalen Klimamodell entspricht (Gitterweite 21 km). Diese Simulationen werden für den 30-Tages-Zeitraum des LITFASS-2003 Experiments durchgeführt.

Zwei Heterogenitätsparameterisierungen, der Mosaic- und der Tile-Ansatz, sind in das LM eingebaut worden. Beide Methoden zerlegen die Oberfläche innerhalb einer atmosphärischen Gitterbox in verschiedene Untergebiete, um kleinskalige Variabilität unterhalb der Modellmaschenweite aufzulösen. Der Mosaic-Ansatz verwendet ein explizites, geographisches Untergitter, wohingegen der Tile-Ansatz die Oberfläche nach einem bestimmten Kriterium, z.B. der Landnutzung, aufteilt. Im allgemeinen benötigt der Tile-Ansatz weniger Rechenzeit, da weniger Untergebiete verwendet werden. Der Mosaic-Ansatz ist flexibler, da auch multivariate Heterogenitäten berücksichtigt werden können.

Zwei wesentliche Modifikationen des operationellen Modells sind nötig, um die während LITFASS-2003 beobachteten Austauschflüsse erfolgreich zu modellieren: landnutzungsabhängige Parameter des Stomatawiderstands und der Pflanzenalbedo, sowie genaue Bodenfeuchteanalysen. Letztere lassen sich aus mehrjährigen Assimilationsläufen mit dem Bodenmodell des LM bei ausschließlichem Antrieb mit Messdaten erstellen. Diese Technik garantiert einen balancierten Modellzustand und ermöglicht es, Heterogenitätseffekte infolge regeninduzierter Bodenfeuchtevariationen wiederzugeben.

Die Flussvorhersagen aller Modellläufen, die diese Modifikationen nutzen, geben die Beobachtungen im Rahmen der Messgenauigkeit gut wieder - unabhängig von der Berücksichtigung von Heterogenitäten. Diese genauer modellierten Austauschflüsse reduzieren auch Fehler in den Vorhersagen des atmosphärischen Zustands. Verwendet man hochaufgelöste Modellintegrationen (z.B. mit einer Maschenweite von 1 km) als Referenz, so ergibt sich eine klare Rangfolge für die verschiedenen Parameterisierungsmethoden: Der Mosaic-Ansatz führt zu sehr genauen Flussvorhersagen, gefolgt vom Tile-Ansatz und dem operationell verwendeten Ansatz einer homogenen Oberfläche. Die Unterschiede in den vorhergesagten bodennahen Flüssen verringern sich deutlich, wenn Mittel über größere Skalen betrachtet werden. Die Rangfolge der Methoden kann durch eine Analyse kleinskaliger Varianzen in hochaufgelösten Simulationen erklärt werden: Die Varianz von Oberflächenvariablen ist deutlich größer als die von entsprechenden atmosphärischen Größen und rechtfertigt damit die dem Mosaic- und Tile-Ansatz zugrundeliegenden Annahmen, nur die Oberfläche höher aufzulösen. Während LITFASS-2003 wird ein beachtlicher Anteil der Variabilität der bodennahen Flüsse durch Bodenfeuchtevariationen erklärt, die nicht mit der Landnutzung korreliert sind. Solche kleinskaligen Heterogenitäten können nur vom Mosaic-Ansatz aufgelöst werden, nicht aber durch ein Tile-Schema.

Contents

Contents

1 Introduction

1.1 Motivation

The land-surface is the interface between the two geophysical systems atmosphere and soil including vegetation. It controls the interaction between both systems via surface fluxes, which are in particular the fluxes of heat, moisture, momentum, radiation, and of various chemical constituents. An impact of these exchange processes on weather and climate is accepted in atmospheric science without any dispute (see review articles of Garratt, 1993; Betts et al., 1996). Momentum, heat, and moisture fluxes modify the wind field (Findell and Eltahir, 2003), directly affect screen level weather conditions like temperature and humidity (Dai et al., 1999; Ronda et al., 2002; Seuffert et al., 2002), and influence the formation of clouds and precipitation (Chen and Avissar, 1994; Avissar and Liu, 1996; Eltahir and Pal, 1996; Lynn et al., 1998; Findell and Elthair, 1999; Pielke, 2001)

The surface cannot be seen as a static boundary condition independent of the atmospheric system because the state of the surface is partly determined by atmospheric forcings. Various feedback mechanisms between atmosphere and soil exist, like differential heating caused by varying insolation due to cloud shading (Lipton, 1993) or differential moistening due to soil moisture variablity introduced by rainfall patterns (Clark et al, 2004). Therefore, soil modules became essential and indispensable parts of all climate and numerical weather prediction (NWP) models and interactions between the two systems atmosphere and soil are calculated fully prognostically.

If atmosphere and soil are coupled in one model, one of the most important discrepancy between these two systems should be taken into account: their horizontal diffusivities. The atmosphere is quite diffusive and gradients of all quantities are rapidly reduced by turbulent motion. In contrast, horizontal diffusion at the surface or in the soil is very slow; pronounced contrasts, like e.g. between water and land at a coast, may exist for geological timescales. Consequently, the atmospheric state can be described much more accurately on a coarse grid than the state of surface and soil. This has severe implications for measuring and modelling efforts: It might be sufficient to determine the atmospheric state by point measurements (e.g. by standard ground based synoptical observations or radiosonde ascents) with a coarse network ($o(\Delta x) = $ 10-100 km) and to model its evolution on a correspondingly coarse grid, but a description of the surface state with similar accuracy requires observations and simulations with a much higher resolution ($o(\Delta x) = $ 1 m - 1 km).

These theoretical demands are in contrast to what is feasible in practice and the arising difficulties are in general subsumed in atmospheric sciences as 'land-surface heterogeneity problems'.

Surface vegetation-atmosphere transfer (SVAT) schemes, which consist of a soil model plus components to calculate surface fluxes, are in general developed using the assumption of horizontal homogeneity of all surface and soil parameters. Although some processes, like e.g. plant transpiration, are rather complex, these models demonstrate a good performance if they are used as local one-dimensional models driven and evaluated by point observations at a single measuring site (e.g. Hendersonsellers et al., 1993; Boone et al., 2004). It is common practice, to implement these models one-to-one into climate and NWP models to predict grid-box averaged fluxes at scales of 1-100 km. In principle, neither the assumption of homogeneity is valid nor input parameters are known at the relevant scales. These shortcomings might result in large errors of predicted surface fluxes (e.g. Mölders and Raabe, 1996; Schlünzen and Katzfey, 2003; Heinemann and Kerschgens, 2005).

The main objective of this study is to asses what strategies are needed to consider effects of heterogeneous land-surfaces adequately in meteorological models. What kind of surface-atmosphere exchange parameterisation should be used, which effects are relevant and how to asses appropriate input data? - These are the main questions. The answers are, however, not independent from the horizontal model resolution (Mahrt, 2000). This study is restricted to the scale range of todays mesoscale NWP models (5-10 km) and of advanced regional climate models ($\sim$20 km). Since the prediction of surface fluxes itself is of minor importance for most applications, also the impact on more relevant quantities, like boundary layer evolution, clouds or precipitation, will be investigated. The following section will give an overview of recent related research activities before outlining the strategy of this study in the last section of this chapter.

1.2 Review of published research results

The most direct and accurate method to consider small scale variability of the land-surface in a model is to refine the horizontal resolution appropriately. This explicit representation of heterogeneous land-surfaces requires excessive computer time. The computational costs increase by the third power of the refinement factor since the number of grid points increases quadratically and a linear increase in the number of time steps is necessary to maintain numerical stability. If it is postulated that the atmospheric resolution of models cannot be enhanced sufficiently due to these practical concerns, the subgrid-scale variability of fluxes at the surface and in the atmosphere is not resolved explicitly and might be considered by parameterisation schemes. The review article of Giorgi and Avissar (1997) presents a comprehensive overview over such methods. They subdivide the parameterisation problem into two aspects: a) The 'aggregation effect' is caused by neglecting subgrid-scale variability

at the surface. Since the relation between state variables and fluxes is nonlinear, the fluxes diagnosed based on spatially averaged state variables differ from spatially averaged fluxes. b) Subgrid-scale anomalies of surface fluxes may cause local instabilities which induce organised subgrid-scale circulations. This subgrid-scale motion has the potential to alter the vertical transport of heat, moisture and momentum in the boundary layer. This process is referred to as the 'dynamical effect'. Both effects are not independent since variations of atmospheric state variables induced by dynamical effects feeds back on to the flux aggregation at the surface. Nonetheless, this distinction proposed by Giorgi and Avissar (1997) is quite useful to classify the approaches which have recently been developed.

Solving the aggregation problem is equivalent to estimating the flux over a heterogeneous surface. No exact theory exists for this problem (Mahrt, 1996). In contrast, Monin-Obukhov similarity theory (see basic textbooks, e.g. Stull, 1988) is an accurate and well accepted theory to diagnose fluxes over homogeneous surfaces. This theory results in the well known bulk aerodynamic formula stating that surface fluxes of momentum, heat and moisture are equal to the bulk difference in corresponding state variables (wind speed, temperature and specific humidity, respectively) at the surface and an atmospheric reference level (e.g. the lowest model level) multiplied by a transfer coefficient. The magnitude of this coefficient depends on the turbulent regime, which is determined by stratification, wind shear, and surface roughness. All approaches to estimate fluxes over a heterogeneous surface are extensions of this homogeneous theory and essentially assume that the homogeneous relation is locally valid at each position of the heterogeneous surface. The flux can then be determined as an average of the local fluxes.

The first category of aggregation schemes are 'effective surface' methods, which try to project the problem of the heterogeneous surface on a similar homogeneous problem by determining characteristics of an equivalent homogeneous surface. The most simple approach is to adopt the surface and soil parameters of the dominant land-use type. It is obvious that the 'dominant land-use approach' will only give satisfactorily results as long as a single type of land-surface prevails. Since this requirement is not fulfilled in general, large errors of this method are reported (Mölders and Raabe, 1996; Friedrich et al., 2000; Schlünzen and Katzfey, 2003). Surface heterogeneity is implicitly considered by the 'effective parameter approach', which aggregates parameters of the heterogeneous surface. The success of this approach depends on the choice of parameters. If rapidly varying parameters, like e.g. the local surface temperature or canopy resistance, are aggregated to obtain corresponding area averaged quantities, the method can give good results (Lhomme et al., 1994; Chehbouni and Njoku, 1995; Hu et al., 1999). But this approach cannot be used in forecast applications, because the local subgrid-scale values of these rapidly varying variables are unknown. Instead it is common practice to average slowly varying variables, which are in general not calculated prognostically, but prescribed externally, like leaf area index or roughness length. Since this parameter averaging method is simple and computational inexpensive it is widely used in operational models. Nonetheless, the relation between these parameters and the fluxes is highly

nonlinear. Consequently, the flux calculated using effective parameters can deviate significantly from the area averaged flux (Ronda and de Bruin, 1999; Schlünzen and Katzfey, 2003; Heinemann and Kerschgens, 2005; Heinemann and Kerschgens, 2006b). All these studies recommend to resolve the surface heterogeneity explicitly and to obtain the mean flux by averaging locally diagnosed fluxes.

There are two options to represent surface heterogeneity explictly: diagnostically by probability density function (PDF) methods or prognostically by discrete methods. PDF methods assume that surface quantities are distributed within a grid cell according to PDF and integrate the flux equations either numerically (e.g. Avissar, 1992) or analytically (Giorgi, 1997) over this PDF. In general, the parameters of the PDF are prescribed externally as constant values. This simplification is not always valid, since surface heterogeneity can be determined by time-varying parameters like soil moisture (Yates et al., 2003; Li and Avissar, 1994).

It is common for discrete methods to simulate surface processes with a higher spatial resolution than atmospheric processes. Unfortunately, the nomenclature of these methods in literature is ambiguous. This study will use the definitions of Heinemann and Kerschgens (2005). Avissar and Pielke (1989) proposed the tile method: The surface is subdivided into patches with similar surface characteristics e.g. according to the type of land-use. Surface fluxes as well as soil processes are calculated for each patch separately and without considering any horizontal exchange processes. The patches are not located geographically and usually consist of multiple areas (e.g. various lakes within a grid-box are subsumed to a single patch). The mean grid-scale flux is obtained as the averaged flux of the individual patch fluxes weighted by their fractional coverage. Seth et al. (1994) presented the mosaic approach, which is a modification of the tile method: Surface processes are calculated on a refined subgrid, which subdivides an atmospheric grid-box into N^2 surface subgrid-boxes. Grid-scale fluxes are determined by the same procedure which is applied by the tile approach. Both methods may be simplified by assuming homogeneous soil conditions (e.g. Mölders and Raabe, 1996), which essential means that only fluxes, but not soil processes are calculated on a finer grid. The fundamental approximation of mosaic and tile methods is to neglect subgrid-scale atmospheric variability at the lowest model level.

The impact of these methods on simulations can be assessed most easily by model studies which compare results obtained by various formulation: The by far greatest impact on the mesoscale is reported by Mölders and Raabe (1996) and Mölders et al. (1996). They performed three-dimensional mesoscale simulations with 4-8 km atmospheric resolution and 1 km surface resolution for a domain covering the northern part of Germany at a single case. Mölders and Raabe (1996) compared results of runs with different atmospheric resolutions using both the dominant land-use type approach and the tile approach with homogeneous soil: Surface fluxes were hardly affected by the atmospheric resolution, but the latent heat fluxes were three times smaller, if the tile approach was used. Accordingly cloud formation and precipitation were significantly modified. A comparison of tile and mosaic approach in Mölders et al. (1996) revealed that the mosaic approach results in significantly higher latent

heat fluxes and accordingly reduced sensible heat fluxes.

Schlünzen and Katzfey (2003) evaluated integrations of the mesoscale model ME-TRAS using operational observations and SYNOP stations at a single case. The runs were conducted on 18 km and 4 km resolution with three different surface heterogeneity parameterisations (dominant land-use, effective parameters and mosaic approach). The performance of the mosaic scheme turned out to be the best and showed similar accuracy to predict surface parameters at both atmospheric resolutions; in contrast the other methods gave better results if the atmospheric grid was refined. It is remarkable that runs with the effective parameter approach had less skill than runs based on the dominant land type approach. The finding that runs with a mosaic scheme are less sensitive to atmospheric resolution was also reported by Wen et al. (2000).

Heinemann and Kerschgens (2005) and (2006b) tested the effective surface method, the tile and the mosaic approach for selected days of the LITFASS-98 (Beyrich et al., 2002) and the LITFASS-2003 (Beyrich et al., 2006a) campaigns, respectively. They conducted high resolution integrations with the mesoscale model FOOT3DK at horizontal grid spacings of 250m-1km. These runs were validated against observations and then used as reference in a purely model-based testbed. All aggregation methods are evaluated by an offline diagnosis of fluxes based on coarsening the high-resolution results. This analysis revealed that the mosaic method is the most accurate method with a small tendency to underestimate the latent heat flux, closely followed by the tile approach and the effective surface method gives the largest errors. They report significantly smaller differences in predicted fluxes due to various methods than Mölders and Raabe (1996) and Mölders et al. (1996).

The impact of surface heterogeneity schemes is not only documented for mesoscale weather prediction, but also for climate simulations (e.g. Zeng et al., 2002; Essery et al., 2003). Climate simulations presented by Hahmann and Dickinson (2001) revealed that heterogeneity in roughness length and albedo influence precipitation in the tropics, whereas surface temperature is most sensitivity to surface heterogeneities in the mid-latitudes. These findings are confirmed by Giorgi et al. (2003), who conducted integrations of a regional climate model with the mosaic approach and demonstrated that improved near surface temperature forecasts due to the mosaic technique result in a more accurate representation of snow cover in the Alpine region.

As already mentioned, both the mosaic and the tile approach assume that subgrid-scale variability at the lowest atmospheric model level is negligible. In other words, the blending height (defined as altitude at which differences in turbulent fluxes due to heterogeneity are no longer detectable; for a detailed definition see Mason, 1988; Claussen, 1991) is assumed to be at the lowest model level. This assumption is not fulfilled in general, because the blending height depends on the length scale of surface heterogeneities, the wind speed and the friction velocity and thus may vary in time. If the blending height is above the lowest model level, a part of the anomalies in the surface state variable (temperature or humidity) should be added to the atmospheric reference value before diagnosing the local flux of an individual

patch. Such a disaggregation technique was originally proposed by Seth et al. (1994) and is used by Arola (1999) and Molod et al. (2003). As an alternative method, the blending concept developed by Claussen (1991) may be used to correct for varying blending heights, as e.g. utilised by Arola (1999) or Schlünzen and Katzfey (2003). This method is also applicable if the blending height is below the lowest model level. A method for extreme low blending heights was introduced by Koster and Suarez (1992) as 'mixing approach' by assuming that the fluxes of different patches are already mixed at the top of the vegetation layer.

Despite these corrections of atmospheric reference values, all aforementioned studies highlight, that it is more important to represent the surface variablity accurately than the atmospheric variablity. Even experimental works support this hypothesis (Mahrt and Sun, 1995). To the knowledge of the author, the only study which draws different conclusions was published by Shao et al. (2001). They compared integrations of a mesoscale model with coarse atmospheric resolution (4 km) and high surface resolution (1 km) and vice versa to a reference run with high resolution for both atmosphere and surface. The run with high atmospheric and low surface resolution was in closer agreement to the reference run.

After the review of research on the aggregation effect, the following paragraphs will present results concerning the dynamical effect. Well-known sea breeze circulations are initiated by pronounced contrasts in surface fluxes between water and land-surface. In principle, heterogeneities in land-surface parameters, like soil moisture or vegetation cover, can also induce such contrasts. Many mesoscale model studies with idealised heterogeneities have proven the existence of such circulations (e.g. Mahfouf et al., 1987; Pinty et al., 1989; Chen and Avissar, 1994; Lynn et al., 1995; Avissar and Liu, 1996; Seth and Giorgi, 1996). Doran et al. (1995) documented measurements of a circulation that was initiated at edges of steppe and irrigated farmland regions with a typical patch size of 10 km. A comprehensive large eddy simulation (LES) study of Avissar and Schmidt (1998) based on idealised heterogeneity revealed that random turbulent eddies become organised, if a surface heterogeneity with sufficiently high amplitude and a wavelength of at least 5-10 km is prescribed. These organised circulations can only exist under low wind speed conditions and are almost totally removed at wind speeds larger than 5 m/s. LES simulations conducted by Uhlenbrock (personal communications) demonstrated that even microscale land-surface contrasts in the order of 1 km may induce organised circulations, which can account for up to 10% of the total turbulent transport. According to Uhlenbrock, this increase of vertical transport is almost perfectly compensated by a decrease of the turbulent transport due to random eddies and the total flux is consequently maintained. A spectral analysis of high resolution mesoscale simulations by Roy (2003) indicates that organised circulations due to realistic land-surface heterogeneities evolve preferably at scales of 10-20 km.

It is an ongoing debate how such meso- and microscale circulations should be considered by parameterisation schemes of coarse scale climate or weather prediction models. Lynn et al. (1995), Liu et al. (1999) and Arola (1999) have developed parameterisations for global circulation models (GCM) based on simulations

by mesoscale models. They assumed that all resolved transport of the mesoscale model at scales below the grid spacing of a GCM must be considered by a new parameterisation. In contrast, Heinemann and Kerschgens (2006a) demonstrated that resolved turbulent motion and parameterised, random turbulent transport cannot be considered independently. Consequently, the parameterised flux of the GCM may already account partly for the transport due to mesoscale circulations. Nonetheless, although the total transport may remain unaffected by organised circulations, the spatial distribution of subgrid-scale variability within a coarse grid box is altered. These changes can induce systematic deviations via nonlinear processes, like e.g. condensation (Heinemann and Kerschgens, 2006a).

1.3 Strategy

The review of literature presented in the last section revealed that the existence of effects due to land-surface heterogeneity on scales of mesoscale models is well documented. Nonetheless, recent research results differ significantly as far as the magnitude and the impact of these effects is concerned. Most of these studies concentrate either on single case studies or on idealised cases. Case studies lack representativeness and are likely affected by inaccurate initial conditions since hydrological processes in the soil require long spin-up times. Idealised studies are well suited to investigate isolated effects, but at the same time they tend to overestimate their impact. Therefore, the overall strategy of this study is to asses the impact of land-surface heterogeneities on the meso-γ-scale in a framework, which is as close as possible to operational weather forecasting applications. This means in particular, that realistic model integrations over a longer, continuous period are considered.

The model of choice in this study is the Lokal-Modell (LM) (Steppeler et al., 2003), which is currently used as operational limited area weather forecasting model with a horizontal grid spacing of 7 km by weather services of Germany, Switzerland, Greece, Poland, Italy, and Romania. Research applications (e.g. Seuffert et al., 2002; Ament et al., 2004) have demonstrated that the model can also be applied successfully at high resolutions up to 1 km. The model integrations are evaluated using two data sets: observations of the field experiment LITFASS-2003 and high resolution LM simulations. The 30-day integration period in May and June 2003 as well as the model domain located over the eastern part of Germany and western parts of Poland, were selected to cover the LITFASS-2003 experiment in time and space. To assess what kind of model modifications are needed to predict fluxes over heterogeneous terrain more accurately, various model enhancements have been implemented and tested: Modifications of existing parameterisations, prescription of improved input data and implementation of two heterogeneity parameterisations (mosaic and tile approach).

The experiment LITFASS-2003 and the model LM along with the newly implemented enhancements will be described in Chapter 2. A careful configuration of the

model experiment is needed to obtain realistic simulations, which have the potential to be compared to observations, and to ensure that the differences between runs with different heterogeneity parameterisations are not caused by unwanted side-effects. These issues and in particular methods to obtain appropriate initial soil moisture data will be discussed in Chapter 3. A comprehensive evaluation of predicted latent and sensible heat fluxes at the surface in comparison to both observations and high resolution model results will be presented in the Chapter 4. This chapter highlights the relevance of accurate input data, especially of soil moisture, evaluates the performance of heterogeneity parameterisations and verifies the approximations underlying these schemes by analysing the high resolution model runs. Momentum fluxes are not included in this evaluation, because this process was not in the focus of the LITFASS-2003 experiment. Chapter 5 addresses how surface fluxes propagate within the atmospheric boundary layer and describes their impact on the evolution of the atmospheric state. Model results are compared to in-situ observation by airborne systems, remote sensing sensors and results of a large eddy simulation, which resolves fluxes almost completely.

The main findings of chapter 3-5 will be summarised briefly at the end of each chapter. However, the last chapter presents a comprehensive summary of all results formulated as answers to fundamental questions concerning surface-exchange processes. Each statement is linked by references to those previous sections at which the corresponding issue is discussed in detail. Consequently readers, who are mainly interested in a general overview or only in certain aspects, might use the final chapter as a starting point.

2 Model and data

2.1 LITFASS-2003 experiment

The LITFASS project ("Lindenberg Inhomogeneous Terrain - Fluxes between Atmosphere and Surface: a Long-Term Study") was established in 1995 by DWD in order to determine surface fluxes of momentum, heat and water vapour at the meso-γ scale (2-20 km). The target area covers a square of 20 by 20 km^2 including the Meteorological Observatory Lindenberg (MOL, see Fig. 2.1). The LITFASS domain resembles approximately one grid-box of a regional climate model or 3 by 3 boxes of the operational mesoscale weather forecasting model LM. The domain is located $\sim$65 km southeast of Berlin. Its corners are defined by the following geographical coordinates:

$$52° \, 05' \, 30'' \, \text{N}, \, 13° \, 54' \, 00'' \, \text{E and } 52° \, 16' \, 30'' \, \text{N}, \, 14° \, 12' \, 00'' \, \text{E .}$$

Forest and farmland are the dominant land-use classes within the LITFASS domain (see Fig. 2.1). The remaining area is either covered by lakes or settlements. Orographical contrasts are of minor importance because the altitude varies only between 50 and 120 m above sea level. The forest-farmland contrast between the western and eastern part of the domain induces the most pronounced heterogeneity in surface properties.
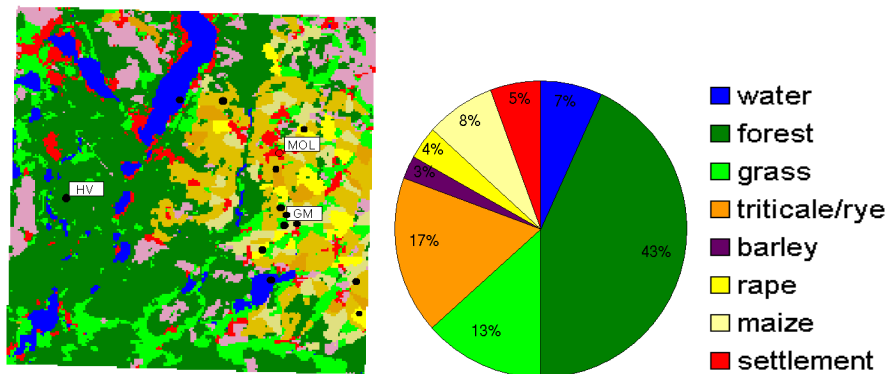

Figure 2.1: Map of the land-use within the LITFASS domain. Indicated are the measuring sites at the observatory Lindenberg (MOL), the boundary layer measuring site GM Falkenberg (GM) and the forest site (HV). (Plots by the courtesy of C. Heret, DWD Lindenberg.)

A first field campaign (LITFASS-98) was performed in May and June 1998. A combination of groundbased in-situ measurements, remote sensing sensors, aircraft observations and vertical profiling of the atmosphere gave insight into the exchange between surface and atmosphere (Beyrich et al., 2002a; Beyrich et al., 2002b; Bange et al., 2002; Engelbart et al., 2002; Görsdorf et al., 2002). As an outcome of LITFASS-98, a long-term measurement program was established in summer 2001 comprising the following facilities: the boundary layer field site ('Grenzschicht-Messfeld', GM) Falkenberg equipped with a 99 m tower, a SODAR/RASS and a RADAR/RASS instrument (both measuring temperature and wind profiles), a network of four energy balance stations (situated over forest, grassland, farmland and water), a network of rain gauges, a network of global radiation sensors and a large aperture scintillometer with a path length of 4.7 km. This data set is completed by routine observations at MOL like synop observations, radiosonde ascents every 6h and radiation measurements in the framework of the baseline surface radiation network.

The second field experiment, LITFASS-2003 (Beyrich et al., 2004; Beyrich and Mengelkamp, 2006), was conducted along the same lines as LITFASS-98, but with a huge number of additional observation facilities. In total 14 energy balance stations were set up, which provided measurements of latent heat flux λE_0 and sensible heat flux H_0 as well as in-situ measurements of all relevant near surface and soil state variables. All characteristic land-surfaces except forest and settlement were monitored by more than one station, which allows for studies about the internal variability within each land-use class. Uniform processing of all eddy-covariance data comprising state-of-the-art checks and corrections (Mauder et al., 2006) ensured a very high data quality. These observations were used to derive composite time series of λE_0 and H_0 for all relevant land-use types (Beyrich et al., 2006). The area averaged fluxes for the whole LITFASS domain are estimated by averaging these time series weighted by the fractional coverage of each land-use type.

The differential absorption lidar technique (DIAL) (Hennemuth et al., 2006) was applied for accurate profiling of absolute humidity in the lower troposphere with high vertical and temporal resolution. Efforts to combine these measurements with vertical wind observation from SODAR/RASS to determine latent heat fluxes in the boundary layer were, however, only successful for integration times of more than one hour due to the limited representativeness of point measurements. Boundary layer fluxes were also obtained by the HELIPOD system (Bange et al., 2002; Bange et al., 2006), i.e. a measuring platform mounted by a rope below a helicopter. Long flight tracks were necessary to reduce the statistical error and only a single average flux value is available per flight leg. These results have been extrapolated down to the surface by using inverse modelling theory in order to obtain area-averaged λE_0 and H_0 values. The HELIPOD measurements additionally provided information about the variability of atmospheric quantities and the surface temperature along the flight track. Scintillometer observations of the long term program were supplemented by additional observational paths and one microwave scintillometer (Meijninger et al., 2006), which allows for line averaged measurements of the latent heat flux.
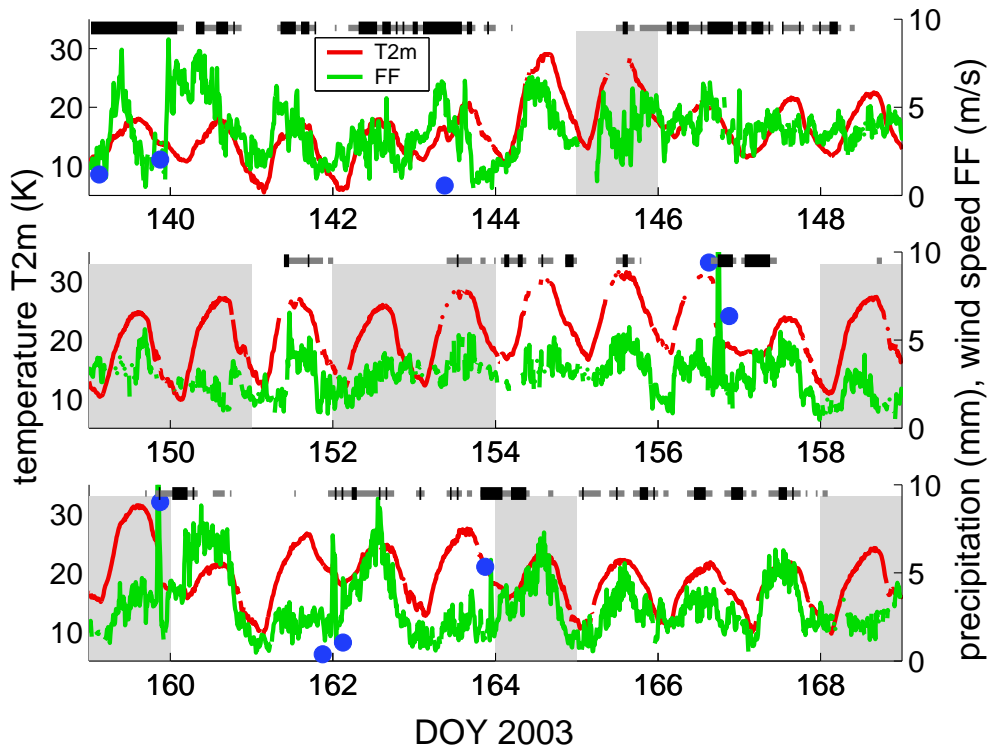
Figure 2.2: Weather conditions during LITFASS-2003: Temperature at 2 m height (red), wind speed at 10 m (green), 3 hourly accumulated precipitation (blue dots) and cloud cover (overcast black, brocken grey; derived from ceilometer observations) at the GM Falkenberg site.

Comparing all aforementioned methods to measure areal averaged fluxes the compositing technique turned out to be the most direct and reliable approach with a nearly full temporal coverage of the experimental period. Therefore, this data set is used in this study as a reference for model evaluation and other measurements are only referred to if they provide additional information.

An overview over the weather conditions during the 30-day experiment period LITFASS-2003 (19 May until 17 June 2003) is given by Fig. 2.2. From the beginning until Julian day 144, the weather at Lindenberg was determined by low pressure systems passing by over the Atlantic and Baltic sea. This episode is further characterised by moderate temperature, high wind speeds and mostly cloud covered situations. Compared to surrounding areas only light rainfall was detected at Lindenberg. Subsequent to this episode, a high pressure systems established over central Europe, which was connected with increasingly warm, dry, clear sky and low wind speed weather conditions at Lindenberg. A cold front of an Atlantic cyclone reached Lindenberg on day 156 and initiated strong thunderstorms with precipitation sums up to 50 mm in the evening. During the rest of the LITFASS-2003 campaign, frequent changes between weak troughs and high pressure ridges influenced the local weather conditions: Cloudy situations were observed more often than before, three rain events occurred, but fair weather conditions were still dominating.
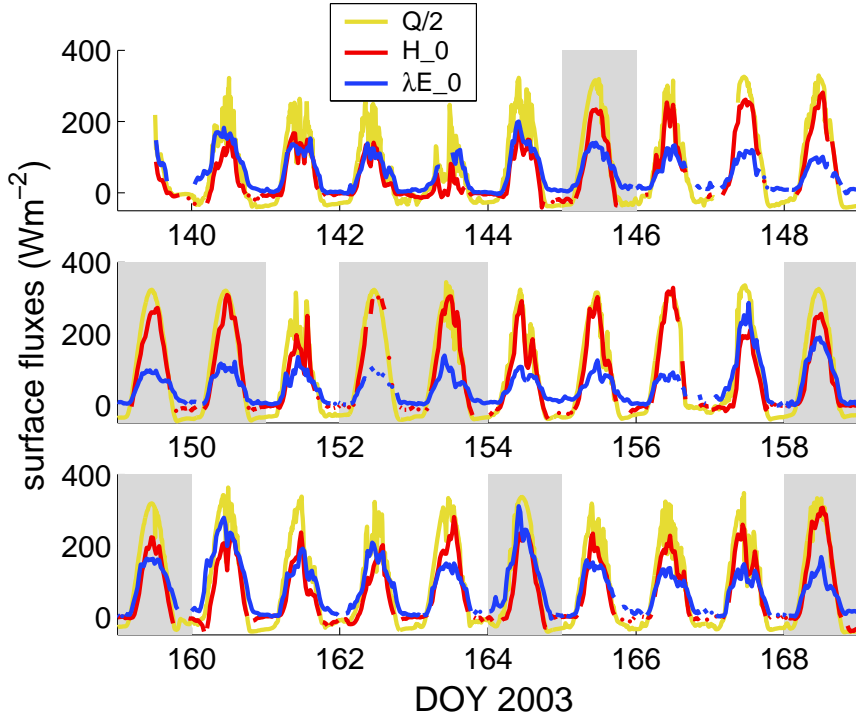
Figure 2.3: Surface fluxes during LITFASS-2003: LITFASS domain average of net radiation Q (yellow), sensible H_0 (red) and latent heat flux λE_0 (blue).

Heterogeneity effects are pronounced if the insolation is high, and are less superposed by advection if the wind speeds are low. From this point of view, weather conditions during LITFASS-2003 were very suitable. Nine days, the so called golden days (grey shaded in Figures 2.2 and 2.3), have been selected for special case studies. Most of them meet the requirements mentioned above, but also two days with more complex weather conditions (day 145 and day 164) where included to enhance the representativeness of the sample.

The flux measurements (Fig. 2.3) can easily be related to the weather conditions: First of all, it is obvious that clouds directly affect the net radiation Q. During the high pressure, fair weather episode until day 156, the soil dried out. Consequently, the sensible heat flux increases constantly, whereas the latent heat flux decreases. The strong rain event at day 156 wettens the soil and as direct response, the turbulent fluxes are partitioned almost equally the next day. During the last part of LITFASS-2003 sensible (latent) heat fluxes increase (decrease) again. This evolution is most pronounced at the last five days, when no precipitation occurres.

The data set of LITFASS-2003 is not only suitable to study the temporal flux evolution, but also its spatial distribution, which is largely determined by the contrast between forest in the east and farmland/grass in the west. A comparison of averaged fluxes (Fig. 2.4) reveals significant differences in all flux components. At first, the albedo of forest is much lower compared to grass, which explains that more radiation is absorbed by forests. Secondly, trees are more sensitive to soil moisture stress and
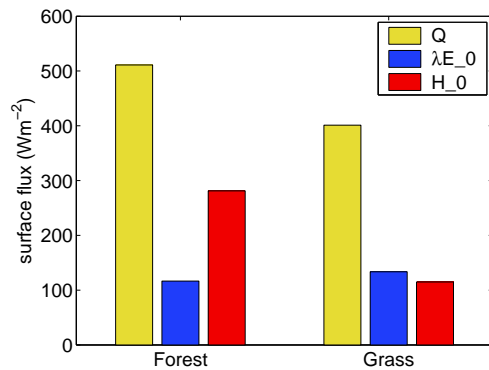
Figure 2.4: Averaged daytime (8-14 UTC) net radiation Q, sensible H_0 and latent heat
flux λE_0 measured during LITFASS-2003 at the station HV (forest) and at
GM Falkenberg (grass).
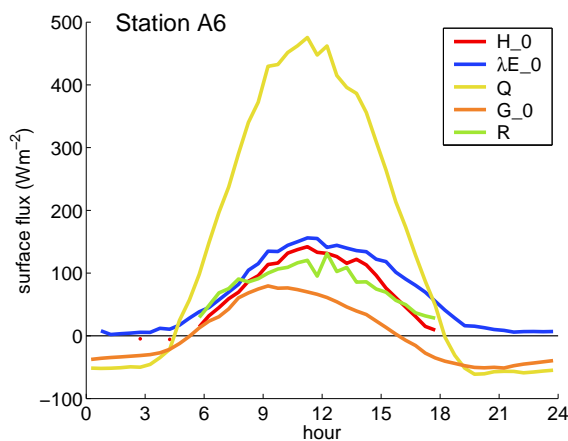
Figure 2.5: Mean daily cycle during LITFASS-2003 of all measured components of the
surface energy balance equation above a corn field (station A6). Additionally
the residual term R due to the non-closure of the energy balance is displayed.

increase their stomatal resistance to prevent wilting. Therefore, the partitioning of
turbulent fluxes is shifted towards sensible heat flux over forest areas.

Simulating the temporal and spatial structure of measured fluxes during LITFASS-
2003 is a challenging testbed for models. Nevertheless, it is important to discuss a
serious uncertainty, which is inherent to eddy-covariance measurements - the non-
closure of the surface energy balance. To preserve energy, the sum of latent, sensible
and ground heat flux must be equal to the net radiation, but measurements often
result in a positive residuum $R := Q - G - \lambda E_0 - H_0$ (Fig. 2.5). This effect is
common to eddy-covariance measurements and already frequently published in lit-
erature (e.g. Foken and Oncley, 1995; Laubach and Teichmann, 1999; Beyrich et
al., 2002b). The magnitude of the residuum varies, but most publications report
estimates in the range of 15%-30% Q. Mauder et al. (2006) assumes a residuum
of 20-25% Q for the LITFASS-2003 measurements. The residuum is an artefact of
measurements. This means that in principle all components must be corrected to

remove the residuum, but it is not clear how to distribute the systematic error. It is unlikely that the soil heat flux has a significant impact, because of its small magnitude; adding the residuum to G_0 would result in an unrealisticly large heating of the soil. Uncertainties in the radiation measurements may be a reason, but recent improvement of the instruments tend to give higher values of Q, making the non-closure problem even more severe. It is most likely to attribute the error to the eddy-covariance measurements.

Hypotheses to explain this shortcoming are summarised by Culf et al. (2004): Theoretically, the energy balance equation is only valid for fluxes determined at an infinitesimal small volume close to surface, but in practice, flux components are measured at various heights. Therefore, the imbalance may be caused by horizontal advection or storage terms. Nonetheless, these effects result in errors having both signs and do not explain the dominance of a positive residuum. This systematic effect is probably caused by measurement problems in combination with the eddy-covariance technique: All time series, which are used by the eddy-covariance technique, are measured independently. Any measurement problem, like e.g. flow distortion at an sonic anemometer, tends to add white noise and thus reduces correlations and fluxes. Although such effects are reduced by correction formulas, considerable uncertainties remain.

It is important to take the residuum into account while comparing model data to measurements. In the following, the residuum will be estimated as $25\%\,Q$ as proposed by Mauder et al. (2006) and will be added as a range of uncertainty to measurements of both H_0 and λE_0.

2.2 Lokal-Modell (LM)

The Lokal-Modell (LM) is used by German Meteorological Service ("Deutscher Wetterdienst", DWD) as operational, limited area forecast model since December 1998. Since then, the model has been advanced constantly and has undergone many modifications. This section describes the LM Version 3.2, which was operational during LITFASS-2003, along with its operational settings at that time. The LM is a fully compressible non-hydrostatic model, which is operated by DWD with a horizontal resolution of 7 km. The time integration is implicit in the vertical direction and split-explicit in horizontal directions following the concept of Klemp and Wilhelmson (1978). The LM has a generalised terrain-following vertical coordinate with the highest vertical resolution close to the surface. Equations are discretised spatially by finite differencing operators and the corresponding prognostic atmospheric variables are stored on an Arakawa-C-grid: thermodynamic quantities (e.g. temperature, pressure or specific humidity) are evaluated at the centre of a grid-box, whereas dynamic variables (e.g. wind speed, turbulent kinetic energy or diffusion coefficients) are calculated at the boundaries of grid-boxes.

The state variables of land-surfaces are soil temperature profile, soil moisture profile, temperature and water content of the snow storage and the amount of water in the interception storage. The discretisation of the profiles depends on the version of the soil module TERRA: In the framework of the operational two layer version (TERRA-2L) the temperature profile is determined by values at three different depths: the temperature at the (snow-free) surface, at an intermediate depth and a constant so called climatological boundary. The depth of the latter two temperature values is not fixed, but depends on the thermal conductivity and the heat capacity of the soil. This choice allows an optimal discretisation according to the extended force restore method (Jacobsen and Heise, 1982). The soil moisture profile is represented by the water content of an upper layer ranging down to 10 cm depth, the moisture in the deep layer (10 cm-100 cm) and in the climatological layer (100 cm-190 cm). In contrast, the new multi-layer version (TERRA-ML, Heise, 2002; Schrodin and Heise, 2001), which was, however, not operational during LITFASS-2003 and will only be used for a sensitivity study in this work, allows an arbitrary choice of soil layers. Soil temperature and moisture are stored at similar levels and soil temperatures are interpreted as mean values of a layer.

In addition to these prognostic surface state variables, the characterisation of the LM surface is completed by the following set of time constant or only seasonally varying fields: the fraction of land within the grid-box c_{land}, the soil type c_{soil}, roughness length z_0, plant cover f_{veg}, leaf area index f_{LAI} and root depth z_{root}. These fields must be provided to initialise the model and are kept constant throughout the integration time. Seasonal variations, e.g. of f_{LAI}, are considered by varying the initial data, but not by the forecast model itself. Using a lookup-table (Schrodin, 1995), each soil type is assigned to various physical material constants like e.g. heat conductivity or pore volume. Subgrid-scale variability of all surface state variables is neglected and homogeneous surface conditions are assumed within each grid-box.

Two surface types require a special, but simplified treatment: The state of water surfaces is completely defined by surface temperature and roughness length. Since no lake or ocean module is implemented in the LM, the water surface temperature is not a prognostic variable and is kept constant during an integration. Roughness length is diagnosed according to a modified Charnock formula (Doms and Schättler, 1999) during the model integration. As a second exception the surface of soil type 'rock' is assumed to be impermeable for water. Therefore, no soil moisture related processes are considered at rock points and only the thermal heat equation is solved.

In addition to the soil module, the LM comprises a state of the art package of parameterisations of all relevant non-resolved processes: Radiative fluxes are calculated by a delta-two-stream scheme developed by Ritter and Geleyn (1992). A microphysical package with various options is implemented: Cloud condensate can either be considered in a single prognostic variable as cloud water or subdivided into liquid and ice phase. Precipitation as rain and snow can either be diagnosed or simulated as a prognostic variable. Subgrid-scale turbulence within the atmosphere is parameterised with a level-2.5 closure developed by Mellor and Yamada (1982). Transfer coefficients for momentum K_m and for heat and moisture K_h between surface and atmosphere are calculated using a modified Louis scheme (Louis, 1979) or by a yet unpublished newly developed turbulent kinetic energy (TKE) based scheme (Raschendorfer, personal communication). Moist convection is parameterised by a Tiedtke (1989) mass-flux scheme. A Davies (1976) relaxation technique is implemented to nudge the prognostic values at the lateral boundary zone (roughly 8 grid points wide) towards externally prescribed boundary values.

The near surface part of the hydrological cycle as it is represented by the LM is illustrated by Fig. 2.6: Precipitation $P_R + P_S$ reaching the ground is partly accumulated in the interception store W_I or in the snow layer W_S. Both storages interact directly with the ambient atmosphere by evaporation or sublimation, and by formation of dew or rime, respectively. The amount of water that can potentially infiltrate into the soil is given by the sum of drained water from the interception store, melted snow and the part of precipitation which passed by the interception store. Infiltration is limited by the maximum infiltration rate, which depends on the soil type and on soil moisture conditions: dry and sandy soils can infiltrate water faster than e.g. moist soils with a high clay content. If the potential infiltration rate is higher than this limit, the excess is converted into surface runoff R_S and removed from the models hydrological cycle. Infiltrated water moistens the soil. Soil moisture $\eta_{1,2}$ is redistributed vertically between different soil layers by drainage and diffusion. Horizontal transports are neglected. Runoff of soil water $R_{1,2}$ is generated if the volumetric soil moisture in a soil layer exceeds the pore volume. Soil moisture is reduced by bare soil evaporation and plant transpiration. The turbulent transport of water vapour and heat in the surface layer, which ranges from surface up to the centre of the first layer at approximately $33\,\mathrm{m}$ height, is parameterised by the transfer scheme. Above this layer water vapour and heat can either be transported by resolved grid-scale motion or by subgrid-scale turbulent motion, which is parameterised by the turbulence scheme.
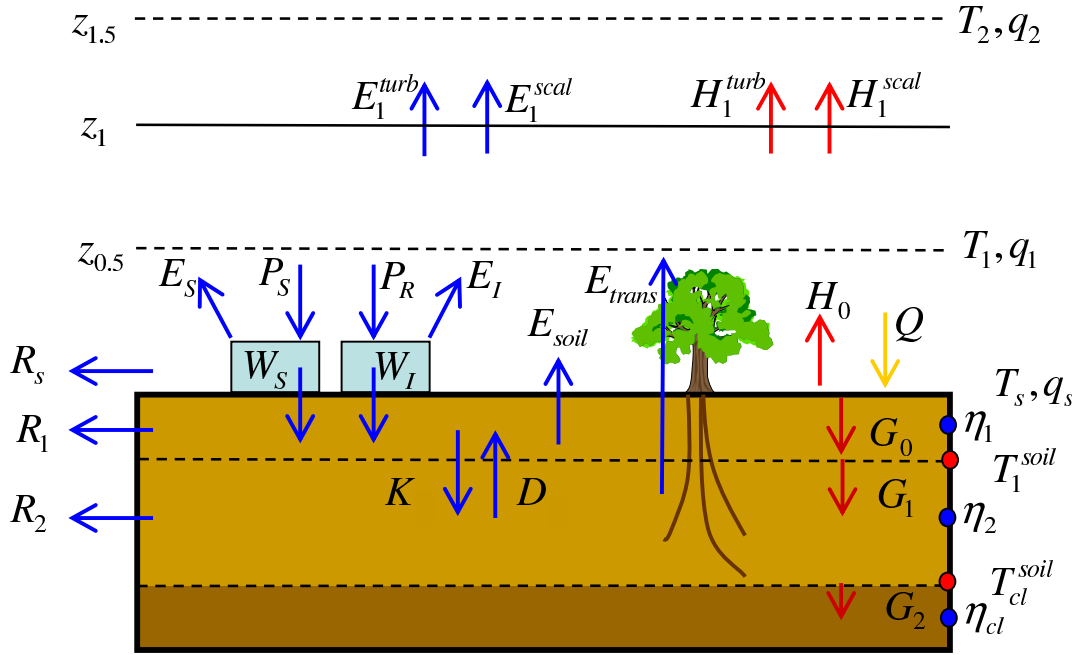
16

Figure 2.6: Scheme of the part of hydrological cycle closely related to the surface using TERRA-2L (see text or Appendix A for a definition of symbols).

The following paragraphs will describe those processes of this hydrological cycle in detail, which are most important for surface-atmosphere exchange processes. Fluxes in the direction of the arrows depicted by Fig. 2.6 will be considered as positive. A complete description of all parameterisations can be found at Doms and Schättler (1999) and Schrodin (1995).

2.2.1 Soil moisture dynamics

The flux of soil moisture in an unsaturated soil is the sum of drainage and diffusion. Horizontal transports are neglected due to the coarse horizontal resolution and therefore the flux of soil moisture F_η can be written as one-dimensional Darcy equation (see standard textbook, e.g. Dingman, 2002):

$$F_\eta = K(\eta) + D(\eta)\frac{\partial \eta}{\partial z} \tag{2.1}$$

The hydraulic conductivity K and the hydraulic diffusivity D depend both on the soil moisture η and the soil characteristics. In the LM, both functions are parameterised by the following exponential laws (Rijtema, 1969):

$$K(\eta) = K_0 \exp\left(K_1 \frac{\eta_{PV} - \eta}{\eta_{PV} - \eta_{ADP}}\right) \tag{2.2}$$

$$D(\eta) \quad = \quad D_0 \exp\left(D_1 \frac{\eta_{PV} - \eta}{\eta_{PV} - \eta_{ADP}}\right) \tag{2.3}$$

The coefficients K_0, K_1, D_0 and D_1 as well as the pore volume η_{PV} and the soil moisture at air dryness point η_{ADP} depend on the soil type (for the look-up table see Schrodin, 1995).

The temporal tendencies of the mean soil moisture η_i of layer i is proportional to the difference of the soil moisture fluxes at the layer boundaries. Evaluating (2.1) at these boundaries requires a vertical interpolation of the soil moisture contents. In TERRA-2L, a weighted average of the adjacent layers is applied:

$$\eta_{i+\frac{1}{2}} = \alpha\eta_{min} + (1 - \alpha)\eta_{max} \tag{2.4}$$

with $\alpha = 0.8$, η_{min} the minimum, and η_{max} the maximum soil moisture content of adjacent layers. In contrast, TERRA-ML assumes a linear soil moisture profile between centres of two layers.

The lower boundary condition at the bottom of the deep layer in TERRA-2L is formulated as a rigid lid at which all soil water fluxes are set to zero. In contrast, a free drainage boundary condition is implemented in TERRA-ML: Soil water can drain from the lowest layer, but the flux due to diffusion is neglected. This means, ground water cannot wetten the soil by capillary rise from below. These formulations are the two most extreme variants of lower boundary conditions: The rigid lid results in very wet soils, because drainage at the lowest boundary is completely omitted; TERRA-ML will tend to dry soil conditions, since soil water drains at the bottom without a compensating flux due to capillary diffusion.

2.2.2 Evapotranspiration

The net evapotranspiration of a grid-box is the sum of bare soil evaporation E_{bare}, plant transpiration E_{trans}, sublimation from the snow E_s and evaporation from the interception store E_I weighted by their areal coverages:

$$E = (1 - f_I - f_{snow})\left[(1 - f_{veg})E_{bare} + f_{veg}E_{trans}\right] + f_I E_I + f_s E_s, \tag{2.5}$$

with f_I the areal fraction covered by interception water, f_s the areal fraction covered by snow and f_{veg} the areal fraction covered by plants. An important quantity to determine these evaporation rates is the potential evaporation rate E_p:

$$E_p(T_s) = -\rho K_h |\vec{v_h}| (q_{atm} - q^*(T_s)) \tag{2.6}$$

with the transfer coefficient K_h for heat, air density ρ, wind speed $|\vec{v_h}|$ and humidity at the atmospheric reference level q_{atm} and saturation humidity $q^*(T_s)$ at surface temperature T_s. The evaporation from the interception E_I and snow store E_s is equal to the potential evaporation at the corresponding temperatures:
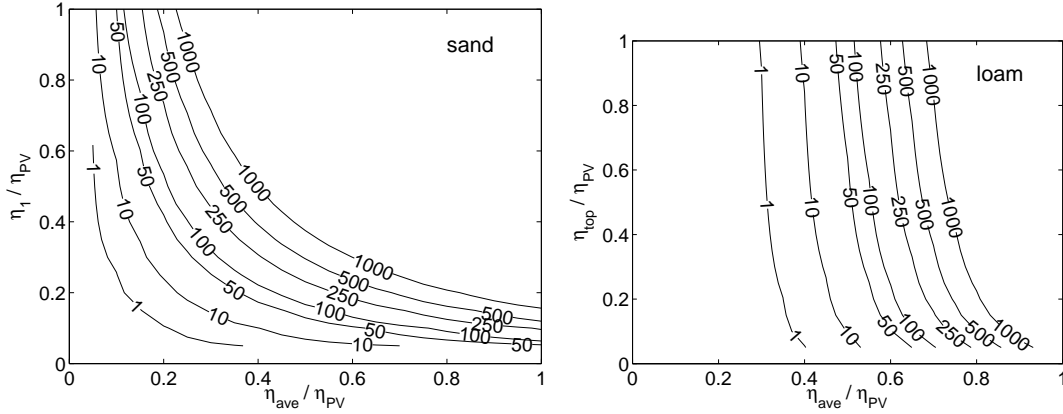
$$E_I = E_p(T_s) \qquad\qquad E_s = E_p(T_{snow}) \tag{2.7}$$

Figure 2.7: Maximum latent heat flux in Wm^{-2} above bare soil for the soil types sand (left) and loam (right) depending on the soil moisture contents at the top-level layer η_1 and the average content throughout the soil column η_{ave} scaled by the pore volume η_{PV}.

Bare soils evaporation is parameterised according to the BATS scheme of Dickinson (1984): It is assumed that bare soil evaporates at potential rate as long as the upward diffusion of soil moisture can supply enough water:

$$E_{bare} = \min\left(E_p, E_{bare}^{max}\right) \tag{2.8}$$

The maximum evaporation rate E_{bare}^{max}, which can be sustained by soil moisture diffusion, is parameterised in terms of the soil moisture of the upper layer η_1, the average soil moisture η_{ave} of both layers and in terms of the soil type. The functional relations were determined by regressions from simulations with a high resolution soil module. Fig. 2.7 shows two examples of E_{bare}^{max} for sand and loam. Sand is less sensitive to the average soil moisture because vertical diffusion is smaller compared to loam.

The BATS scheme of Dickinson (1984) is also applied for plant transpiration E_{trans}:

$$E_{trans}^{dick} = -\rho\left(q_{atm} - q^*(T_s)\right)\left(\frac{1}{r_{ca} + \frac{1}{f_{LAI}}(r_{lc} + r_{stom})}\right) \tag{2.9}$$

This formula is based on the following conceptual model: Air within the stomata of leaves is saturated with water vapour and the temperature of leaves is set to T_s. The transport of this humidity to the lowest atmospheric level is controlled by a sequence of three resistances: the stomatal resistance r_{stom}, the resistance r_{lc} between air directly outside of the leaves and ambient canopy air, and the resistance r_{ca} between the canopy air and the lowest atmospheric level. To take into account that the leaf surface is in general larger than a plane surface the last two resistances are divided by the leaf area index f_{LAI}. Like for bare soil evaporation, r_{ca} is equal to $K_h|\vec{v_h}|$. It is assumed that r_{lc} is proportional to the square root of the friction velocity $u^* = \sqrt{K_m}|\vec{v_h}|$ (with the transfer coefficient for momentum K_m) and a factor of proportionality of $0.05\,(\text{m/s})^{\frac{1}{2}}$.
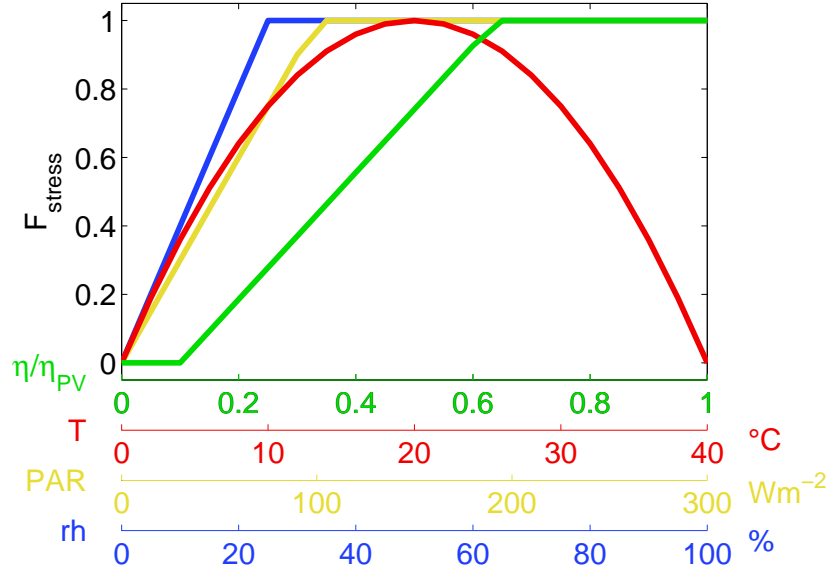
19

Figure 2.8: Parameterisation curves of the four stress factors limiting plant transpiration: soil moisture stress (green), temperature stress (red), insolation stress (yellow) and humidity stress (blue). Note, that low values indicate stress. (Curve of soil moisture stress is not exact; soil moisture threshold values are slightly soil type dependent.)

The stomatal resistance r_{stom} is in the range of a minimal value, when environmental conditions are optimal for photosynthesis/transpiration, and a maximum value under unfavourable conditions. The actual value is determined by four stress factors, which are zero if the stress is highest. They consider stress due to shortage of insolation (F_{rad}), shortage in soil moisture (F_η), improper ambient temperature (F_{tem}) and humidity (F_{hum}):

$$r_{stom}^{-1} = r_{stom}^{max\,-1} - \left(r_{stom}^{min\,-1} - r_{stom}^{max\,-1} \right) F_{rad} F_\eta F_{tem} F_{hum} \qquad (2.10)$$

Fig. 2.8 depicts the functional relation for the stress functions. The radiation stress depends on the incoming photosynthetically active radiation PAR (wavelength of 200-750 nm). The soil moisture stress is evaluated from the average soil moisture content down to the root depth. The stress function increases linearly between the permanent wilting point and the turgor loss point. Both parameters are soil type dependent, but the indicated values of 10% and 68% relative soil moisture (Fig. 2.8) are good approximations. F_{tem} and F_{hum} are based on the interpolated temperature at 2 m height and the humidity at the lowest atmospheric level, respectively. As the functional form of F_{hum} is still in dispute, the humidity stress is switched off in the operational LM ($F_{hum}=1$).

In the LM, the transpiration predicted by the Dickinson scheme is artifically reduced by a factor proportional to the root depth z_{root}:

$$E_{trans} = (z_{root}/1.0\,\mathrm{m})\, E_{trans}^{dick} \qquad (2.11)$$

This formula was not implemented for scientific reasons, but as a pure emergency action to reduce the excessive evaporation in the LM (E. Heise, personal communication).

After the total evapotranspiration has been diagnosed according to (2.5), the following bulk formula is inverted to derive a virtual specific humidity q_s at the surface:

$$E_0 = -\rho K_h |\vec{v_h}| (q_{atm} - q_s) \qquad (2.12)$$

This virtual specific humidity q_s equals the humidity that is required at a flat surface to sustain the diagnosed latent heat flux. Since most surfaces are not flat, e.g. due to leaves, q_s is in general not measureable and may be greater than the saturation humidity $q^*(T_s)$.

It is still state-of-the-art to use strongly parameterised scheme, like the BATS approach, to calculate plant transpiration in mesoscale NWP models. Schemes with similar complexity like those from Chen and Dudhia (2001) (implemented into the models WRF and MM5) or the ISBA scheme of Noilhan and Planton (1989) (implemented into the models HIRLAM, ALADIN, and MESO-NH) are frequently applied. As an exception, the Unified Model of UK MetOffice uses an advanced parameterisation with a physiological description of the photosynthesis process (Essery et al., 2001).

2.2.3 Surface energy balance

At the surface, the energy fluxes of net radiation Q, latent λE_0 and sensible heat H_0, and the ground heat flux G_0 are in balance:

$$Q = H_0 + \lambda E_0 + G_0 \qquad (2.13)$$

(with the latent heat of vaporisation λ). Melting and freezing processes as well as sublimation will be neglected here for simplicity, because they are irrelevant during LITFASS-2003. The net radiation as primary source of energy at the surface is evaluated by the radiation scheme and is composed by the sum of shortwave and longwave down- and upward radiative fluxes:

$$Q := S_{down} - S_{up} + L_{down} - L_{up} \qquad (2.14)$$

The interactions of radiation at the surface are described by the solar broadband albedo α_{so} and infrared broadband albedo α_{IR}. Both relate downward and upward fluxes:

$$S_{up} = \alpha_{so} S_{down} \qquad (2.15)$$
$$L_{up} = \alpha_{IR} L_{down} + (1 - \alpha_{IR}) \sigma T_g^4 \qquad (2.16)$$

with the Stefan-Boltzmann constant σ. The effective surface temperature T_g is an area weighted average of the snow temperature T_{snow} and the snow-free surface

temperature T_s. This average is linear in temperature neglecting the nonlinear effect due to the fourth power temperature dependency of the infrared emission. α_{IR} is set to a fixed value of 0.004. Since α_{so} varies significantly between snow covered, vegetated or bare surfaces, a more sophisticated parameterisation is applied in the solar spectral range:

$$\alpha_{so} = f_{snow}\alpha_{snow} + (1 - f_{snow})\left(f_{veg}\alpha_{veg} + (1 - f_{veg})\alpha_{bare}\right) \qquad (2.17)$$

with α_{snow} equal to 0.7 and α_{veg} equal to 0.15. The albedo of the bare surface α_{bare} is set to 0.07 for water surfaces and varies between 0.2 and 0.3 for land-surfaces depending on soil type and top-level soil moisture.

The sensible heat flux H_0 is parameterised by a bulk formula corresponding to 2.12:

$$H_0 = -\rho K_h |\vec{v_h}| \left(T_{atm} + \frac{g}{c_p} z_{ref} - T_g\right) \qquad (2.18)$$

with the acceleration of gravity g, the isobaric heat capacity of air c_p and the reference height z_{ref}, at which T_{atm} is valid. The term $\frac{g}{c_p} z_{ref}$ corrects for the adiabatic lapse rate of atmospheric temperature.

The ground heat flux G_0 is determined as residuum of the three other energy flux components according to equation (2.13) and is used as forcing at the upper boundary to calculate the soil temperature profile by the extended force restore method (Jacobsen and Heise, 1982). This method is able to solve the heat transfer equation exactly for two arbitrary harmonics, which have been chosen in the LM to capture the daily variations with a 24 h period and synoptical perturbations with a 5 day period. The effect of soil moisture on the heat conductivity has been neglected because otherwise the extended force restore method cannot be applied.

In TERRA-ML the heat transfer equation requires the solution of a tridiagonal linear system of equations which results from an implicit numerical treatment. Since TERRA-ML calculates temperature only at the centre of layers the skin temperature of the surface T_s is not directly given. Various sophisticated schemes to extrapolate T_s are implemented, but the most easiest assumption, setting T_s equal to the mean temperature of the top layer, is actually used.

As the energy balance equation (2.13) is explicitly used to determine G_0, the LM inherently closes the energy budget at the surface. Energy conservation might not be fulfilled perfectly only due to numerical problems in treating the melting or freezing processes.

The most difficult task in solving the energy balance equation is to determine the correct partitioning of latent and sensible heat fluxes, which can be expressed in terms of the Bowen ratio $\beta := H_0/\lambda E_0$. Assuming a constant forcing of the total turbulent fluxes

$$\text{const} = H_0 + \lambda E_0 = Q - G_0 \qquad (2.19)$$

in combination with (2.18) and (2.12) gives a set of equations, which can be solved for β depending on the effective stomatal resistance r_{stom}/f_{LAI}, the atmospheric
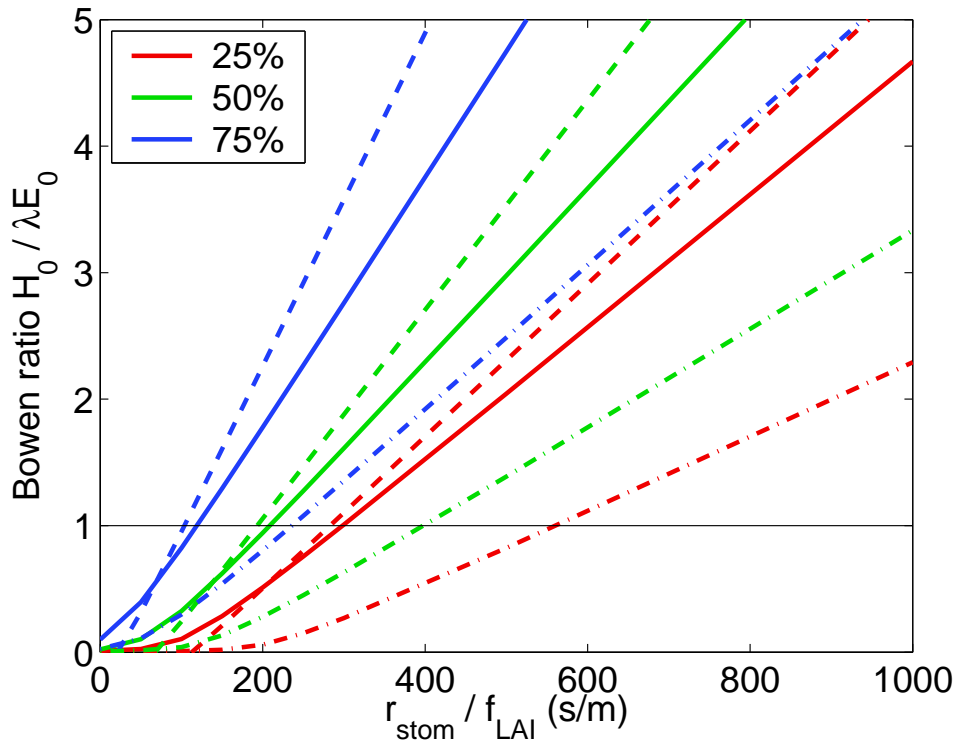
Figure 2.9: Bowen ratio depending on the effective stomatal resistance r_{stom}/f_{LAI}. The relative humidity at the atmospheric reference height (33 m) is varied between 25 and 75%. Solid lines: $|v_h|$=2 m/s, T_{atm}=20 °C; dashed lines: $|v_h|$=10 m/s, T_{atm}=20 °C; dashed-dotted lines: $|v_h|$=2m/s, T_{atm}=30 °C. The net available turbulent energy $Q - G_0$ is set to 500 W/m^2 and z_0 is fixed to 0.1 m.

temperature and relative humidity, wind speed and the total turbulent flux $H_0+\lambda E_0$. The impact of $H_0+\lambda E_0$ on the Bowen ratio is small; all other dependencies are shown in Fig. 2.9. Bearing in mind that the stomatal resistance of plants varies in the range of 100 s/m to 5000 s/m, it is evident that the bowen ratio is largely determined by the stomatal resistance. Accurate stomatal resistance parameters (r_{stom}^{min} and r_{stom}^{max}) and LAI information as well as a good parameterisation of the daily variations of stomatal resistance due to stress factors are essential. It is reasonable that low atmospheric humidity favours evaporation and results in low Bowen ratios. The same effect occurs if the atmospheric temperature is increased because the specific humidity spread in the equation (2.12) for λE_0 increases exponentially following the curvature of the humidity saturation pressure relation, while the temperature spread in the equation (2.18) for H_0 increases only linearly. Increased wind speed directly enhances the transfer coefficient in the equation (2.18) for H_0, whereas the net transfer coefficient in the equation (2.12) for λE_0 remains limited by the stomatal resistance. Consequently, higher wind speed causes slightly higher bowen ratios.
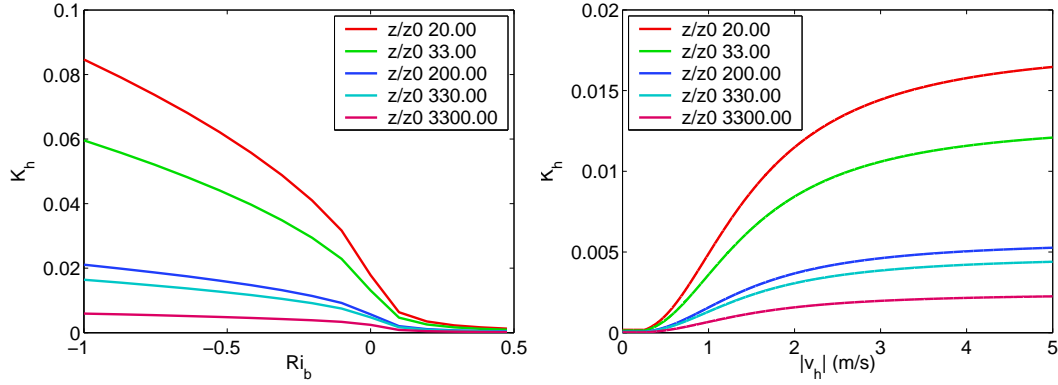
Figure 2.10: Transfer coefficients K_h determined by the Louis scheme with respect to the bulk Richardson number Ri_b (left) and for different wind speeds assuming a constant temperature difference $T_s - T_{atm} = 4\,K$ (right). Atmospheric reference height is fixed to the height of the lowest LM level (33 m).

2.2.4 Transfer scheme

The first of two available transfer schemes in the LM is a modified Louis scheme. It is based on the concept presented by Louis (1979), but uses a slightly different Prandtl number and modified fitting functions. Using Monin-Obukhov similarity theory, flux-profile relationships can be integrated up to the lowest model level in order to obtain relations between the bulk differences in state variables, corresponding fluxes and the Monin-Obukhov length. The universal functions appearing in these relations have been adopted from experimental data by Businger (1971). As the Monin-Obukhov length itself depends on the fluxes, no analytical solution to determine the transfer coefficients exists. Iterative solutions are computationally expensive and result in too small coefficients under stable conditions and infinite values in the free convection limit. These shortcomings can be avoided without loosing significant accuracy by fitting suitable functions to the analytical solution as proposed by Louis. Fig. 2.10 shows the resulting transfer coefficients of heat as a function of the bulk Richardson number $Ri_B = gz(\Theta_{atm}(z) - \Theta_s)/(\overline{\Theta}v_h^2(z))$. Large transfer coefficients are obtained under unstable situations ($Ri_B < 0$) and for either large roughness length z_0 or low reference heights z.

The bulk formulas (2.18) and (2.12) suggest that the surface fluxes are proportional to the wind speed. This is only valid if the transfer coefficient is independent from the wind speed. According to the Louis scheme, this condition is only fulfilled at high wind speeds (Fig. 2.10, right). At lower speeds, the surface fluxes increase more than linearly with increasing wind speeds. Subgrid-scale variance in the input variables of the bulk formulas (2.18) and (2.12) is neglected in the LM. This approximation will result in biased flux estimates, if significant subgrid-scale correlations among these variables exist. The transfer scheme has the potential to induce such correlations: Positive anomalies in the temperature difference $\Delta T = T_s - T_{atm}$ will directly result in a positive anomaly of the transfer coefficient, because the atmo-
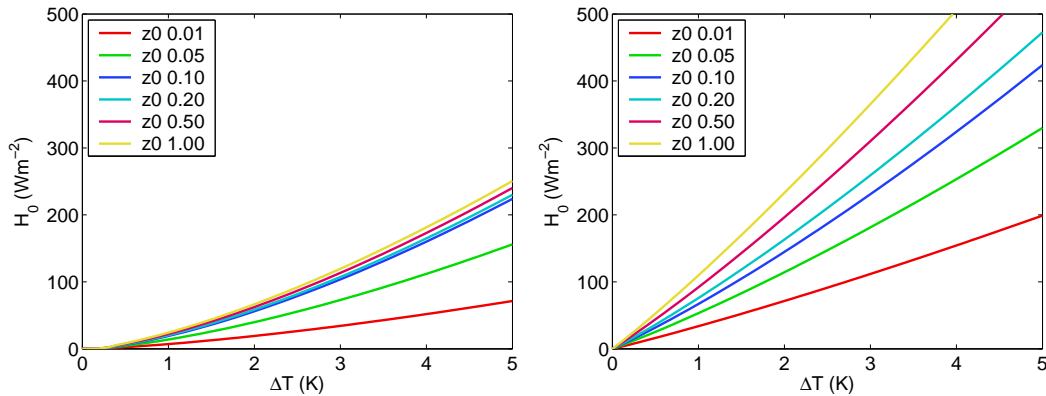
Figure 2.11: Relation between sensible heat flux H_0 and temperature spread ΔT up to the lowest model level $(33\,\mathrm{m})$ for $2\,\mathrm{m/s}$ (left) and $10\,\mathrm{m/s}$ wind speed (right) as well as varying roughness length z_0.

spheric stratification is less stable. In essence, unlike to what might be expected from the formula, the sensible heat flux is not linear in terms of the temperature difference ΔT as demonstrated by Fig. 2.11. The nonlinearity is stronger in case of low wind speed conditions.

The second transfer scheme has been developed by M. Raschendorfer and is used in the operational LM. The surface layer is subdivided into a laminar and a constant flux layer. Assuming certain interpolation rules, scaling arguments and laminar parameters, the problem can be reduced to estimate the turbulent velocity scale at the boundary between the laminar and the constant flux layer. This is done by solving a TKE equation similar to the approximated TKE equation of Mellor and Yamada (1982), which is applied in the turbulence scheme above the surface layer. Although this scheme has some advantages like a consistent treatment of turbulence throughout the whole atmosphere and no need for empirical functions, it is only documented by an incomplete internal report. Therefore, the scheme is not suitable for research applications and will not be considered in this study except in the framework of the operational LM simulations.

2.2.5 Transport above the surface layer

Above the surface layer, heat and humidity can be transported either by resolved eddies in terms of grid-scale variables or by subgrid-scale circulations, which are parameterised by the turbulence scheme and the Tiedtke (1989) mass-flux scheme of moist convection. Surface fluxes and the boundary evolution are mostly affected by the turbulence scheme, which will be presented in more detail: Mellor and Yamada (1982) derived a hierarchy of second order turbulence closure by successive simplifications of the budget equation for second order turbulent moments using order analysis. In the level-2.5 approximation, the system of equations is reduced to a simplified prognostic equation for the TKE e and diagnostic relations for all

other remaining second order moments. Since the horizontal grid spacing is in general large compared to the vertical discretisation, horizontal turbulent mixing is neglected (boundary layer approximation).

The turbulent vertical fluxes of sensible H and of momentum M can be expressed by a flux-gradient relation similar to the bulk formulas in the surface layer:

$$H_{i+\frac{1}{2}} = -\rho_{i+\frac{1}{2}} c_p K_{h,i+\frac{1}{2}}^{atm} \frac{\theta_{i+1} - \theta_i}{z_{i+1} - z_i} \quad (2.20)$$

$$M_{u,i+\frac{1}{2}} = -\rho_{i+\frac{1}{2}} K_{m,i+\frac{1}{2}}^{atm} \frac{u_{i+1} - u_i}{z_{i+1} - z_i} \quad (2.21)$$

with the layer index i; $i + \frac{1}{2}$ denotes the boundary of layers i and $i + 1$. Analogue formulas apply for the latent heat flux λE and the flux of zonal momentum M_v. The turbulent diffusion coefficients are $K_{m,h}^{atm}$ given by

$$K_{m,h}^{atm} = l_{tur} \sqrt{e} S_{m,h} \quad (2.22)$$

with the turbulent length scale l_{tur} and the stability functions S_m and S_h. These stability function depend on the wind shear, stability, the turbulent length scale l_{tur} and the TKE e. Both stability functions approach zero if the stability or the wind shear is increased. Consequently, considerable transport of heat, humidity or momentum requires unstable conditions. The turbulence scheme is closed locally, which means that turbulent mixing occurs only at the same level where turbulent motion is initiated. Non-local effects, like subgrid-scale thermals invoked at the surface, which may rise up throughout a neutrally or even slightly stable stratified boundary layer, cannot be considered. The turbulent length scale l_{tur} is parameterised according to Blackadar (1962) and increases almost linearly with height at low altitudes before approaching its asymptotic value l_{tur}^*, which is set to $500\,\mathrm{m}$:

$$l_{tur} = \frac{\kappa z}{1 + \kappa z / l_{tur}^*} \quad (2.23)$$

with the von-Karman constant κ and the height above ground z.

2.3 Model enhancements

A comparison of model results and measurements, which will be presented in Chapter 4, reveals that the operational version of the model has be to enhanced in order to reproduce observed surface fluxes during the LITFASS-2003 period realistically. Those modifications which are specific to the LITFASS-2003 integrations, especially appropriate initial data, will be discussed in the next chapter, but general improvements, which should in principle become part of the operational model system, will be presented in this section. At first, model errors in terms of disagreement between model coding and scientific knowledge have been removed. Secondly, existing parameterisations have been improved by small reformulation. Finally, two new parameterisation schemes for heterogeneous land-surfaces have been implemented. These changes will be documented in the following.

2.3.1 Removal of model errors

The artificial reduction of transpiration proportional to the root depth (2.11) is the most relevant model error with respect to surface fluxes. The correction factor has a large impact because the values of z_{root} vary operationally between 0.03 m and 0.6 m. In the light of LITFASS-2003 observations, the additional root depth dependency deteriorates the model performance: It reduces the modeled latent heat flux over grass surfaces or farmland areas stronger than over forest due to the large root depth of trees. Measurements give the opposite picture (see Fig. 2.4). Removing the correction is essential to model the spatial flux distribution realistically, but requires additional efforts with respect to initial soil moisture analysis: Due to the reduced transpiration, the operational soil moisture analysis of DWD tends to higher soil moisture values. If the improved model is initialised with this data, the model will excessively overestimate evaporation. A considerably long spin-up phase is needed to ensure that the improved model is in a balanced state with respect to soil moisture.

All other coding errors, which have been discovered and eliminated during this study, do not have a direct impact on surface fluxes and will be discussed in Appendix D. Anyway, it is worthwhile to correct them because indirect effects cannot be excluded due to the nonlinear interactions between all parts of the model. A physical consistent model systems is an overall prerequisite for any scientific effort based on numerical simulations.

2.3.2 Improvement of existing parameterisations

The albedo of plants and the parameters for computing stomatal resistance are set to constant values in the operational LM. The discussion of Fig. 2.4 revealed that this simplification is not valid. Both albedo and stomatal resistance parameters vary significantly between different types of vegetation. The importance of accurate stomatal resistance parameters was additionally highlighted by algebraic considerations summarised in Fig. 2.9. Consequently, land-use was introduced as an additional input field to characterise the land-surface; plant albedo and stomatal resistance parameters are prescribed according to a look-up table (see Appendix B) which assigns typical values to each land-use class.

The LM lacks a lake or sea module to compute surface temperatures of water surfaces prognostically. Water surface temperatures are provided by the initial data and then kept constant throughout the integration. This approximation is justified for shortrange (a couple of days) and coarse scale runs since the temperature of large water surfaces, like e.g. the Baltic sea, vary only slowly in time. In contrast, surface temperatures of small lakes exhibit a clear diurnal cycle and considerable day to day variations, which cannot be ignored (see Fig. 2.12). Small lakes are resolved at high resolutions of e.g. 1 km. Developing a lake module was not feasible and not the objective of this study. As a simple and practical approach, the measured lake
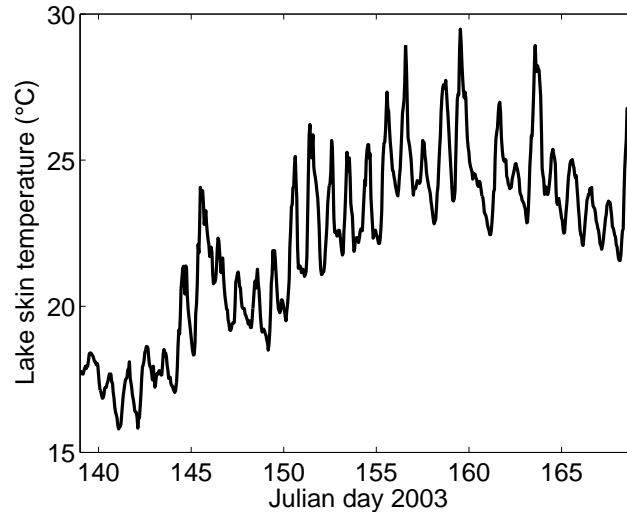
Figure 2.12: Time series during LITFASS-2003 of lake surface temperature measured at the Glubigsee, which is situated in the southeastern part of the LITFASS domain.

surface temperature of the Glubigsee (Fig. 2.12) was prescribed every hours at all lake points within the model domain.

To calculate drainage rates, the soil moisture at the interface of adjacent layers must be interpolated using the average soil moisture of both layers. The standard interpolation formula weights the dry layer strongly (see equation 2.4). This formulation may cause a deadlock: If the lower soil layer dries out, drainage towards this layer is nearly totally suppressed and the layer can never be refilled by draining precipitation from above. This unphysical effect can be avoided by introducing a upstream numerical formulation: The soil moisture at the source layer, i.e. the upper layer, determines the drainage rate. To avoid excessive wetting of the lower layer due to this change, the rigid-lid lower boundary condition is replaced by a free drainage boundary condition similar to TERRA-ML: Soil water can drain at the lower boundary, but the flux due to diffusion is neglected. The relevance and positive impact of these modifications will be demonstrated in Section 3.3.

2.3.3 Implementation of new schemes for heterogeneous land-surfaces

Subgrid-scale variability in surface characteristics as well as the soil properties within one grid-box of the operational LM is neglected. The LM employs the effective parameter approach to account for small scale land-surface heterogeneities: High resolution land-use maps are converted into high resolution maps of all relevant land-surface parameters by look-up tables. These fields are aggregated to effective parameters on the coarse model grid by arithmetic averaging of all variables, except roughness length which is averaged logarithmically and additionally considers effects of roughness due to subgrid-scale orography.
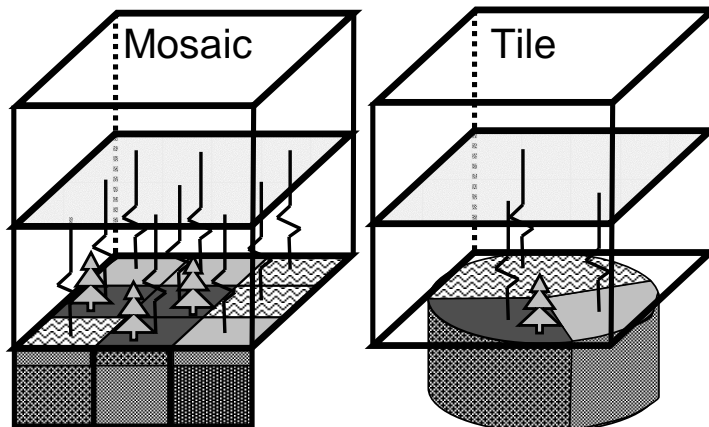
Figure 2.13: Schematic overview of surface-atmosphere exchange represented by the mosaic (left) and the tile approach (right).

As alternatives, the tile approach (Avissar and Pielke, 1989) and the moasic approach (Seth et al., 1994) have been implemented into LM during this study. The mosaic method simulates all surface and soil processes on a explicit subgrid within one atmospheric grid-box, whereas the tile method subdivides the surface within an atmospheric grid-box into several typical classes and simulates all surface and soil processes for each class separately (Fig. 2.13). The advantage of the mosaic scheme is that each subgrid-point has a geographical position which can e.g. be used for hydrological run-off models or to assimilate high resolution data from an land-surface data assimilation scheme. The tile method with its subdivision into non-localised classes is in general faster because less classes than subgrid-pixels are needed to capture the subgrid-scale heterogeneity. But the tile method is based on a subjective classification and can only resolve surface variablity due to this classification. For example, if land-use is selected to define the surface classes of the tile scheme, only variablity due to land-use will be considered and other effects, e.g. due to differential soil moisture contents, will be neglected.

The coarse atmosphere model component and the higher resolved surface and soil module are coupled in both methods by disaggregating fluxes directed to the surface and averaging fluxes in the opposite direction. The surface within one atmospheric grid column is subdivided into N sub-patches, which have their individual prognostic surface and soil state variables, and surface parameters. The fraction covered the patch i is given by f_i, so that $\sum_{i=1}^{N} f_i = 1$. The mosaic approach can be seen as special case with $f_i = 1/N$. The latent heat flux $E_{0,i}$ for one patch is given by a bulk relation formally equivalent to the operationally used parameterisation (2.12):

$$E_{0,i} = -\rho K_{h,i} |\vec{v_h}| (q_{atm} - q_{s,i}) \tag{2.24}$$

Analogue formulas apply for the local sensible heat flux $H_{0,i}$ and momentum transport $M_{0,i}^{u,v}$. These local fluxes as well as the local transfer coefficients $K_{h,i}$ and $K_{m,i}$ are determined from both coarse scale atmospheric variables (T_{atm}, q_{atm}, $|v_h|$ and ρ) and local fine scale surface variables (e.g. $q_{s,i}$, $z_{0,i}$).

This reveals the approximation which is the basis of the mosaic and tile methods: subgrid-scale variablity of atmospheric variables is neglected. It is assumed that small scale anomalies in surface fluxes have no significant impact on atmospheric state variables at the lowest model level. In other words, the blending height of surface heterogeneities is assumed to be at this level. Physically, tile and mosaic schemes can be interpreted as all-or-nothing approximations of subgrid-scale horizontal diffusion: There is no diffusion below the lowest model and no horizontal coupling between the patches. But at the lowest model level and above, subgrid-scale horizontal diffusion is assumed to be extremely strong and to remove all subgrid-scale variability efficiently. Results from high resolution model simulations will show that these assumptions are in general well justified (see Section 4.3.3).

Grid-box averaged fluxes, which are needed as lower boundary conditions of the atmospheric model, are obtained by area weighted averaging

$$E_0 = \sum_{i=1}^{N} f_i E_{0,i}. \tag{2.25}$$

Similar formulas apply for H_0 and $M_0^{u,v}$.

Precipitation and downwelling radiation are distributed homogeneously among all patches, but also other distributions might be used to mimic subgrid-scale variability in precipitation and cloud cover. Upwelling radiative fluxes can be calculated locally according to (2.15) and (2.16) and then be aggregated by an area-weighted average. Technically, it is more convenient to solve the equivalent problem of calculating the radiative transfer equation for the whole atmospheric column with a homogeneous, effective solar albedo $\alpha_{so}^{eff} = \sum_{i=1}^{N} f_i \alpha_{so,i}$ and the effective radiative surface temperature $T_g^{eff4} = \sum_{i=1}^{N} f_i T_{g,i}^{4}$ and secondly disaggregating the short and longwave net radiation S_{net} and L_{net}:

$$S_{net,i} = \frac{(1 - \alpha_{so,i})}{\alpha_{so}^{eff}} S_{net} \tag{2.26}$$

$$L_{net,i} = L_{net} + (1 - \alpha_{IR})\sigma \left(T_{g,i}^{4} - T_g^{eff4} \right) \tag{2.27}$$

The mosaic and the tile method may be simplified by assuming homogeneous soil conditions within one atmospheric grid-box. Consequently, the same soil temperature and soil moisture values are used for all sub-pixels of the mosaic approach or all land-use classes of the tile approach; only different surface parameters like roughness length or stomatal resistance are applied to calculate the individual fluxes. The computational advantage is that all processes within the soil, like heat conduction or drainage, have to be calculated only once per atmospheric grid-box.

By implementing these parameterisations for subgrid-scale surface heterogeneities, the enhanced LM draws level with most other mesoscale models: Tiles scheme with a few sub-patches are frequently implemented into mesoscale models (e.g. HIRLAM, MESO-NH, ALADIN or Unified Model). For example, the HIRLAM model (Uden

et al., 2002) distinguishes between five surface classes (water, ice, bare soil, forest and low vegetation) within each atmospheric grid-box. To the knowledge of the author, mosaic schemes are not used operationally. Beside the standard LM, there are, however, still some models (e.g. WRF and MM5), which neglect subgrid-scale variability and assume homogeneous surface conditions.

3 Setup of model experiments

3.1 Sensitivity study of parameters influencing surface fluxes

The model description in the previous chapter showed that near surface fluxes are influenced by many parameters, which can be subdivided into three groups: variables which are constant in time or vary only seasonally (e.g. soil type or leaf area index), slowly varying variables (e.g. soil moisture) and rapidly varying variables (e.g. atmospheric temperature). The first group of variables, called surface parameters, is prescribed externally. This means that the model performance depends directly on accurate input data. Although the second group of variables is prognostic in a mesoscale NWP model, the model cannot alter these variables significantly due to short integration times and therefore the initial values are of great importance, too. Only the third group is less sensitive to externally prescribed conditions and depends more on the dynamics and parameterisations of the model itself. The aim of the sensitivity study, which will be presented in this section, is to quantify the impact of all relevant parameters on the prediction of near surface fluxes. This gives an indication how accurately surface parameters and slowly varying variables should be prescribed.

To ensure representativeness in space and time, this sensitivity study consists of model integrations for the whole LITFASS domain and the whole LITFASS-2003 period. Since such integrations are computationally too expensive when run with the full LM model, only its soil module TERRA in a stand-alone version is integrated. 'TERRA stand-alone', as a surface-vegetation-atmosphere transfer (SVAT) scheme, consists of the soil module, the Louis transfer scheme and those parts of the radiation scheme which concern interactions of surface and radiation (Fig. 3.1). All processes in the soil as well as surface fluxes are computed prognostically, but the following atmospheric forcings at a certain reference height (e.g. the height of measurements) are prescribed externally: atmospheric temperature T_{atm}, atmospheric humidity q_{atm}, surface pressure p_s, wind speed $|v_h|$, precipitation rate RR and downwelling radiation Q_{down}.

Consequently, any feedback of the surface fluxes on the atmosphere is neglected. This approximation is common practice for SVAT model integrations. It is valid as long as the surface fluxes do not deviate too much from the real fluxes which have determined the true temporal evolution of the atmospheric state variables. A
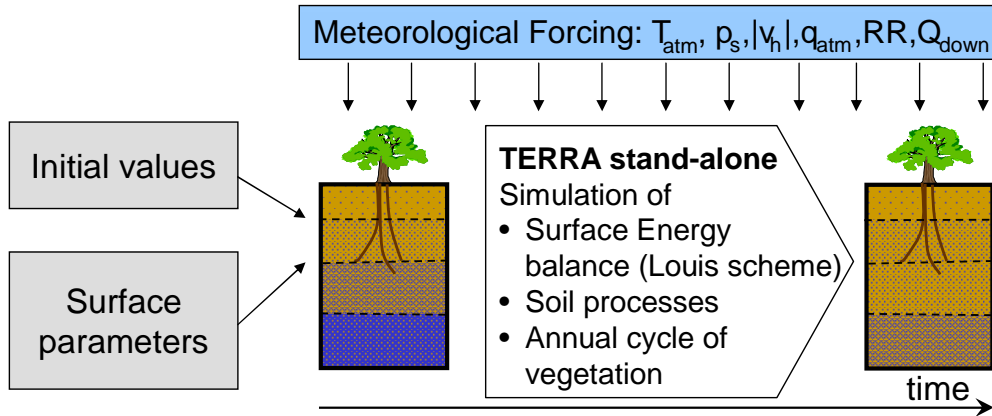
Figure 3.1: Scheme of TERRA stand-alone: Initial values (soil temperature and moisture) and surface parameters (e.g. soil type or plant cover) have to be provided once at the starting time. In contrast, the boundary conditions consisting of the meteorological forcing are prescribed throughout the entire simulation periode.

comparison of a stand-alone integration without feedback and a atmospherically coupled run will be given at the end of Section 3.3.

Regarding the sensitivity study, the unmodified input data of the control run is chosen to represent the conditions during LITFASS-2003 as close as possible: Initial soil conditions (moisture and temperature) are obtained from the measurement driven soil moisture analysis, which will be discussed in Section 3.3. Surface parameters are provided by the improved data set, which will be derived in Section 3.2. Meteorological forcing except precipitation is prescribed homogeneously as measured at the GM Falkenberg site. Photosynthetically active incoming radiation (PAR) is not measured, but approximated by $0.5\,S_{down}$; this formula was obtained by a fit to results of the LM radiative transfer scheme. Precipitation rates are retrieved from radar observations (for details see Section 3.3). Sensitivities are investigated by varying all selected influence parameters separately by a factor between 0.25 and 4. As exceptions, the atmospheric temperature is not disturbed relatively, but absolutely by increments between -2 and 2 K, and the range of humidity variations is limited to avoid unrealistically dry and wet conditions.

The results in terms of temporally and spatial averaged net radiation, sensible and latent heat flux are summarised in Fig. 3.2. It shows clear impacts concerning the partitioning of latent and sensible heat flux. The influence of the atmospheric forcing variables T_{atm} and q_{atm} is reasonable: low air temperatures result in a large spread between surface and air temperature and thus enhance the sensible heat flux, whereas a dry atmosphere supports increased latent heat flux. Soil moisture, especially the deep soil moisture, has a strong influence. The deep layer has a greater influence on the soil moisture stress of plants because large fractions of roots reside in this layer. Soil moisture conditions during LITFASS-2003 are in the transition regime between the extremes of a wet soil which allows plants to transpire
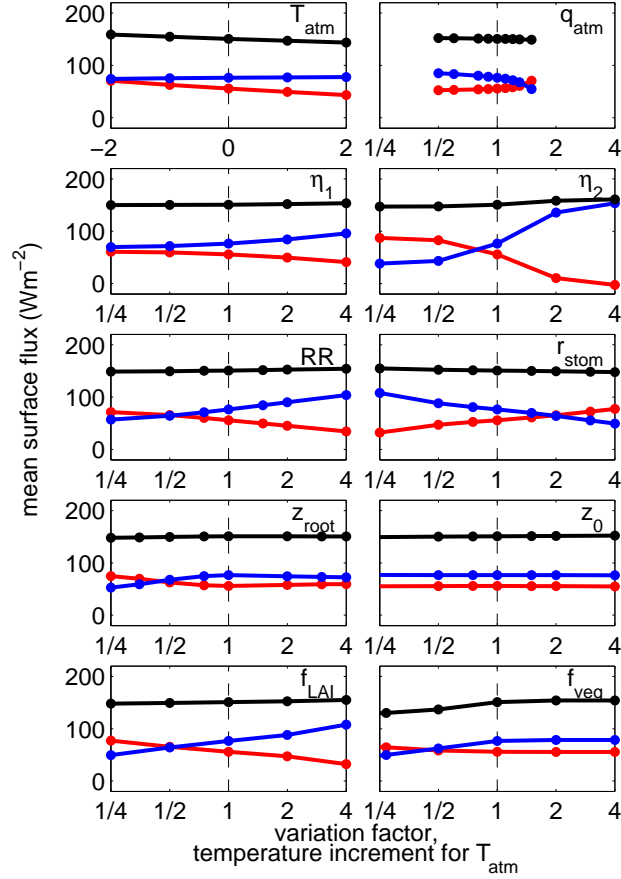
Figure 3.2: Net radiation (black), sensible (red) and latent (blue) heat flux (averaged over the LITFASS-2003 periode and LITFASS domain) simulated by TERRA stand-alone depending on variations of the following parameters: atmospheric reference temperature T_{atm}, atmospheric reference humidity q_{atm}, top level soil moisture η_1 (0-10 cm) and deep soil moisture η_2 (10-100 cm), rain rate RR, stomatal resistance r_{stom}, root depth z_{root}, roughness length z_0, leaf area index f_{LAI} and plant cover f_{veg}. (Stomatal resistance is varied by modifying its minimal and maximal values, see equation 2.10.)

at their potential rate and a dry soil suppressing transpiration nearly completely. This sensitive regime makes the precipitation rate an important quantity because the amount of rain reaching the ground alters the soil moisture. Concerning the surface parameters, f_{LAI} and r_{stom} have the greatest impact. It is worthwhile to highlight the importance of stomatal resistance because its representation in the operational LM is strongly simplified by assuming a similar stomatal parameters for all plant species. If plant cover f_{veg} is decreased, evapotranspiration will be reduced; plant transpiration is obviously more effective than bare soil evaporation. Greater root depth leads to higher evaporation since the root reaches deeper into the moist deep soil layer. Surprisingly the roughness length has no visible impact. Although higher roughness length result in higher transfer coefficients, this effect is perfectly compensated by smaller gradients in the state variables of the bulk formula.

Concerning net radiation, all parameters have only a small or no effect. Plant cover f_{veg} is somewhat relevant since the albedo of bare soil is in general higher than the albedo of plants. In general, larger sensible heat fluxes tend to result in smaller net radiation because the surface is warmer and emits thus more energy in the infrared spectral range.

In essence, parameters of all three groups have a significant impact on surface fluxes. It is essential for any study which aims at investigating the impact of model formulations (e.g. concerning representation of heterogeneity) to take care of accurate input data in order to avoid unwanted side effects. Especially a good analysis of leaf area index, stomatal resistance parameters and soil moisture is important. The following section will describe a procedure to obtain accurate surface parameter estimates and Section 3.3 will present an appropriate soil moisture analysis scheme.

3.2 Surface parameters

Maps of surface parameters for the use in atmospheric models shall describe the surface characteristics on a scale corresponding to the horizontal resolution of the model grid. Such a data set can be derived by using a map of land-use classification and by assigning characteristical parameter values to each land-use class. This technique is applied by DWD and has also been adopted in this study: The estimation of surface parameter maps is based on the CORINE land-cover data set (EEA, 2000) in combination with a look-up table (see Appendix B). The CORINE data set has been retrieved from satellite observations allowing a high spatial resolution of approximately 100 m. In principle, some land surface parameters, like leaf area index, can also be estimated directly from NDVI measurements of satellites. But these methods have not been used, because recent research results (e.g. Tittebrand et al., 2005) revealed large uncertainties in the regression formulas relating NDVI and land-surface parameters.

High resolution land-use maps or derived parameter maps must be aggregated on the coarser model grid. Classified variables like land-use are aggregated by the dominant type approach, which means that a coarse grid-box is assigned to the most frequent class within the box. Continuous variables may be aggregated either by first aggregating the land-use map and then applying a look-up table ('dominant type approach') or by deriving the parameters at high resolution and subsequent averaging of the parameter fields ('effective parameter approach'). The first concept results in a physical consistent combination of parameters, but may lack representativeness for the grid-box. As an another drawback, this aggregation method depends on the subjectively chosen classification: If a certain class is subdivided into sub-classes (e.g. subdividing forest into broadleaf and coniferous forest), each of these sub-classes may not form the majority within a grid-box in contrast to the non-splitted class. In essence, classes, which are resolved in detail, because they are of special interest, are oppressed by the dominant type method. In order to avoid
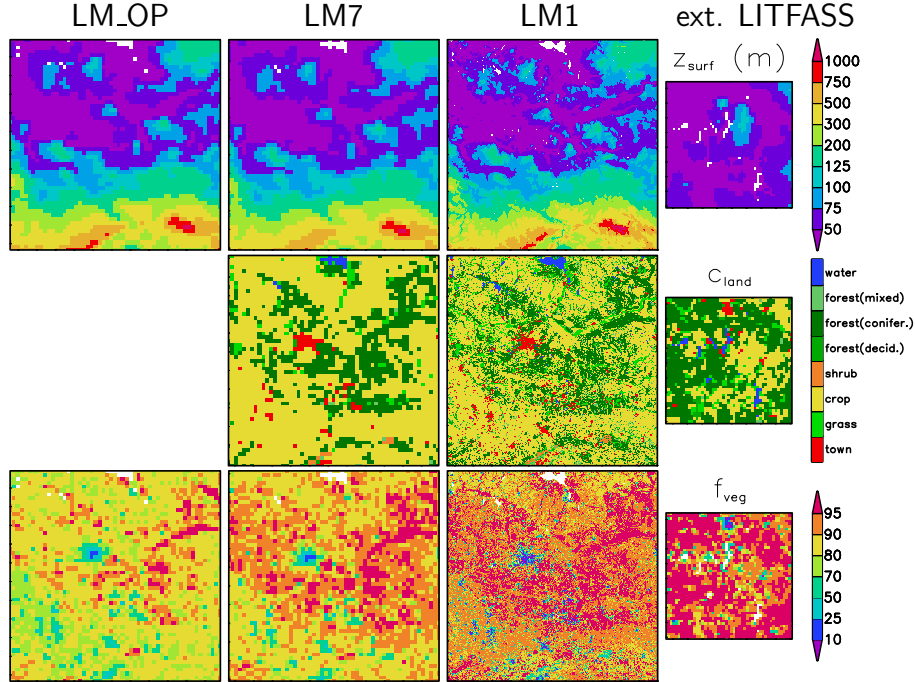
Figure 3.3: Surface parameter sets from left to right: Operational LM (LM_OP; 7 km grid spacing); newly derived data sets at 7 km (LM7) and at 1 km (LM1) resolution. These maps cover an area of $385 \times 385 \, \mathrm{km}^2$ centred over the LITFASS domain ('LM domain' according to Fig. 3.14). Last column: Zoom into newly derived 1km data set for an area of $49 \times 49 \, \mathrm{km}^2$ centred over the LITFASS domain ('Extended-LITFASS domain' according to Fig. 3.14). Seasonal varying parameters (f_{LAI}, f_{veg} and z_{root}) are valid for 30 May.

these problems, the effective parameter method, which is also operationally used by DWD, will be applied as basic method in the following.

Almost all parameters are averaged arithmetically, except the roughness length. In this case, it is reasonable to assume an arithmetical averaging of surface fluxes, which are proportional to the logarithm of the roughness length under neutral stratification. Consequently, the roughness length is aggregated by logarithmic averaging. For the sake of simplicity and to save computer memory resources, the two additionally added parameters α_{veg} and $r_{stom}^{min,max}$ are not prescribed externally by additional input files, but internally generated during the model execution according to the land-use map. Consequently, these fields are always aggregated by the dominant type method.

Surface elevation is adopted from the GTOPO30 (USGS, 1997) data. The soil type classification is merged from different data sources. For the LITFASS domain and its surrounding, a special soil type map from the 'LITFASS-Lokal-Modell' (Herzog et al., 2002) project was available. The information for the rest of the model domain is based on the operational soil type map of DWD. Basic requirements of consistency between the parameter fields, e.g. similar land-sea masks given by the land-use map and by the soil type distribution, are assured by a series of final checks.
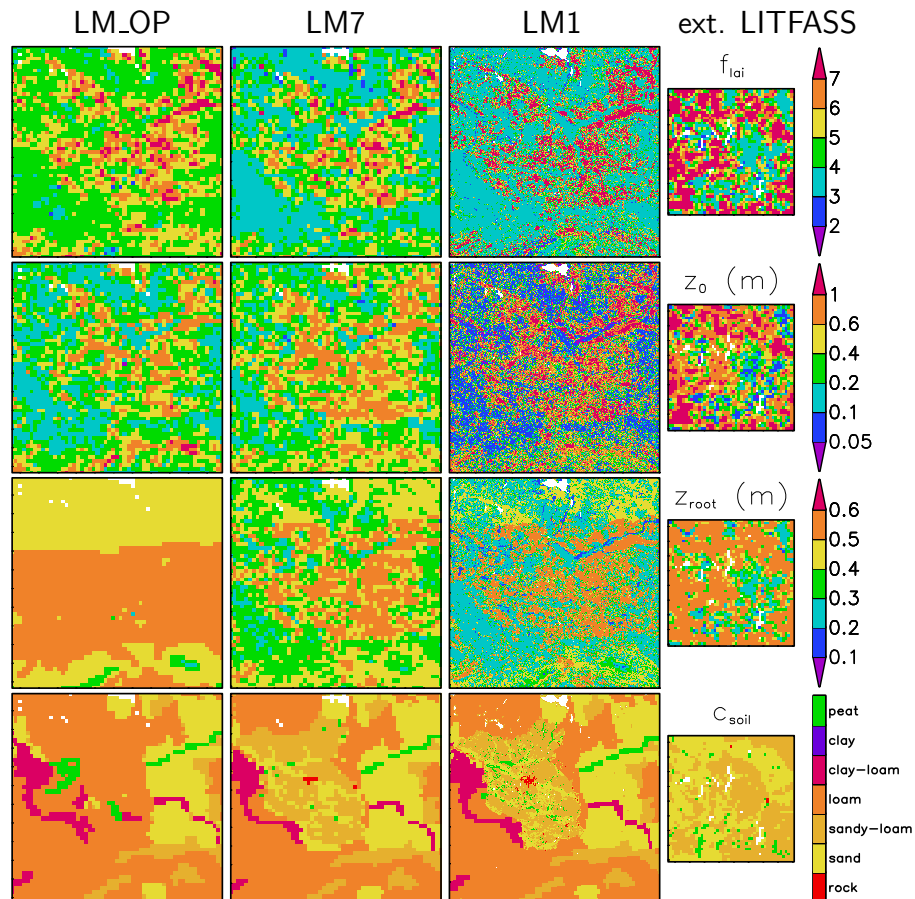
Figure 3.3: (continued)

Fig. 3.3 presents an overview of the derived fields at different resolutions and in comparison to the operational parameter sets of DWD. In principle, DWD applies the same techniques and utilises only slightly different look-up tables and versions of CORINE land-cover data. Therefore, the operational data set and the newly derived one look quite similar. Exceptions are the fields of root depth and soil type: In contrast to the documentation of LM, the operationally used root depth is obviously only a function of latitude and elevation. Adding additional soil type information introduces much more structure into the soil type distribution and changes the prevailing soil type in the LITFASS region from loam to sandy-loam and sand, which is much more realistic. Beside these two corrections, the newly derived parameters have the advantage that they are available consistently at all horizontal resolutions that are needed for model integrations. Comparing the 7 km resolution data to the high resolution 1 km data, it becomes obvious that the high resolution maps have significantly more variablity and more steep gradients. Consequently, surface parameter maps contain information at small scales which cannot be deduced from coarse scale maps. Looking at the zoomed image of the Extended-LITFASS domain $(49 \times 49 \mathrm{km}^2)$ the contrast between forest in the west and farmland in the east of the LITFASS domain is visible in the land-use map and nearly all other derived parameter maps. The topography in the domain is quite flat and thus no great impact on the local weather can be expected.

3.3 Soil moisture analysis

The sensitivity study at the beginning of this chapter demonstrated that accurate soil moisture (SM) analysis data is essential to simulate latent and sensible heat fluxes realistically. Generating such an analysis is a very challenging data assimilation task because area averaged SM contents are hardly measurable. In situ measurements are only representative for an area of some square meters, whereas satellite retrievals give only information on regional scales in the order of 50 km due to large footprints of microwave radiometers (e.g. Jackson and Hsu, 2001). Additionally, these retrievals are limited to the upper 10 cm of the soil due to the small penetration depth of microwave radiation.

Therefore, any data assimilation system for SM at NWP scales depends strongly on the background field, which is simply the model prediction of SM. Variational algorithms may be implemented to incorporate indirect observations like temperature and humidity at 2 m height in an analysis scheme as proposed by Mahfouf (1991): These algorithms search those SM values that minimise the prediction errors of 2 m values at the preceding day. Such an algorithm (Hess, 2001) is currently used by DWD to produce SM analyses for operational purposes. However, variational methods have two drawbacks: If the SM field is updated by the fully coupled atmospheric-soil model, all atmospheric variables influencing the SM evolution, especially rain rates, are model variables with errors due to model shortcomings and limited predictability. Secondly, the variational SM assimilation may introduce additional errors in analysed SM because not all errors in predicted variables at the 2 m level are caused by poor SM data (see Seuffert et al. (2004) for the potential of similar problems in the ECMWF assimilation scheme).

As an alternative, SM analysis can be retrieved from soil module integrations which are completely driven by measured data. Such measurement driven soil moisture analysis schemes (MSMA) have recently been applied successfully on continental scales (Mitchell et al., 2004) as well as on the mesoscale (Trier et al., 2004). The MSMA scheme presented in the following is based on TERRA stand-alone integrations.

Two factors are determining the quality of any MSMA scheme: quality of the model formulation and accuracy of the forcing data. The first issue can be tested by point integrations at a single measuring station, where all forcing variables as well as the SM evolution are known. Fig. 3.4 presents the result of such an integration (MSMA_lind) at the GM Falkenberg site for the year 2003. Modelled and measured top level SM coincide very well. Deep SM is also in good agreement except an underestimation by the model in autumn and winter at the end of the year. This error is likely due to the neglect of ground water uptake in the model (see Sections 2.2.1 and 2.3.2). Anyway, this test demonstrates that an MSMA based on TERRA has a good potential to provide realistic SM analyses.

The second ingredient of a MSMA scheme, which should deliver areal SM estimates, is areal forcing data. Especially high quality maps of precipitation rate are
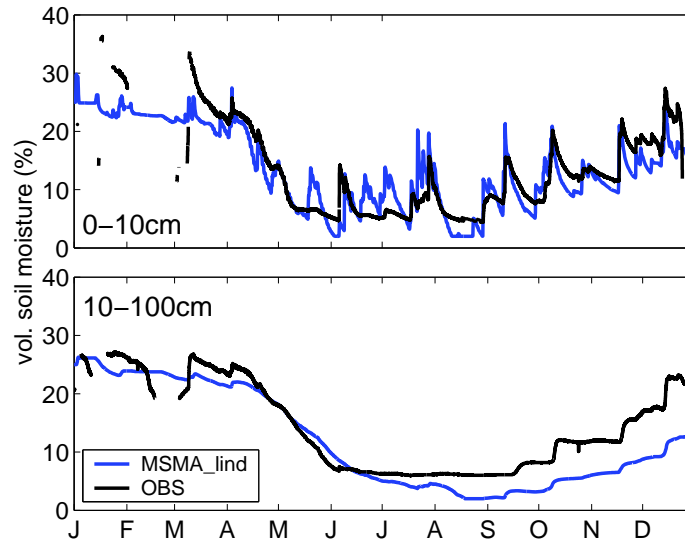
Figure 3.4: Observed soil moisture during 2003 at the GM Falkenberg site (OBS) and simulated by a single point integration of TERRA stand-alone (MSMA_lind) driven by local measurements.

essential because precipitation has usually the largest influence on SM and can be very variable in space. A network of four rain gauges in the LITFASS domain was available in the years 2001 and 2002. This network became denser by 6 additional stations in the year 2003 (see all sites in Fig. 3.5 b,c) and during LITFASS-2003 radar observations at 1 km resolution from the DWD radar Berlin are used.

A simplified optimal interpolation method is applied to interpolate the rain gauge information in space: Fig. 3.5a shows the spatial autocorrelation of rain gauge measurements estimated from the network of ten sites during the first half year of 2003. It can be seen, that longer averaging intervals result in larger autocorrelation. An averaging interval of 30 min was chosen as a compromise between large spatial representativeness and high temporal precision required by the soil model to simulate infiltration processes realistically. The spatial representativeness limits the domain size of the MSMA, because rain gauge measurements cannot be extrapolated too far. Therefore, the MSMA is only performed for the so-called Extended-LITFASS domain covering an area of $49 \times 49 \, km^2$ centred over the LITFASS area. The rain rate at an analysis point is estimated by an average of all rain gauge information weighted by their spatial autocorrelation at the given distance between observation and analysis point. This method is equivalent to an optimal interpolation scheme (minimum error variance estimator, e.g. Daley, 1991) if no background field is available and the redundancy among the gauge measurements does not differ significantly. The second assumption is well justified since the rain gauge stations are distributed quite evenly.

The analysed field based on rain gauge observations (Fig. 3.5b) gives the right mean value, but is clearly too smooth. Precipitation during LITFASS-2003 was dominated by a few strong convective events. The interpolation algorithm which
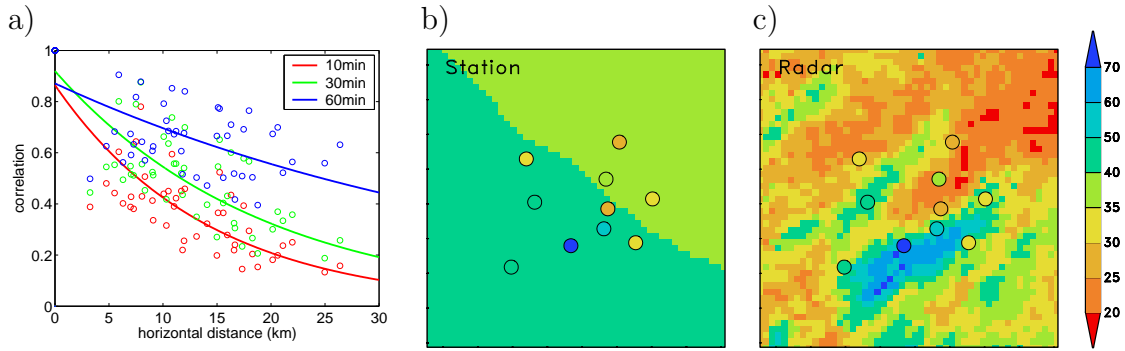
Figure 3.5: a) Spatial correlation of precipitation rates estimated from measurements of ten rain gauges within the LITFASS domain during the first half year of 2003. b) Spatial distribution of accumulated precipitation (Extended-LITFASS domain of $49 \times 49 \, \text{km}^2$) during LITFASS-2003 interpolated from rain gauge measurements. c) same as b), but derived from radar observations. Coloured circles indicate values of local rain gauge measurements.

was calibrated in terms of autocorrelation for the first half year of 2003 with more stratiform rain events cannot reveal these convective structures. Under these conditions it is advantageous to use radar observations, which can capture the spatial structure very well (see Fig. 3.5c). The conversion from radar reflectivity to precipitation rate is performed by a quantile matching calibration: Reflectivity classes are calibrated in a way that the frequency distribution of radar derived rain rates and colocated rain gauge measurements are similar. All forcing variables other than precipitation are prescribed homogeneously by the measurement at the GM Falkenberg. The impact of this simplification will be discussed at the end of this section.

Any MSMA needs information about the initial SM conditions. Usually integrations are started in winter time assuming SM saturation. But SM, in particular at deeper soil levels, varies only slowly and may depend over a long time range on the initial conditions. Long time integrations are the only way to minimise the impact of uncertain initial conditions on MSMA results. Therefore, all integrations of this study start at 1 January 2001, which is roughly 2.5 years before the period of interest.

The need for a long spin up phase is demonstrated by the time series of the modelled LITFASS-domain averaged SM content (Fig. 3.6). Although the SM approaches field capacity in winter, this level is not always reached. In particular the deep SM seems to be in balance with slightly drier values in winter time. The SM of the deep soil layer additionally stores information about the interannual variability and its value at the end of each year is related to the total precipitation amount during the year: The year 2002 was quite wet with 700 mm accumulated precipitation followed by 2001 with 544 mm and finally 2003 was extraordinarily dry with only 376 mm. This compares qualitatively with the wintertime deep SM (Fig. 3.6).

Beside the above mentioned adaptations to the model balance, the MSMA multi-year integration shows no dubious trends. This is an important feature of a realistic
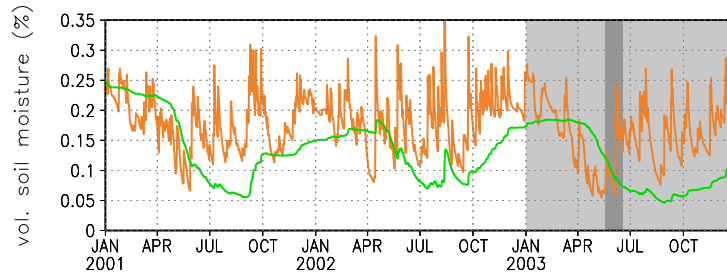
Figure 3.6: Time Series of LITFASS domain averaged soil moisture calculated by a 3-year
TERRA stand-alone integration including all model improvements (top level
soil moisture (0-10 cm), orange line; deep soil moisture (10-100 cm), green
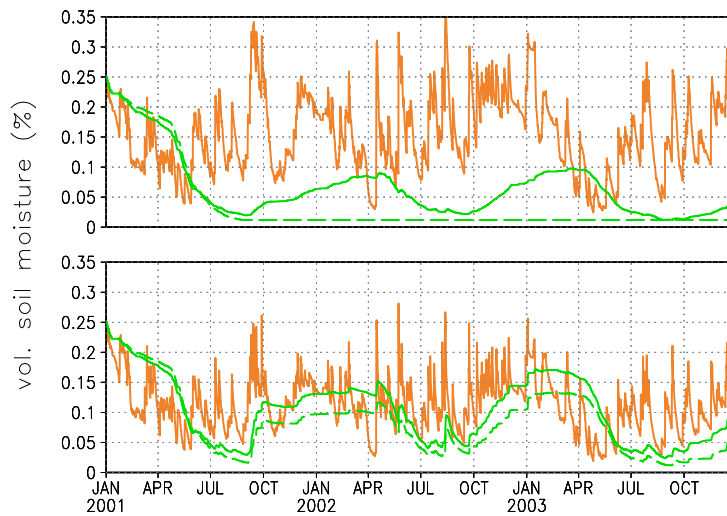line).

Figure 3.7: Top panel: TERRA stand-alone integration with standard drainage calcula-
tion at a forest grid-pixel (top level soil moisture (0-10 cm), orange line; deep
soil moisture (10-100 cm), green line). Bottom: same as top, but with an
up-stream scheme for drainage. Omitting soil moisture diffusion leads to a
deep soil moisture following the green dashed line.

SVAT model and an important prerequisite for MSMA applications. The standard
TERRA of DWD without improved formulation of drainage (see Section 2.3.2) does
not fulfil this requirement: Fig. 3.7 shows a three year integration of TERRA stand-
alone at a grid-box covered with forest using the operational upstream formulation
of drainage. The operational formulation results in a strong drying of the deep
soil layer, whereas the top level remains temporarily rather wet. Trees withdraw
a lot of water from the deep soil layer during spring of the first year, which leads
to very low drainage rates according to the operational drainage formulation. Both
layers become decoupled with respect to drainage and the deep soil layer cannot be
refilled by draining rain water. Only vertical diffusion slightly refills this layer (see
dashed curve), which is not very realistic; usually diffusion of soil water is an upward
directed process to rise water from deep wet layers. The unrealistic decoupling is
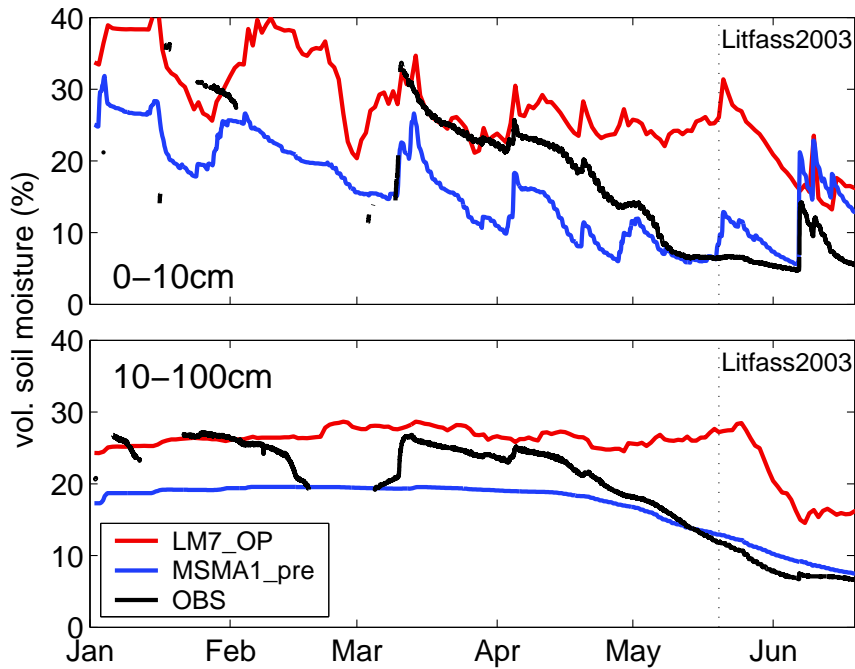removed by the upstream formulation of drainage (Fig. 3.7, lower panel).

Figure 3.8: Temporal evolution of LITFASS domain averaged soil moisture during the first half year of 2003: observations at the GM Falkenberg site (OBS), operational LM analysis (LM7_OP) of DWD and MSMA (MSMA1_pre) results.

In the framework of MSMA integrations, all TERRA settings have been chosen to match the configurations of the experimental runs as close as possible. These LM simulations have been performed with various surface descriptions in order to investigate heterogeneity effects. For each of these descriptions, an individual MSMA has been created to ensure balanced initial conditions with respect to SM. The most important MSMA integrations are an analysis with 1 km horizontal resolution (MSMA1), a coarse scale analysis with 7 km resolution (MSMA7) and an analysis with a tile representation of the surface for 7 km grid-boxes (MSMA7_tile). Each of these analyses consists of a 2.5 year prerun (e.g. MSMA1_pre) which is driven by interpolated rain gauge data followed by a run for the LITFASS-2003 period which is driven by radar based precipitation estimates.

Fig. 3.8 shows a comparison of SM observations at GM-Falkenberg with LITFASS-domain averaged SM of the operational analysis of DWD together with the results of MSMA1_pre. In wintertime and in early spring until April, MSMA results are too dry, which again supports the earlier hypothesis that the model balance tend to too dry SM during winter. This deficiencies may be removed by revising the lower boundary condition and e.g. considering ground water uptake. Nonetheless, it is obvious that the MSMA can describe the drying out throughout spring 2003 much more realistically than the operational analysis of DWD. Consequently, MSMA gives reasonable dry SM values during the LITFASS-2003 period, whereas the soil is almost saturated in the operational analysis of DWD. Measurements and MSMA do not agree as well as in the pointwise MSMA integration displayed in Fig. 3.4.
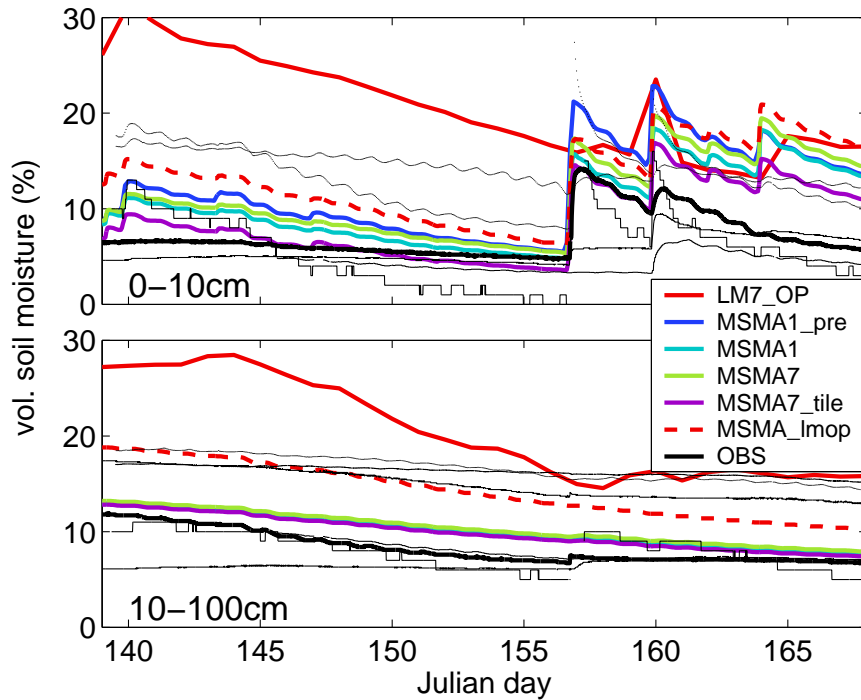
Figure 3.9: Same as Fig. 3.8, but only for the LITFASS-2003 period and additionally in comparison to observations at various LITFASS-2003 energy balance stations (thin, black lines) and results of MSMA using radar data with various surface representation: 1 km grid spacing (MSMA1); 7 km grid spacing (MSMA7); tile representation with 7 km resolution (MSMA7_tile); operational 7 km surface parameters (MSMA_lmop).

This discrepancy indicates that an exact quantitative verification of modelled area averaged SM values with point measurements is difficult.

More insight into the details during LITFASS-2003 is given by Fig. 3.9. This plot additionally presents the SM observations which have been conducted at LITFASS-2003 energy balance stations and the results of MSMA integrations based on radar observations with different surface descriptions. Obviously, Radar observations allow more accurate estimates of the areal precipitation: MSMA1 using radar data is less overestimating the response in top level SM to rain events than MSMA1_pre based on rain gauge data (Fig. 3.9). The differences between MSMA runs with different surface representation are small, but visible; they prove that the balanced model state with respect to SM is not independent from the surface description. A part of the improvements compared to the operational SM may be attributed to the improved surface parameters and model improvements. The effect of the MSMA method itself can be inspected by looking at the result of the MSMA_lmop integration, which is a 7 km MSMA run with all settings and surface parameters similar to the operational LM version. This run resembles the other MSMA runs more than the operational SM analysis and demonstrates that most of the analysis improvement is due to the MSMA concept.
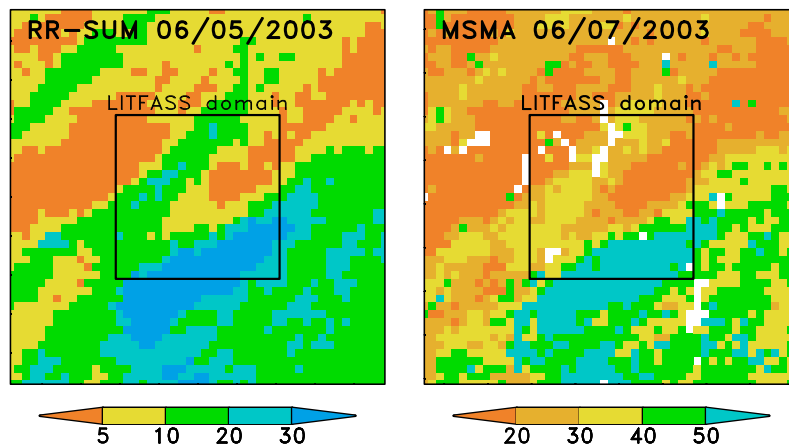
Figure 3.10: Accumulated rain fall (in mm) at 5 June 2003 (left) and the resulting top level soil moisture (in vol. %) distribution (right) two days later in the surrounding of the LITFASS domain.

The MSMA scheme also provides more reasonable estimates of the spatial SM distribution. Fig. 3.10 shows the response of the top level SM to the convective rain event at 5 June 2003. No precipitation occurred for two weeks prior this event and therefore the soil dried out very homogeneously. The convective rain event exhibited large variations in precipitation amount. This heterogenous precipitation pattern is clearly reflected by the SM distribution two days later. Note, that assimilating radar data is the only method to capture rain induced SM patterns reasonably because modelled precipitation rates will always exhibit positioning errors and ground based in situ measuring networks will be too coarse to resolve convective structures.

The general idea of the MSMA concept is to model SM dynamics in a physical consistent manner. Not only the SM evolution should agree with measurements, but also other prognostic quantities like e.g. the fluxes between surface and atmosphere. A comparison of daytime fluxes modelled by MSMA1 and observed above three different surface types is presented in Fig. 3.11. TERRA stand-alone can distinguish the different flux conditions above these surfaces. The temporal evolution of partitioning latent and sensible heat flux is well represented, too. Biases of the model with respect to observations are always positive, that means the sum of the modelled turbulent fluxes is larger than measured. This is again an artefact due to the non-closure of the measured energy balance.

Despite all these promising results, it is important to mention, that TERRA stand-alone integrations may differ from integrations of the full LM system, which couples TERRA to the atmospheric model (see Fig. 3.12). At 7 June 2003, large differences in predicted fluxes occur due to the variations of SM (see Fig. 3.10) in combination with the homogeneously prescribed atmospheric conditions in the TERRA stand-alone simulation: The prescribed measurements are taken from GM-Falkenberg, which is located in the dry part of the domain. The sensible heat flux and the temperature at 2 m height are consequently comparatively high there,
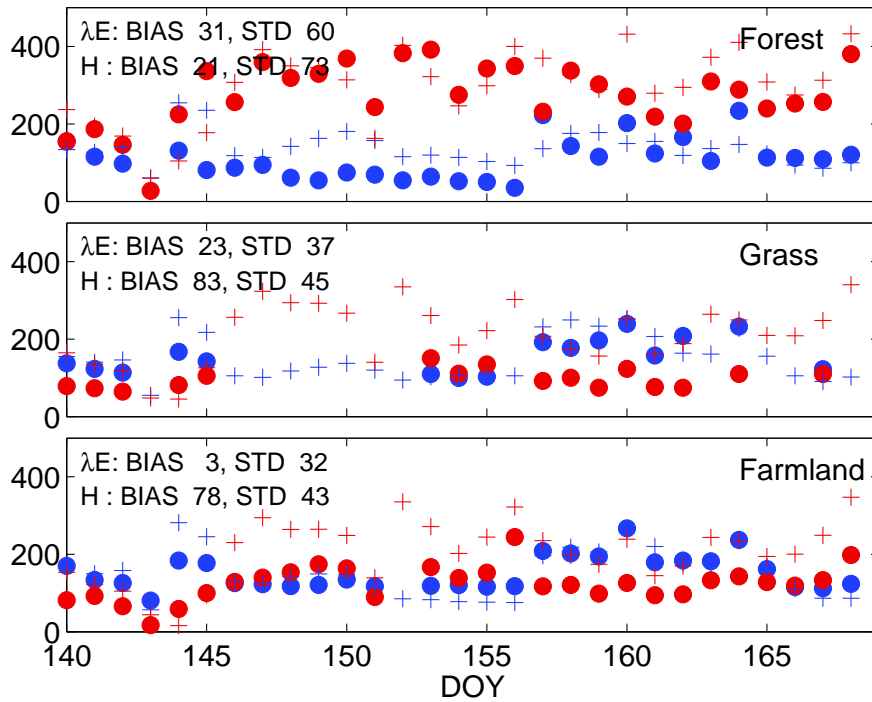
Figure 3.11: Daytime (10-14 UTC) averages of sensible (red) and latent (blue) heat fluxes over different types of land-surface. Simulation results from MSMA1 integration are marked by crosses and measurements by solid circles.

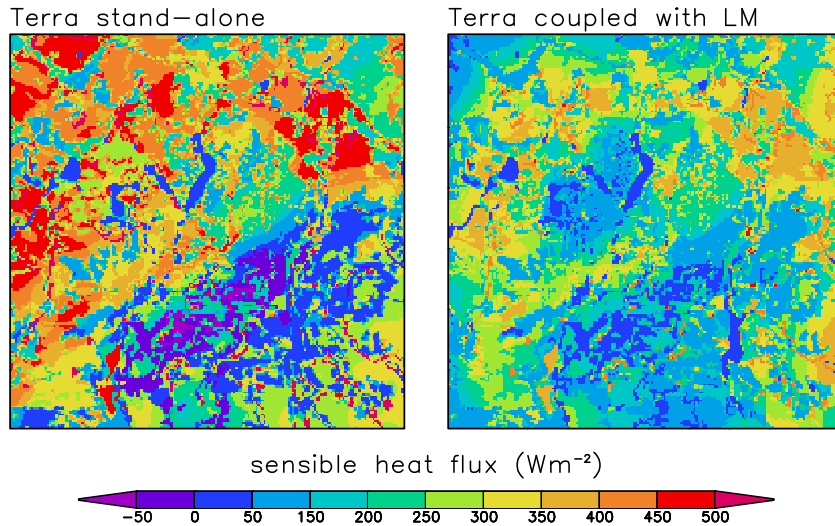Figure 3.12: Modelled sensible heat flux at 7 June 2003, 12 UTC within the Extended-LITFASS domain (area of 49x49km², centred over the LITFASS domain). Surface parameters and soil moisture are similar in both integrations. The TERRA stand-alone integration (left) are driven by homogeneously prescribed atmospheric forcings, whereas surface and atmosphere are dynamically coupled in the LM integration (right).

whereas the surface remains rather cool at areas with high SM. If these low surface values are combined with the high 2m-temperature forcing values observed at GM-Falkenberg, even negative sensible heat fluxes may be diagnosed. This effect explains the large variability in modelled fluxes of the TERRA stand-alone. Under such conditions it is favourable to use a coupled soil atmosphere model, which can adapt the atmospheric state variables at reference height to local flux conditions. Margulis and Entekhabi (2001) present a comprehensive analysis of the errors which may arise from uncoupled simulations. Averaged over longer periods, such errors tend to cancel each other. Therefore, MSMA is less affected, but studies analysing flux predictions at certain cases should always use a coupled model.

3.4 Model configuration

The main objective of this study is to improve model predicted fluxes over heterogenous land-surfaces. To this goal, model simulations with various heterogeneity parameterisations are evaluated by comparisons to both observations and high resolution model results. Such comparisons are only usefull if the model simulation fulfil three constraints: At first, the simulations must be as realistic as possible to mimic the real situations. Secondly, the model needs enough degrees of freedom to simulate all interactions between surface and atmosphere without artifical forcings from boundary or initial conditions. Finally, the setup of all model integrations should be as similar as possible except for the model formulation of interest. Otherwise differences between the model integration cannot be definitely ascribed to the investigated process. This section will describe how model domain, assimilation cycle and model configuration have been chosen to fulfil these requirements as good as possible.

From a scientific point of view, large model domains are favourable. Under these conditions, the model can evolve freely in the interior of the domain without any unphysical forcings due to poor boundary conditions. But in practice, the domain size is limited by the computer resources. The following convergence test addresses the issue of choosing an appropriate domain size: The edge size of integration domains has been varied between 140 km and 490 km for two case studies and the predicted latent heat flux in the LITFASS-domain, which is situated in the centre of all domains, is analysed (Fig. 3.13). It is evident from the results of the first day (Fig. 3.13, left) that convergence can be found at edge sizes equal or larger than 350 km. At that day, the surrounding air, which is introduced via the lateral boundaries, is slightly drier than the air mass in the interior, which is in balance with the surface fluxes and local boundary layer development. This perturbation may propagate by diffusion and advection to the centre of the domain and causes increased latent heat fluxes there. Such simple boundary effects are avoided by selecting a sufficiently large domain. If nonlinear atmospheric effects become important, boundary effects
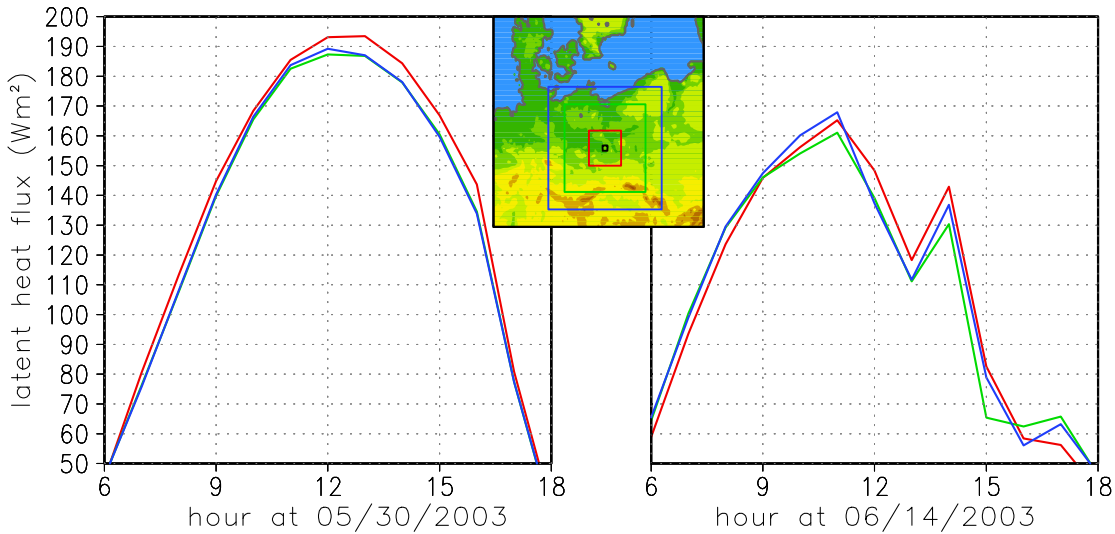
Figure 3.13: LITFASS domain (black square) averaged latent heat flux predicted by the LM simulations for two cases (30 May and 14 June 2003) with 7 km horizontal resolution using three different domain sizes: $140 \times 140 \, km^2$ (red), $350 \times 350 \, km^2$ (green) and $490 \times 490 \, km^2$ (blue).

are more difficult to handle: The second case (see Fig. 3.13, right) was a cloudy day. Due to the nonlinearities in cloud processes and surface-atmosphere interactions, small differences in boundary conditions may result in significant deviations of fluxes in the interior of the domain at all domain sizes.

The most effective method to suppress such unwanted boundary effects is to use equal boundary conditions for all model runs. This rule has two implications: At first, the same domains should be used for all integrations that are analysed simultaneously. Secondly, as far as runs at different horizontal resolutions are concerned, the decrease of the nudging coefficient in the boundary zone must depend on the geometrical distance from the boundary and not on the number of grid-boxes as originally proposed by Davies (1976). Consequently, the original formulation of Davies is only applied at the coarsest scale and the boundary zone at higher resolutions is adequately extended.

The first implication narrows the range of horizontal resolution scales which can be investigated at the same time: If one domain is used for all resolutions, it must be large enough to allow the model to develop its own dynamics at the coarsest resolution. But the domain should still be small enough to allow integrations at the highest resolution from the point of view of computational costs. The following three scales have been selected to be investigated in this study: the 21 km scale, which resembles approximately the grid-box size of todays high resolution regional climate models; the scale of 7 km, which is the grid spacing of todays mesoscale weather forecasting models, and finally the 1km scale, which is fine enough to resolve most of the heterogeneity which are relevant for the atmosphere (Heinemann and Kerschgens, 2005). Integrations with 1 km and 21 km grid spacing at the same
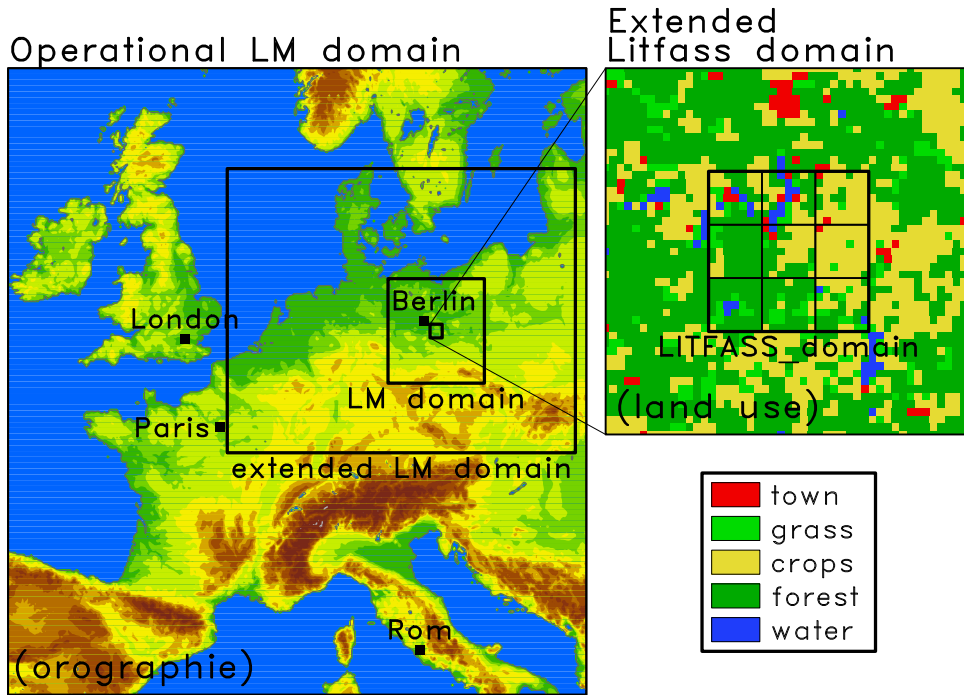
Figure 3.14: Domains: Measurements are available at the Litfass domain ($20\text{x}20\text{km}^2$); soil moisture analyses are calculated at the Extended-LITFASS domain ($49\text{x}49\text{km}^2$); LM runs with 1 and 7 km atmospheric grid spacing are performed at the LM domain ($385\text{x}385\text{km}^2$); the LM with grid spacings of 7 and 21 km is integrated at the Extended-LM domain ($1386\text{x}1050\text{km}^2$).

domain are not feasible: Either the domain is too large for high resolution runs or the domain is too small to allow the model a free evolution at a coarse grid spacing. Consequently, the considered scale range is splitted into the two intervals from 1-7 km and 7-21 km.

Integrations as well as evaluation is performed separately for both scale intervals using appropriate model domains: A set of runs with atmospheric resolutions of 7 km and 1 km have been calculated at the LM domain (see Fig. 3.14), which covers an area of 385 km x 385 km and is centred over the LITFASS domain. A larger domain, the Extended-LM domain, is used for a set of runs with atmospheric grid spacing of 21 km and 7 km. The Extended-LM domain has a size of 1386 km x 1050 km and is slightly shifted to north-west in order to fit into the operational LM domain and in order to position the southerly boundary not over alpine mountain ridges.

The partly contradicting constraints of realistic and free model evolution have been considered by implementing the following assimilation cycle, which is schematically depicted by Fig. 3.15: LM runs are performed for only 24 hours and then reinitialised by analysis data at midnight. This configuration enables the model to simulate the boundary layer development throughout a day freely, but prevents that errors in this prediction can affect the simulations at the next day. The central tool

Figure 3.15: Assimilation cycle of LM integrations performed in this study.

in this assimilation cycle is LM2LM, a interpolation program especially developed by the author for this study. LM2LM can transform input data from arbitrary input grids to the model grid and is able to combine maps with different resolution and size. Information about the atmospheric state for initial and boundary conditions are exclusively taken from the operational LM analysis of DWD. This analysis is produced by a nudging scheme, which is a continuous LM integration that is nudged by artificial source terms towards observations (Schraff and Hess, 2003). Compared to intermittent analysis schemes, nudging disturbs the model balance only slightly and thus LM runs initialised with this analysis have little spin-up problems. LM analyses are available every hour at 7 km resolution for the operational LM domain. LM2LM interpolates this information on the model grid by subdividing each level of the source grid into triangles, by a subsequent linear horizontal interpolation within each triangle and finally by a linear vertical interpolation. This simple interpolation scheme does not introduce any artificial variance at fine scales and has already successfully applied for other studies (Ament et al., 2004; van Lipzig et al., 2006).

All prognostic surface and soil variables except soil moisture are also interpolated from LM analysis data alone. To avoid artificial sharp gradients a quadratic function fitting technique is locally applied for interpolation. Soil temperature is only prescribed at the first day of the integration period and then taken over from the prediction at the end of the previous day. It is important to simulate soil temper-
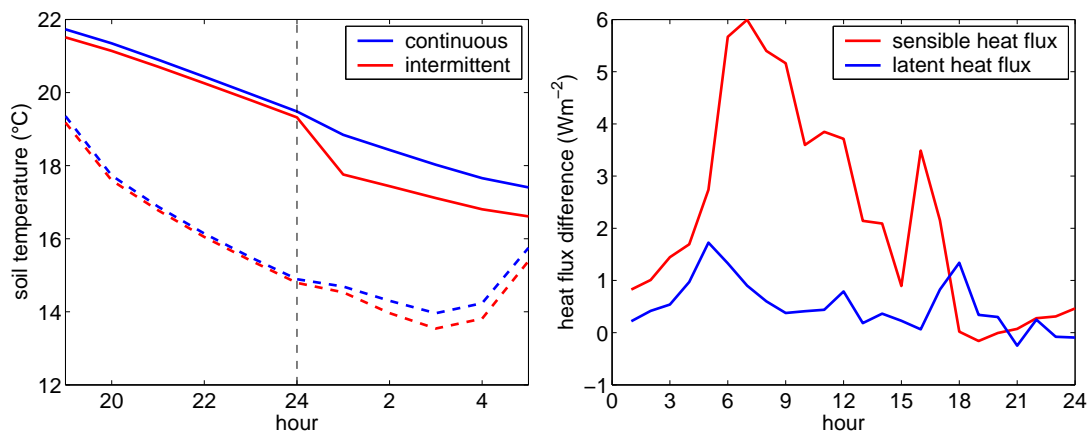
Figure 3.16: Left: Nighttime evolution of soil temperature at the surface (solid) and at 10 cm depth (dashed) with and without intermittent assimilation of soil temperatures. Right: Deviation of simulated surface fluxes using intermittent assimilation with respect to integrations using continuous soil temperatures. Both plots are averages over the whole LITFASS-2003 period at a single grid point within the LITFASS domain.

ature continously because adapting the soil temperature can be interpreted as an unphysical energy flux at the surface which violates the closure of the surface energy balance. Fig. 3.16 demonstrates the systematic drops in soil temperature of an intermittent soil temperature assimilation cycle and the resulting errors in surface fluxes.

Initial soil moisture values are provided by the MSMA for the Extended-LITFASS domain and by the LM analysis for the whole domain. LM analysis data must be interpolated spatially and both data sets have to be merged. Volumetric soil moisture is not a suitable quantity for interpolation and merging since it is also a function of soil type: The dynamic range of volumetric soil moisture is confined by the air dryness point and the pore volume, which vary among different soil types. In short, volumetric soil moisture needs to be scaled appropriately before interpolation and merging. From a meteorological point of view, soil moisture has the main function to control evapotranspiration. Accordingly, the scaled SM should describe the evapotranspiration regime with respect to soil moisture stress independently from the soil type.

TERRA stand-alone integrations for a single pixel and prescribed LITFASS-2003 weather conditions have been performed to check various scaling techniques. Soil moisture is kept constant throughout each integration. In addition to the pore volume scaling (PORV) which is operationally used by DWD, a scaling by pore volume and air dryness point (PORV-ADP) and a scaling by field capacity and
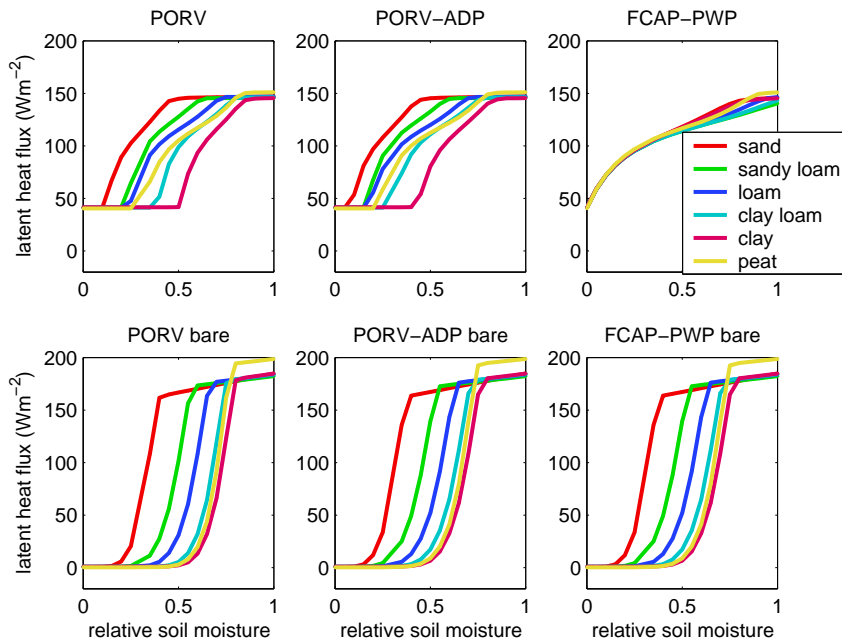
Figure 3.17: Relation between mean latent heat flux and relative soil moisture η_{rel} calculated for various soil types. Three different definitions of η_{rel} (see text) have been applied. Top row shows results of a TERRA stand-alone integration driven by LITFASS-2003 weather conditions at a pixel, which is totally covered by vegetation. Bottom row: same as top, but for a bare soil pixel.

permanent wilting point (FCAP-PWP) have been tested:

$$\text{PORV} \quad : \quad \eta_{rel} = \frac{\eta}{\eta_{PV}} \tag{3.1}$$

$$\text{PORV-ADP} \quad : \quad \eta_{rel} = \frac{\eta - \eta_{ADP}}{\eta_{PV} - \eta_{ADP}} \tag{3.2}$$

$$\text{FCAP-PWP} \quad : \quad \eta_{rel} = \frac{\eta - \eta_{PWP}}{\eta_{FCAP} - \eta_{PWP}} \tag{3.3}$$

Fig. 3.17 shows the average latent heat flux for all scaling techniques and soil types. For pixels fully covered by vegetation, the scaling by field capacity and permanent wilting point is by far the best choice. No scaling is successful, however, at bare soil pixels because bare soil evaporation is a nonlinear function of both top-level and deep soil moisture (see also Fig. 2.7). Fortunately, this problem is not very relevant in the framework of LITFASS-2003 because most of the grid points are densely vegetated. The scaling by field capacity and permanent wilting point will be applied in the following.

Soil moisture for the Extended-LITFASS domain is directly adopted from the MSMA. Outside this area, it is assumed that the operational soil moisture analysis represents the correct spatial structure, but might exhibit a bias. The bias is estimated by comparing the results of MSMA with the operational soil moisture analysis in the overlap area; the bias is then corrected additively for the whole
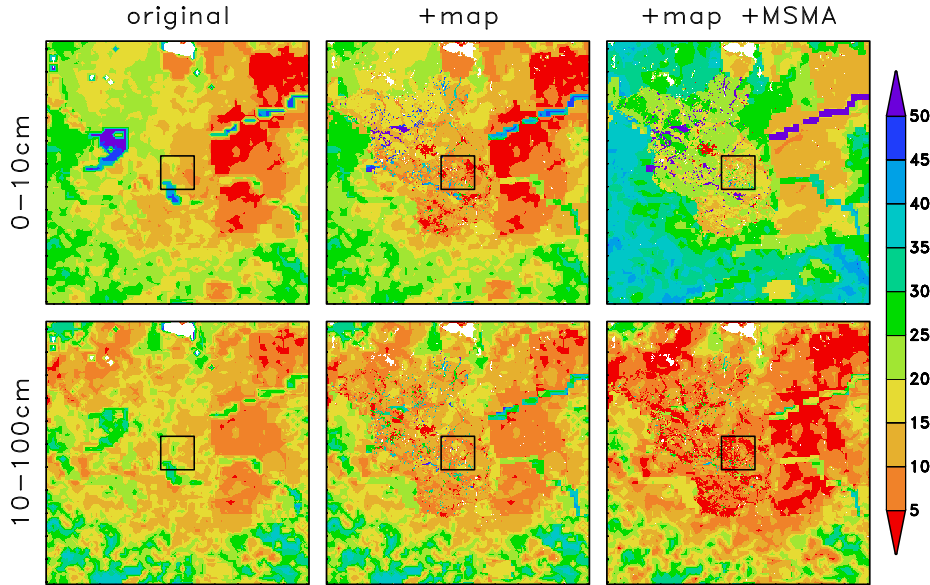
Figure 3.18: Merging of volumetric soil moisture analysis (LM domain, 13 June 2003). Left column shows the original soil moisture analysis of DWD, which is adapted to the new soil map by scaling with field capacity and permanent wilting point (middle column) and finally merged with MSMA results (right). The black square denotes the Extended-LITFASS domain.

external domain. Fig. 3.18 presents an example of this interpolation and merging procedure. The left column shows the LM analysis interpolated on a 1km grid. This field is scaled to account for the new soil type map at the second column and the right column shows the final product with inserted MSMA data at the centre and bias correction outside. The soil moisture regime provided by MSMA data differs from those of operational analysis - essentially to be in balance with the modified parametrisation (e.g. no artificial reduction evaporation depending on root depth, drainage formulation). Thus the adaptions in the last step of the merging are in general large.

Beside the domain and the assimilation cycle, the model configuration is as close as possible to the operational settings during LITFASS-2003. This means in particular, that 35 vertical layers were used with the thinnest layer of 66 m depth next to the surface. Prognostic cloud ice scheme and prognostic advection of precipitation are not used. However, the following settings differ from the operational pratice:

- The transfer scheme of Louis is switched on instead of the TKE scheme because the Louis scheme is the only well documented scheme that is implemented into the LM. Consequently, only this scheme could be modified to be operated with mosaic or tile approach.

- The moist convection scheme is switched off for high resolution runs with 1 km grid spacing, since these runs almost resolve deep convection (e.g. Weisman et al., 1997).

Table 3.1: Overview of major model runs that will be analysed in this study.

Operational domain (2275x2275km²) no MSMA, no model improvements	
	LM_OP
integration period	LITFASS-2003
Resolution of Atmosphere	7 km
Resolution of surface fluxes	7 km
Resolution of soil	7 km

LM domain (385x385km²) with MSMA data and model improvements						
	LM7	**LM7_ DOM**	**LM7_ MOS1**	**LM7_ TILE**	**LM7_ MOS1_ hsoil**	**LM7_ TILE_ hsoil**	**LM1**
integration period	LITFASS-2003	LITFASS-2003	LITFASS-2003	LITFASS-2003	LITFASS-2003	LITFASS-2003	golden days
Resolution of Atmosphere	7 km	7 km	7 km	7 km	7 km	7 km	1 km
Resolution of surface fluxes	7 km	7 km	1 km	7 km 8 classes	1 km	7 km 8 classes	1 km
Resolution of soil	7 km	7 km	1 km	7 km 8 classes	7 km	7 km	1 km

Extended-LM domain (1386x1050km²) with MSMA data and model improvements						
	LMe21	**LMe21_ MOS7**	**LMe21_ MOS1**	**LMe21 TILE**	**LMe7**	**LMe7_ MOS1**	**LMe7_ TILE**
integration period	golden days	golden days	golden days	golden days	golden days	golden days	golden days
Resolution of Atmosphere	21 km	21 km	21 km	21 km	7 km	7 km	7 km
Resolution of surface fluxes	21 km	7 km	1 km	21 km 8 classes	7 km	1 km	7 km 8 classes
Resolution of soil	21 km	7 km	1 km	21 km 8 classes	7 km	1 km	7 km 8 classes

- All model improvements mentioned in Section 2.3 are utilised: assimilation of lake surface temperature, fixed coding errors, upstream drainage formulation, land-use dependent vegetation albedo and stomatal resistance parameters.

- The update interval of the radiative fluxes was decreased from 1 hour to 15 min in order to model cloud-radiation interactions more accurately.

Tab. 3.1 gives an overview of the major runs that will be analysed in the following two chapters to investigate the exchange processes over heterogeneous land-surfaces and their implications for weather prediction. Data from the operational model integration (LM_OP) has been retrieved from the data base of DWD; all other runs have been performed especially for the purposes of this study. The runs differ with respect to the model domain (LM domain 'LM'; Extended-LM domain 'LMe'), their atmospheric resolution (given in kilometres by the number following the domain identifier) and their surface representation. The standard parameterisation of surface

heterogeneity are effective parameters (names without an appendix). Non-standard schemes are: dominant land-use parameters ('DOM'), mosaic approach ('MOSx', with surface grid resolution of x kilometres) and the tile approach ('TILE') with 8 land-use classes (defined by look-up table in Appendix B plus a seperate class 'water'). The last two methods have also been investigated in a simplified version with homogeneous soil conditions ('hsoil'). Most of these integrations cover the whole LITFASS-2003 period. Due to limited computer resources the LMe and the LM1 runs have only been calculated for the nine golden days (defined in Section 2.1 by Figure 2.2).

3.5 Main results

The primary goal of this chapter was to describe the preparation of model experiments and not to obtain scientific results. Nonetheless, shortcomings in the design of the model experiment may result in misleading conclusion. Therefore, it is worthwhile to identify key issue in the setup of model runs:

- Soil moisture turned out to be a parameter, which has a great impact on the partitioning between latent and sensible heat flux and consequently good initial conditions of soil moisture analysis are essential. Integrations of the SVAT scheme of LM (TERRA stand-alone) completely driven by observations provide more accurate soil moisture analyses during LITFASS-2003 than the operational, variational scheme of DWD. This measurement driven soil moisture analysis (MSMA) allows additionally for a precise response of soil moisture content on precipitation in space and time. One-dimensional integrations at GM-Falkenberg driven by local measurements demonstrated that TERRA stand-alone can predict the soil moisture evolution very well, if accurate forcing data is provided. The parameterisation of drainage had to be revised in order to avoid unrealistic trends in long-term runs.

- The configuration of model experiments likely influences the prediction of surface fluxes. A careful design of the experiment is essential to ensure that differences between various model runs are exclusively attributed to changes in the representation of the surface. It is of great importance to use similar lateral boundary conditions (in particular similar model domains) and to scale soil moisture properly if the soil type is modified. Intermittent assimilation of soil temperature is not recommended because it may result in systematic deviations of surface fluxes.

4 Evaluation of modelled surface fluxes

In this chapter, the results of the model experiments (see Tab. 3.1) will be evaluated with respect to the surface fluxes during the LITFASS-2003 period. At first integrations using the effective parameter approach - the currently operational method - are verified by comparison with LITFASS-2003 measurements. The advanced parameterisations of land-surface heterogeneities, like mosaic and tile approach, implicitly make use of this technique because it is applied locally to calculate the fluxes at every sub-pixel. Accordingly, the first section has two objectives: At first, to investigate the effect of the model improvements (e.g. MSMA, improved model formulation; see Section 2.3) alone without advanced heterogeneity parameterisation, and secondly, to test whether the effective parameter approach can in principle reproduce the observed surface flux characteristics of various land-use types. Without this ability, the mosaic and the tile method cannot operate properly. The second section will compare runs with advanced heterogeneity parameterisations with LITFASS-2003 flux measurements. Although measurements are the most objective data source for any evaluation, the significance of such comparisons is always limited due to uncertainties of the measurements (e.g. non-closure of the energy balance; see Section 2.1) and the limited sample size. Therefore, high resolution LM runs with 1 km grid spacing will be used as a second reference data set. This model intercomparison will be discussed in the third section. Finally, the same high resolution model data will be utilised to justify the assumptions underlying mosaic and tile approach.

4.1 Verification of the effective parameter method

The LM with its operational configuration (LM_OP) overestimates evapotranspiration excessively during LITFASS-2003, as the time series of domain averaged latent heat flux (Fig. 4.1) indicates (BIAS for the whole period of $48\,\mathrm{Wm^{-2}}$). The simulation also fails to capture the dry-out phases before the rain event on Julian day 156 (5 June 2003) and at the end of the period. This is reflected by a high standard deviation (STD) of $53\,\mathrm{Wm^{-2}}$(based on hourly mean values). These failures are mainly caused by high soil moisture contents prescribed by the operational soil moisture analysis (see Section 3.3), which allows plants to evaporate at maximal rate without any soil moisture stress. In contrast, the LM7 integration, which makes use of improved model formulations (see Section 3.4) and of the more accurate MSMA soil
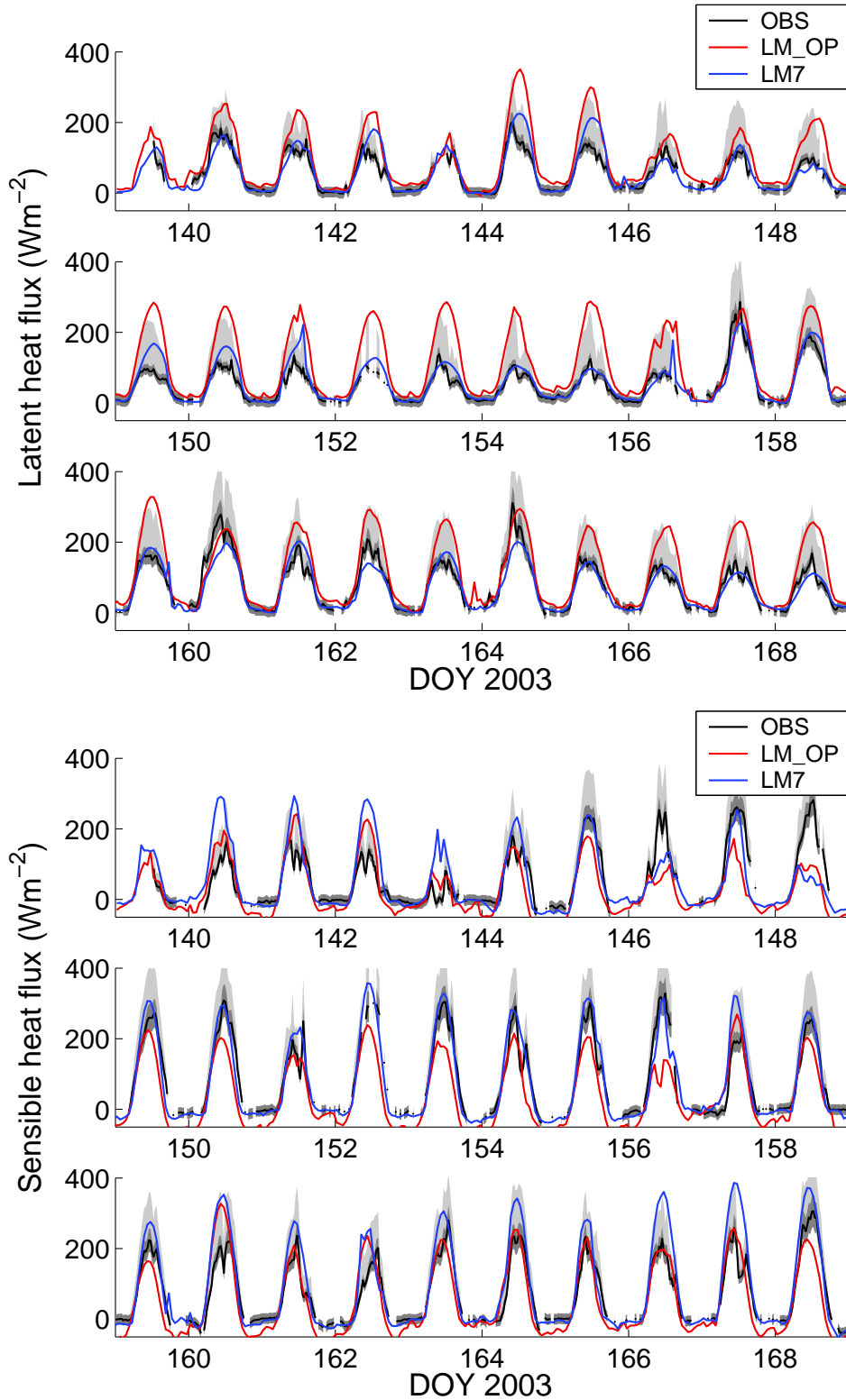
Figure 4.1: Time series of measured and modelled latent (top) and sensible heat flux (bottom) averaged over the LITFASS domain. The observational data (black line) is derived by compositing the measurements of ground based energy balance stations (Beyrich et al., 2006). The ranges of uncertainty due to random errors and the non-closure of the energy balance are shaded in dark and light grey, respectively.

Figure 4.2: Mean daily cycle (average of LITFASS-2003 period) of latent (left) and sensible heat flux (right). The dark and light grey shaded areas indicate the ranges of uncertainty due to random measuring errors and non-closure of the energy balance, respectively. See Tab. 3.1 for definitions of model runs.
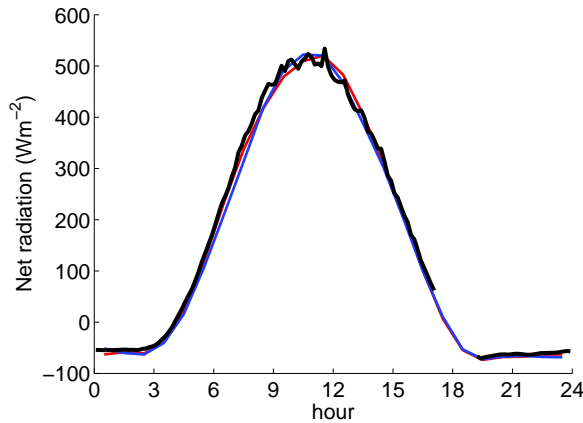

Figure 4.3: Same as Fig. 4.2, but for net radiation and restricted to LM_OP and LM7. Results of other simulations are almost identical to LM7. Error margins of the measurements are not available.

moisture analyses (see Section 3.3), are in very good agreement with the observed latent heat fluxes (BIAS of $2\,\mathrm{Wm^{-2}}$ and STD of $28\,\mathrm{Wm^{-2}}$). The improvement of LM7 compared to LM_OP is also revealed by inspecting the mean daily cycle of the latent heat flux (Fig. 4.2): The line of LM7 is always within the error margin of the observations, whereas LM_OP partly exceeds this range.

Concerning the sensible heat flux H_0, LM_OP tends to underestimate the flux (BIAS $-25\,\mathrm{Wm^{-2}}$). This is essentially a compensation of the large latent heat fluxes λE_0 because the modeled net radiation, which influences significantly the sum of $H_0 + \lambda E_0$, is in very good agreement with the observations (Fig. 4.3). LM7 gives systematically higher H_0 fluxes than observed (BIAS of $16\,\mathrm{Wm^{-2}}$), which are, however, well inside the error margin of the observations. This BIAS is acceptable
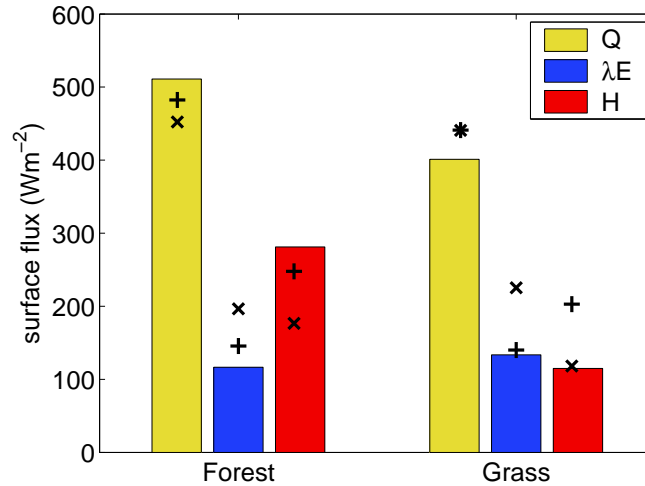
Figure 4.4: Averaged daytime (8-14 UTC) surface fluxes derived from measurements (bars), LM_OP (x) and LM7 (+) during LITFASS-2003. Observations are taken from the forest site HV and GM-Falkenberg (grass), respectively, and model results are retrieved from the corresponding model grid-boxes.

because due to the non-closure of the energy balance in the measurements any model, that fulfils energy conservation, must exhibit a positive bias either in λE_0 or H_0. Especially during night time, LM7 is in much better agreement with the observations than LM_OP, which can be attributed to the Louis transfer scheme. The operational scheme by Raschendorfer has a tendency to predict higher turbulent exchange during stable situations than the Louis scheme due to an additional source term in the turbulent kinetic energy equation, which accounts for generation of turbulent motion by subgrid-scale temperature inhomogeneities. Mironov and Raschendorfer (2001) demonstrate that this enhancement reduces negative biases of 2 m-temperature during nighttime. Nonetheless, during LITFASS-2003 and with respect to the flux predictions, the new source term is not beneficial.

During afternoon, the mean daily cycles of LM_OP and LM7 are outside the error margin of the measurements. This is caused by a phase shift in modelled sensible heat fluxes towards a too early daily maximum. The latent heat flux exhibits a phase shift in the opposite direction in both simulations. This model deficiency is common to all model runs - independently from the treatment of surface exchange processes. Appendix C presents some sensitivity tests concerning this issue and gives some indications that the simplified representation of the canopy layer at forests in the LM parameterisation might be responsible.

LM7 integrations do not only represent LITFASS domain averaged fluxes more accurately than LM_OP, but they are also superior as far as the spatial distribution is concerned (see Fig. 4.4). Over forest, LM_OP overestimates the latent heat flux excessively; this has been almost totally corrected by the model improvements implemented into LM7. The land-use dependent albedo of vegetation in LM7 leads to slightly larger net radiation values over forest, which is also in closer agreement to
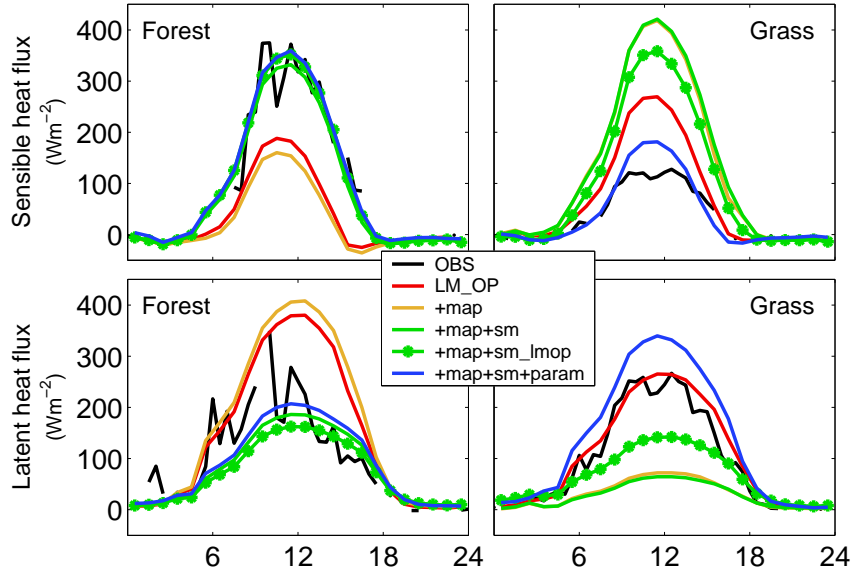
Figure 4.5: Modelled and observed surface fluxes during 13 June 2003 over two different land-surfaces. All model simulations are performed with 1km grid spacing, but different configurations: LM1_op is similar to LM_OP except the resolution; +map uses the improved surface parameter set; +map+sm and +map+sm_lmop are additionally initialised with MSMA1 and MSMA1_lmop soil moisture data, respectively; finally +map+sm+param is operated with improved parameterisation and is similar to LM1.

observations. Taking negative biases of flux measurements due to the non-closure effect into account, the results of both model versions over grass may be valid, and it is not possible to rank them. Note, that the modifications of LM7 in comparison to LM_OP alter the flux partitioning towards higher sensible and lower latent heat fluxes much stronger over forest than over grass. Consequently, the model improvements do not simply correct for an overall systematic error, but also change the spatial structure.

The improvements in LM7 cannot be attributed to one single modification; they are achieved in a combination of all enhancements. This is illustrated by a stepwise introduction of all model enhancements (Fig. 4.5). These investigations are based on high resolution simulation with 1 km grid spacing, because the land-surface contrasts can be resolved better at this resolution. Note, that a single correction, e.g. prescribing new surface parameters ("+map"), might even reduce the model performance. The importance of balanced soil moisture conditions is revealed by comparing two simulations without improved parameterisations: "+map+sm" (based on MSMA7) and "+map+sm_lmop" (based on MSMA_lmop). MSMA7 is more accurate than MSMA_lmop (Fig. 3.9), but was derived with improved parameterisations. In this respect, the soil moisture analysis (MSMA7) and the LM integration "+map+sm" are inconsistent. Although initial soil moisture conditions are more realistic, the inconsistent integration "+map+sm" gives worse results than the simulation ("+map+sm_lmop") with consistent, but less accurate MSMA data. This

Table 4.1: Evaluation of predicted latent/sensible heat fluxes using LITFASS-2003 mea-surements: Systematic error (BIAS) and standard deviation (STD) of the LIT-FASS mean flux time series (see also Fig. 4.1). The model performance to char-acterise the flux anomalies of one 7 km grid-box with respect to the LITFASS domain average is expressed by the mean absolute value of the systematic errors ($\overline{|\text{BIAS}|}$) within a grid-box and by the corresponding mean standard deviation ($\overline{\text{STD}}$). All values in Wm^{-2}; STD based on hourly mean values.

		LM_OP	LM7	LM7_DOM	LM7_MOS1	LM7_TILE	LM7_MOS1_hsoil	LM7_TILE_hsoil
LITFASS mean	BIAS	48/-25	2/16	10/10	8/5	12/0	12/1	14/-1
	STD	53/51	28/57	32/55	27/52	26/49	30/51	29/49
anomaly predic-tion (9-14 UTC)	$\overline{|\text{BIAS}|}$	61/55	24/24	19/18	21/20	20/21	20/25	22/25
	$\overline{\text{STD}}$	108/99	57/72	61/72	51/68	51/68	52/68	51/69

highlights again the importance of balanced initial soil moisture conditions. It might be better to operate a slightly wrong model with consistently wrong soil moisture data than using more realistic data.

4.2 Evaluation of heterogeneity parameterisations using observational data

The last section demonstrated that model integrations (LM7) with model improve-ments (like MSMA soil moisture data or land-use dependent vegetation parameters) reproduce the observation much better than the operational run (LM_OP). By these modifications, the LM is enabled to simulated the spatial flux distribution as well as temporal evolution during LITFASS-2003 successfully. Since this is a prerequisite for evaluating any heterogeneity parameterisation, these improvements are utilised by all runs with enhanced heterogeneity parameterisation, which will be compared to observations in the following.

4.2.1 Prediction of LITFASS domain averaged fluxes

The analysis is started by comparing runs at the LM domain with 7 km atmospheric resolution: The impact of utilising different heterogeneity parameterisations (e.g. effective parameter approach (LM7), mosaic scheme (LM7_MOS1) or tile approach (LM7_TILE)) on modelled fluxes is significantly smaller than the effect of MSMA and of improved model formulations (differences between LM_OP and LM7). These facts are illustrated by the mean daily cycle of LITFASS domain averaged fluxes
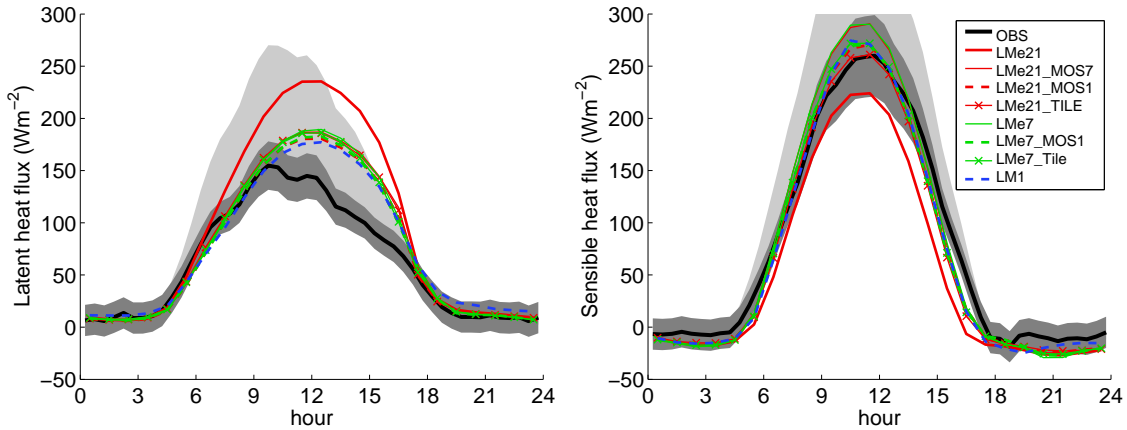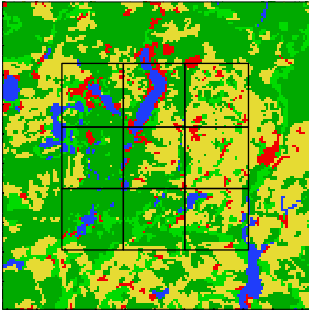
Figure 4.6: Mean daily cycle (average over the nine golden days) of latent (left) and sensible heat flux (right) as LITFASS domain average. The dark and light grey shaded areas indicate the ranges of uncertainty due to random measuring errors and non-closure of the energy balance, respectively.

(Fig. 4.2) and the corresponding BIAS and standard deviation values listed by Tab. 4.1. Disregarding the phase shift error, predicted fluxes of simulations with MSMA and model improvements agree with the observations within the range of uncertainty - no matter how surface heterogeneity is parameterised. Therefore, it is not possible to rank the parameterisation methods at 7 km atmospheric resolution by comparing predicted and observed LITFASS domain averaged fluxes.

Differences of predicted LITFASS domain averaged fluxes are larger if the coarse scale series of runs, which are integrated at the Extended-LM domain, is considered (Fig. 4.6). Using the effective parameter approach at a grid spacing of 21 km (LMe21) results in very high latent and very low sensible heat fluxes at the limits of the uncertainty range of observations since the whole LITFASS area is assigned to the single land-use class 'crops': The small stomatal resistance parameters of 'crops' likely cause the overestimation of evapotranspiration. Nonetheless, all runs except LMe21 are clearly within the error margins, despite of small deviations in the afternoon due to the phase shift problem. Again, a ranking is not possible.

However, (Fig. 4.6) demonstrates that the representation of the surface influences the flux calculations much more than the representation of the atmosphere. Runs with similar surface representation, but different atmospheric resolution are almost identical: Integrations with 7 km surface resolution (LMe21_MOS7 and LMe7) are in close agreement; the same applies for the simulations with a surface grid spacing of 1km (LMe21_MOS1, LMe7_MOS1). Even the results of LM1, which is integrated on the smaller LM domain, fits nicely into the last group. The results of the runs with tile approach (LMe21_TILE and LMe7_TILE) differ since the surface representation using the tile approach also depends on the atmospheric resolution. But as it can be expected, the tile run with higher resolution (LM7_TILE) converges towards the high resolution runs with 1 km surface grid spacing.

61

Table 4.2:   Mean anomalies in Wm^{-2} of surface fluxes at daytime (9-14 UTC) aver-
aged over the LITFASS-2003 period at the nine LM grid-boxes within the
LITFASS-domain. Estimated observations are listed on top followed by LM7
and LM7_MOS1 results. Model results which are in closer agreement to the
estimated observations by at least 5 Wm^{-2} compared to the other model run
are highlighted in bold face. For a legend of the land-use map (centre), see
Fig. 3.14.

Mean anomaly of λE_0				Mean anomaly of H_0		
-3	0	9		7	1	-25
-32	-40	**14**		41	-41	-44
-15	**-10**	-20		**1**	**-29**	10
-9	-1	15		34	19	-50
9	-32	**8**		6	39	**-38**
8	**-19**	-10		**18**	**23**	-4
-11	-6	1		34	10	-31
-4	**13**	64		**24**	23	-81
9	28	**29**		5	**3**	**-28**

4.2.2 Prediction of the spatial flux distribution

Advanced parameterisation schemes of surface heterogeneity are expected to have a
high skill in predicting spatial flux distributions. This quality can be tested by sub-
dividing the LITFASS domain into 3 by 3 grid-boxes (see Figure included into Tab.
4.2) resembling the atmospheric LM grid-boxes of runs with 7 km resolution. Area
averaged fluxes in these sub-areas are estimated likewise the LITFASS domain aver-
aged fluxes by averaging the composite time series for each land-use type (Beyrich
et al., 2006) weighted with the fractional coverage. To distill the spatial variance,
only the anomalies of fluxes with respect to the LITFASS domain average are in-
vestigated. The analysis focuses on daytime (9-14 UTC) fluxes, since differences in
predicted fluxes are most pronounced then. The estimated observations in Tab. 4.2
reflect the land-use dependent characteristics, which have already been discussed in
Section 2.1: Latent heat flux anomalies of forest and farmland dominated grid-boxes
are almost equal with slightly larger values at farmlands, whereas sensible heat flux
anomalies show a pronounced contrast between these two major land-use types.

As a first qualitative analysis, the performance of LM7 and LM7_MOS1 is com-
pared by assuming that those results which are in closer agreement to the estimated
observations by at least 5 Wm^{-2} indicate a better prediction (see values printed in
bold face in Tab. 4.2). Remarkably, LM7 is better at grid-boxes with homogeneous
land-use (two forest dominated grid-boxes in the southwest and two farmland domi-
nated boxes in the northeast), whereas LM7_MOS1 shows better performance at the
other more heterogeneous boxes. Concerning the latent heat flux, this comparison
between LM7 and LM7_MOS1 is undecided because both methods are preferable
at 4 grid-boxes, but with respect to the sensible heat flux LM7_MOS1 gives better
results at 6 boxes and LM7 only at 2.

A quantitative analysis is conducted by calculating bias and standard deviation
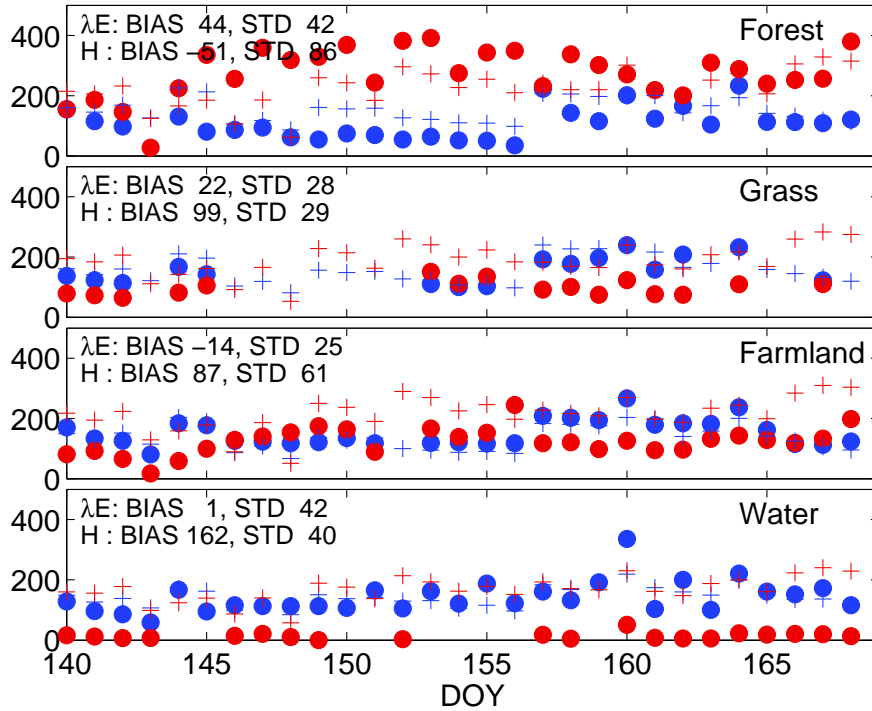
Figure 4.7: Daytime (10-14 UTC) averages of sensible (red) and latent (blue) heat fluxes over different types of land-surface. Simulation results from LM7_MOS1 integrations are marked by crosses and measurements by solid circles.

of the anomaly prediction for each grid-box and then summarising these result as mean bias and mean standard deviation averaged over all boxes (see Tab. 4.1, lower rows). Errors of simulations with model improvements are clearly smaller than those of LM_OP. Although simulations with enhanced parameterisation of heterogeneous land-surfaces tend to exhibit smaller errors than the simulation using the standard effective parameter technique (LM7), an analysis of variance reveals that these results are not statistical significant; the differences in terms of mean bias and standard deviation as well as of the number of grid-boxes are too small to rank the different approaches.

In summary, based on a comparison with observations, it can only be concluded that integrations with model improvements predict the fluxes during LITFASS-2003 more accurately than the operational LM forecasts. A statistical significant assessment of various heterogeneity parameterisation schemes based on LITFASS-2003 observations is not possible. Nonetheless, the following two examples demonstrate, that heterogeneity parameterisations, in particular the mosaic scheme, reproduce spatial and temporal structures of observed fluxes reasonably.

The LM using the mosaic approach (LM7_MOS1) simulates the overall spatial differences of fluxes over various land-surfaces and their temporal evolution successfully (Fig. 4.7). Over forest the model produces larger values of H_0 compared to λE_0, but this difference is smaller than observed. It is remarkable that TERRA stand-alone
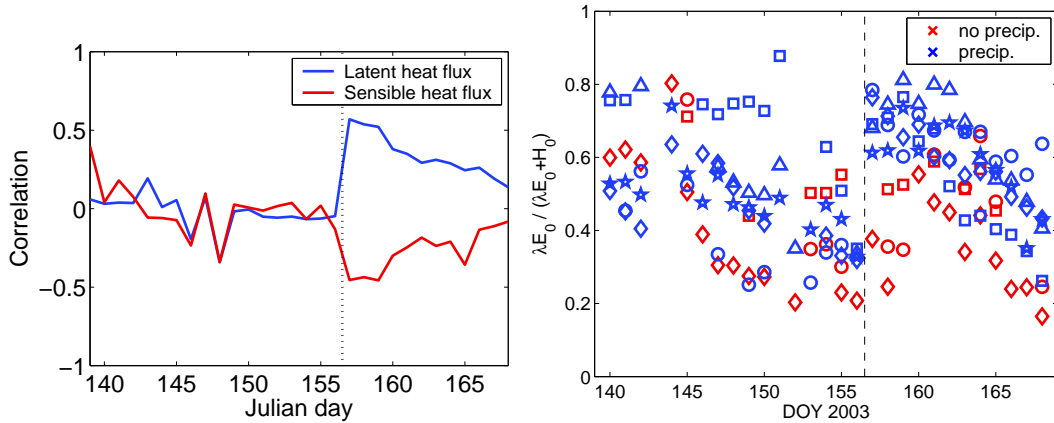
Figure 4.8: Left (model): Pattern correlation of precipitation sum on day 156 (5 June 2005, dashed line) and surface flux predictions (LM7_MOS1) at 12 UTC during the LITFASS-2003 period. Right (observation): Evaporation fraction $\lambda E_0/(\lambda E_0 + H_0)$ at 11-13 UTC measured at various LITFASS-2003 stations. Those sites which observed rain at day 156 are coloured in blue and the stations labled in red kept dry.

integrations, which use exactly the same surface parameters as LM7_MOS1, give systematically higher sensible heat fluxes over forest (Fig. 3.11). The main reason is that atmospheric reference values are homogeneously prescribed by measurements over grass (GM Falkenberg) in TERRA stand-alone integrations and these values cannot adapt to the flux regime over forest, unlike in LM7_MOS1 simulations. Most likely, larger stomatal resistance parameters can reduce this discrepancy between LM7_MOS1 simulations and observations, but tuning based on measurements at a single station is too uncertain. Taking the non-closure problem of measurements into account, the observed and modelled fluxes over grass and farmland coincide well. Above water the latent heat flux is predicted correctly, but the sensible heat flux is clearly overestimated, although lake surface temperatures are prescribed by measurements. This deficiency might be caused by fundamental problems in the surface exchange scheme (e.g. internal boundary layers). Since water surfaces cover only a small part of the LITFASS domain and land-surfaces are the main focus of this study, this issue has not been considered in more detail.

The second example considers spatial flux heterogeneities induced by inhomogeneous rainfall patterns, as e.g. observed during 5 June 2003. Assimilation of these observations by MSMA results directly in inhomogeneous soil moisture distribution, which is maintained for some days (see also Fig. 3.10) and affects the surface fluxes during this time (see also Fig. 3.12). Fig. 4.8 (left) shows the spatial correlation of the rain rate observed during 5 June 2003 with the predicted daytime surface fluxes by LM7_MOS1. Of course, no correlations exist before the rain event. But afterwards a clear connection between rain pattern and surface fluxes is visible, namely a positive correlation with the latent heat flux (wet areas evaporate more) and a negative with the sensible heat flux. These correlations decrease with time, but are

significantly higher than the noise level during nine days after the rain event. A similar response can be diagnosed from flux measurements (see Fig. 4.8, right): Before the rain event stations at which rain occurred at 5 June 2003 and others cannot be separated by inspecting the evaporation fraction $\lambda E_0 / (H_0 + \lambda E_0)$. But afterwards a significant higher evaporation fractions were observed at wet stations only. It can be concluded that under dry soil conditions - as experienced during LITFASS-2003 - rain fall patterns influence surface fluxes on a temporal scale of a week. This offers a forecast potential for mesoscale NWP, which can only be exploited if high resolution rainfall observations (usually radar data) are assimilated (e.g. by MSMA), and if the model is able to make use of localised, high resolution surface information, e.g. by using the mosaic method.

4.3 Evaluation of heterogeneity parameterisations using high resolution model data

The previous section demonstrated that it is not possible to decide on the basis of LITFASS-2003 measurements which parameterisation method of land-surface heterogeneity is superior. It is attractive to utilise high resolution model results instead of observations as reference for an evaluation because these simulations provide a complete data set with a much denser spatial coverage and without measurement artefacts (e.g. non closure problem). Consequently, this method offers the opportunity to draw conclusions with higher significance. Additionally, approximations about subgrid-scale effects, which are used by certain parameterisation methods, can be checked directly by analysing high resolution model runs, since they resolve these effects.

Nonetheless, some essential processes, like transpiration at leafs, must be parameterised even in high resolution simulations. Systematic errors in these parameterisations due to inaccurate formulations or choices of parameters will also affect high resolution simulations. Therefore, such simulations should not be considered as ground truth. Any evaluation based on high resolution model data should be regarded in first place as a consistency test. They can only verify parameterisation schemes if the high resolution simulation converge towards the truth - the results of the last section (Fig. 4.7) provide confidence in this ability of LM.

4.3.1 Analysis at scales of mesoscale weather prediction models

LM simulations with 1km atmospheric grid spacing (LM1) will be utilised as high resolution reference in the following. Consequently, only integrations on the same domain, the LM domain, can be analysed. These runs have been performed with a grid spacing of 7 km, which is typical for todays mesoscale NWP models. An evaluation of runs on the Extended-LM domain with atmospheric grid spacings up to 21 km is postponed to the next subsection.
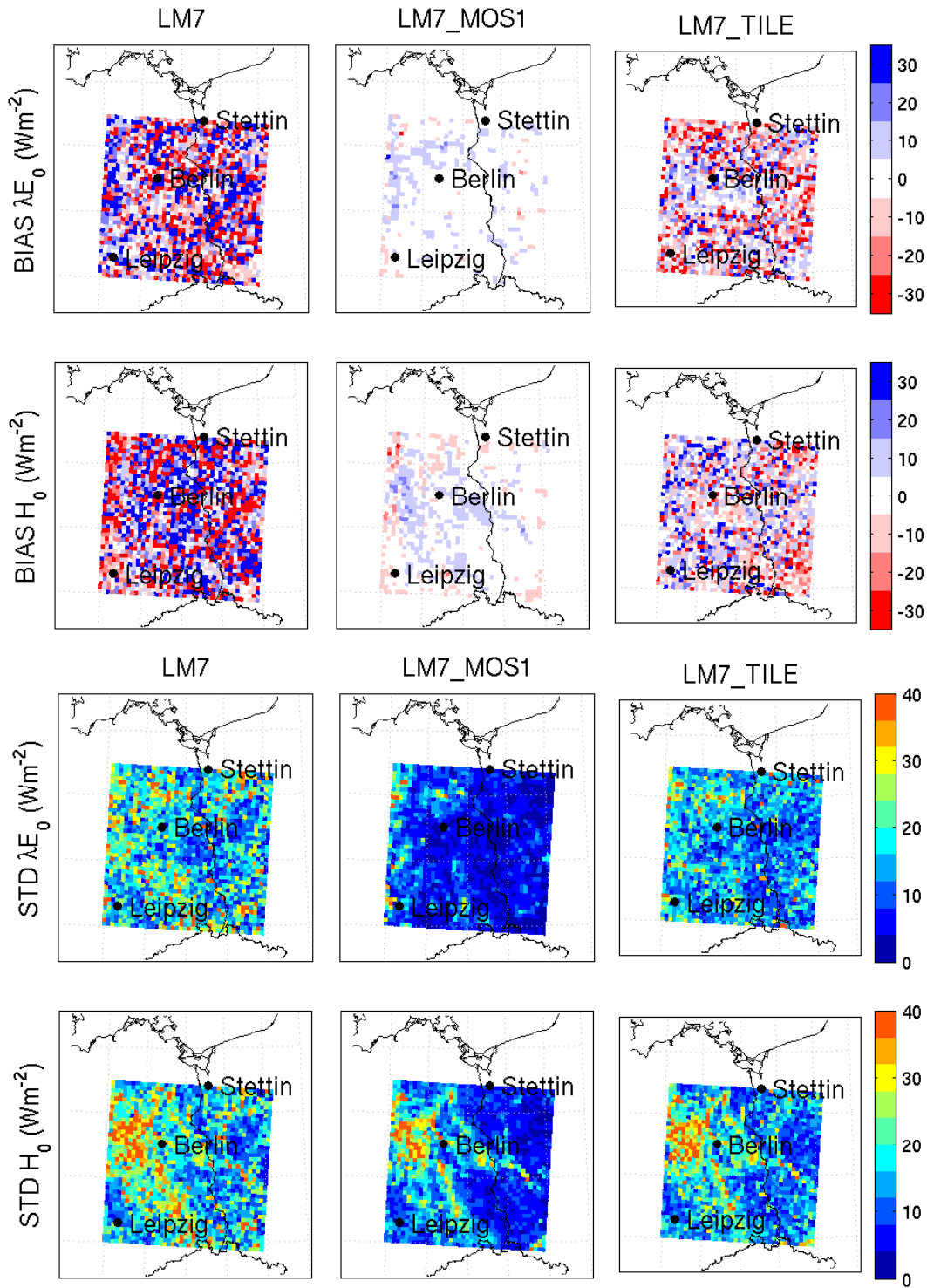
Figure 4.9: Top panel: BIAS map of predicted latent λE_0 and sensible heat flux H_0 with respect to LM1 integrations based on forecasts at the nine golden days at 12 UTC. Bottom panel: same as top, but for the standard deviation. (The boundary zone, which is affected by the lateral boundary conditions, is excluded here and in all following analyses.)

Table 4.3: Evaluation of predicted latent/sensible heat fluxes at 12 UTC within the LM domain using high resolution LM1 model integrations: BIAS describes the systematic deviation of fluxes integrated over the whole model domain, whereas the mean systematic and random deviations at a single grid point are given by $\overline{|BIAS|}$ and $\overline{STD}$. Computational costs are given in arbitrary units, other values in Wm^{-2}.

		LM_OP	LM7	LM7_ dom	LM7_ MOS1	LM7_ TILE	LM7_ MOS1_ hsoil	LM7_ TILE_ hsoil
Consistency w.r.t. LM1	BIAS	30/-27	2/2	2/0	1/1	-3/0	7/-3	6/-5
	$\overline{|BIAS|}$	50/43	27/31	27/24	3/4	16/15	20/17	18/17
	$\overline{STD}$	48/40	19/20	25/24	8/13	15/17	15/17	16/17
Computational cost		1	1	1	2.1	1.2	1.9	1.15

Bias and standard deviation maps of modelled fluxes with respect to LM1 simulations (Fig. 4.9) reveal that runs with the mosaic approach (LM7_MOS1) and the high resolution reference (LM1) agree very well, followed by runs with tile approach (LM7_TILE) and then simulations based on the effective parameter technique (LM7). The statistical indices of this evaluation listed in Tab. 4.3 confirm this ranking, which is in agreement with the model studies of Mölders et al. (1996) and of Heinemann and Kerschgens (2005, 2006b). The random errors in λE_0 are slightly smaller than those of H_0 (Fig. 4.9 lower panel), which is most likely due to the fact, that λE_0 is more controlled by surface properties, in particular by the stomatal resistance of plants, than H_0. In general, bias and standard deviation fields are very patchy and no obvious larger scale structure exists. Averaged over the whole domain all model simulations except the operational run (LM_OP) agree very well with LM1 and deviate by less than $10 \, \text{Wm}^2$ (Tab. 4.3).

Obviously the effect of heterogeneity on surface fluxes depends on the considered horizontal scale: Significant effects occur locally, on small scales; the effect on large scales is negligible. This phenomena can be quantified in terms of a scale dependent root mean square error (RMSE): Fluxes of the reference simulation as well as of the considered run are projected by averaging on a coarse grid and the RMSE is calculated subsequently. A clear reduction in RMSE can be detected for all model integrations if larger horizontal scales are considered (see Fig. 4.10). On all averaging scales, the mosaic approach leads to smallest errors followed by tile approach, and finally effective parameter method (LM7). The differences among various methods are of minor importance on larger scales. The effective parameter approach (LM7) is slightly better than the dominant land-use method (LM7_DOM) with respect to the latent heat flux, but worse if the sensible heat flux is considered. It can be concluded that the effective parameter approach is a very poor or even useless method to parameterise land-surface heterogeneity.
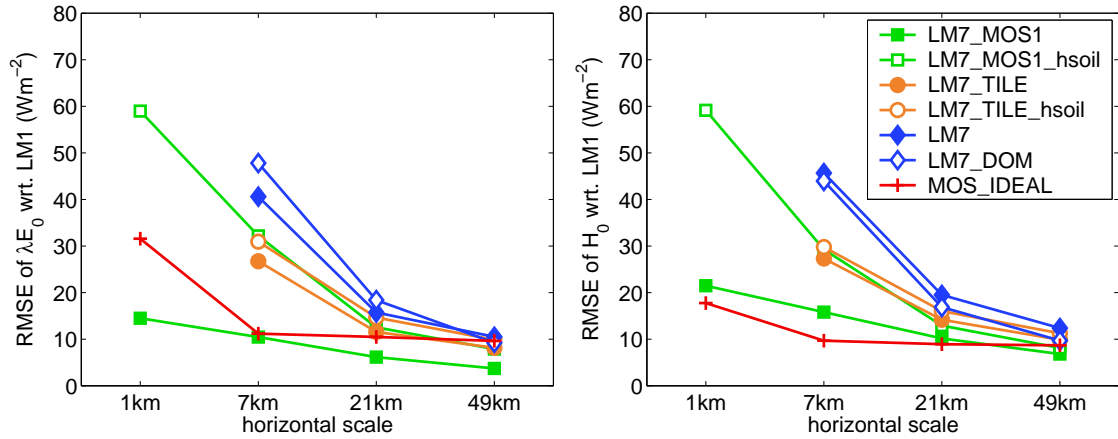
Figure 4.10: Root mean square error (RMSE) at various spatial averaging scales with respect to LM1 integrations. Data basis: 12 UTC forecasts at nine golden days covering the LM domain (without the boundary zone).

Simulations with a non-homogeneous soil representation always give better results than corresponding simulations with a homogeneous soil (compare LM7_MOS1 with LM7_MOS1_hsoil and LM7_TILE with LM7_TILE_hsoil; Fig. 4.10). Differentiated soil physics has a larger, beneficial impact in combination with the mosaic approach than with tile method. This is an indirect indication that most of the soil moisture variability is induced by other effects than land-use contrasts which become resolved by the tile method with differentiated soil physics. A variance analysis at the end of this chapter will prove this hypothesis.

Heinemann and Kerschgens (2005 and 2006b) proposed an idealised mosaic approach for research purposes: The results of a high-resolution integration are post-processed by averaging atmospheric variables on a coarse grid before diagnosing the fluxes offline according to the mosaic approach. This method is of course not applicable in real forecast mode. In contrast to the real mosaic method, the diagnosed fluxes have no feedback on the evolution of the forecast. Heinemann and Kerschgens mention this feature as an advantage, since no errors due to inaccurate flux predictions are accumulated in atmospheric state variables. On the other hand surface fluxes are in a subtle balance with atmospheric state variables which is regulated by feedback processes in order to ensure e.g. energy conservation. Theoretically, the ideal mosaic approach is a cheap method in terms of coding to asses the quality of the mosaic approach, but not physically consistent. In practice (see Fig. 4.10), the errors of the idealised and real mosaic method have the same order of magnitude, but differ in detail.

In addition to the magnitude of surface fluxes also their spatial variance is important to serve as boundary condition for higher order turbulent closures or as an important triggering factor of convection. The analysis of flux variance at different averaging scales predicted by the reference simulation (LM1) reveals considerable amount of variability at small spatial scales (Fig. 4.11, top panel). The mosaic approach (LM7_MOS1) is able to reproduce this variablity very well even at the
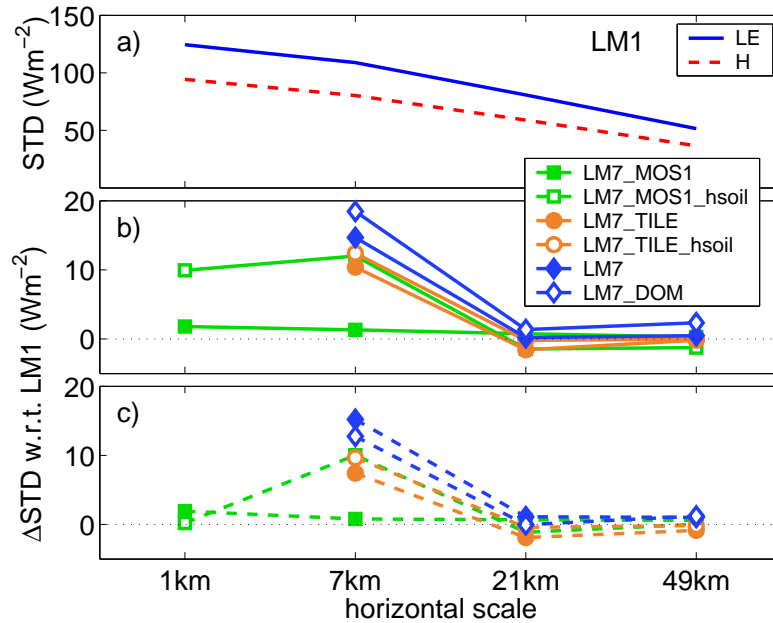
Figure 4.11: (a) Standard deviation of turbulent fluxes estimated from LM1 simulations (nine golden days at 12 UTC) at various horizontal scales. Deviation of simulated standard deviation in latent heat flux (b) and sensible heat flux (c) with respect to LM1 simulations.

smallest scale, but tends to a small overestimation of the variance because local adaptations of the atmospheric reference values to anomalies in the corresponding surface variables are neglected. Nonetheless, all other schemes lead to a much stronger overestimation of small scale variablity. Again, the model versions with differentiated soil lead to better results than those with homogeneous soil. The variance at averaging scales larger than the model resolution (in this case at scales of 21 km and 49 km) is reproduced correctly by all parameterisation schemes.

Computational costs are an important issue for the operational applications of parameterisations. The LM7_MOS1 simulations require about twice the computational time of LM7, whereas LM7_TILE needs only 20% additional computational resources (see also Tab. 4.3). Both factors, which may be further reduced by optimised coding, make practical applications of these methods feasible. In contrast, a grid refinement to 1 km resolution would require 330 times more computational power, which is not affordable for operational applications in near future.

4.3.2 Analysis at scales of regional climate models

The effect of subgrid-scale heterogeneity depends on the grid-scale of the model. Therefore, it is worthwhile to extend the previous analysis to scales of regional climate models in the order of 20 km. The relevance of subgrid-scale heterogeneity at these scales will be investigated by analysing the LM integrations at the Extended-
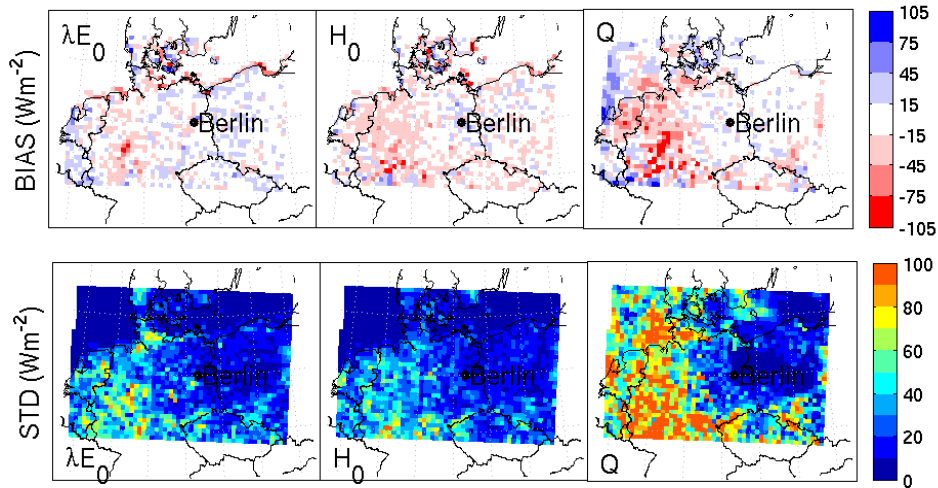
Figure 4.12: Top panel: Bias map (in Wm^{-2}) of predicted latent heat flux λE_0, sensible heat flux H_0, and net radiation Q with respect to reference run at the Extended-LM domain (LMe7_MOS1) based on forecasts at nine golden days at 12 UTC. Bottom panel: same as top, but for the standard deviation.

Table 4.4: Evaluation of predicted latent, sensible heat fluxes and net radiation ($\lambda E_0/H_0/Q$) at the Extended-LM domain using high resolution LMe7_MOS1 model integrations: BIAS describes the systematic deviation of fluxes integrated over the whole model domain, whereas the mean systematic and random deviations at a single grid point are given by $\overline{|\text{BIAS}|}$ and $\overline{\text{STD}}$. All values are given in Wm^{-2} and valid at 12 UTC.

		LMe21	LMe21_ MOS7	LMe21_ MOS1	LMe21_ TILE	LMe7	LMe7_ TILE
Consistency	BIAS	-2/-7/-6	-1/-7/-4	-2/-4/-3	-9/0/-2	1/-2/-2	-5/2/1
w.r.t.	$\overline{|\text{BIAS}|}$	36/35/22	13/14/19	8/8/18	31/26/18	10/10/7	12/8/7
LMe7_MOS1	$\overline{\text{STD}}$	31/27/47	22/20/47	20/18/47	31/25/48	9/8/11	14/8/13

LM domain (see Tab. 4.4 or Tab. 3.1 for a list of runs). Instead of integrations with 1 km grid spacing, which would exceeded computational resources, LMe7_MOS1 integrations are used as high resolution reference, because they are regarded to be the best approximation to simulations with 1 km resolution.

As an example, Fig. 4.12 illustrates the spatial distribution of deviations given by LMe21_MOS7 runs. Note, that for the Extended-LM domain, net radiation Q has to be considered additionally beside the turbulent fluxes: In particular, in the western part of the domain, the errors of Q (both, BIAS and STD) are large and highly correlated with systematic errors in H_0 and λE_0. By chance, due to specific weather conditions during LITFASS-2003 or due to the more continental position, the LM domain is hardly affected by these deviations in Q. This explains why Q

Left matrix (H_0 lower triangle, λE_0 upper triangle):

	LMe21_	LMe21 MOS7	LMe21 MOS1	LMe21 TILE	LMe7_	LMe7 MOS1	LMe7 TILE
LMe21_		59	58	35	65	64	68
LMe21 MOS7	51		21	53	29	34	35
LMe21 MOS1	52	20		50	33	28	36
LMe21 TILE	33	43	40		58	56	55
LMe7_	57	26	31	49		19	23
LMe7 MOS1	58	32	26	47	18		24
LMe7 TILE	60	31	30	48	16	16	

Right matrix (L_{net} lower triangle, S_{net} upper triangle):

	LMe21_	LMe21 MOS7	LMe21 MOS1	LMe21 TILE	LMe7_	LMe7 MOS1	LMe7 TILE
LMe21_		32	33	34	71	71	72
LMe21 MOS7	7		27	33	69	70	71
LMe21 MOS1	7	4		30	70	70	71
LMe21 TILE	7	7	7		71	70	70
LMe7_	13	12	12	13		17	22
LMe7 MOS1	13	12	12	13	4		21
LMe7 TILE	14	13	13	13	6	6	

Figure 4.13: RMS deviation among all integrations at the Extended-LM domain estimated at 21 km resolution in terms of H_0 (left, lower triangle), λE_0 (left, upper triangle), long wave net radiation L_{net} (right, lower triangle) and short wave net radiation S_{net} (right, upper triangle). All values are given in Wm^{-2} and valid at 12 UTC.

had not to be considered in the previous analysis.

Insight into the origin of the deviations in Q is given by an analysis of root mean square deviations among all runs integrated at the Extended-LM domain in terms of net short- and longwave radiation as well as turbulent fluxes (Fig. 4.13). Regarding radiation, it becomes obvious that simulations with different atmospheric resolution agree much less than runs with similar atmospheric grids. Obviously, the representation of clouds strongly depends on the atmospheric resolution. Other studies, e.g. Petch et al. (2002), Bryan et al. (2003) and Ament et al. (2004), support this conclusion.

In essence, two effects modify the predicted turbulent fluxes at the surface: Total turbulent fluxes $H_0 + \lambda E_0$ are affected by the atmospheric resolution via clouds, whereas the partitioning between H_0 and λE_0 is largely determined by the representation of the surface. Accordingly the simulations, which agree in terms of H_0 and λE_0 quite well, can be subdivided into two categories (see Fig. 4.13): At first, runs with similar surface representation (LMe21_MOS7 & LMe7; LMe21_MOS1 & LMe7_MOS1) and secondly runs with similar atmospheric resolution and only slightly different surface representation (LMe21_MOS7 & LMe21_MOS1; LMe7 & LMe7_MOS1; LM7 & LMe7_TILE; LMe7_TILE & LMe7_MOS1).

The effects due to atmospheric resolution (via clouds and net radiation) and due to surface representation have the same magnitude, but act on different horizontal scales: The deviations in net radiation have more large scale structures than the differences induced by the surface. This scaling characteristic is revealed by the scale dependent RMSE depicted by Fig. 4.14. LMe21_MOS1 simulations are superior at small scales, whereas LMe7 and LMe7_tile take over at scales equal or larger than 21 km. Apart from the effect of atmospheric resolution, the afore established ranking of surface heterogeneity parameterisation (best mosaic, followed by tile and
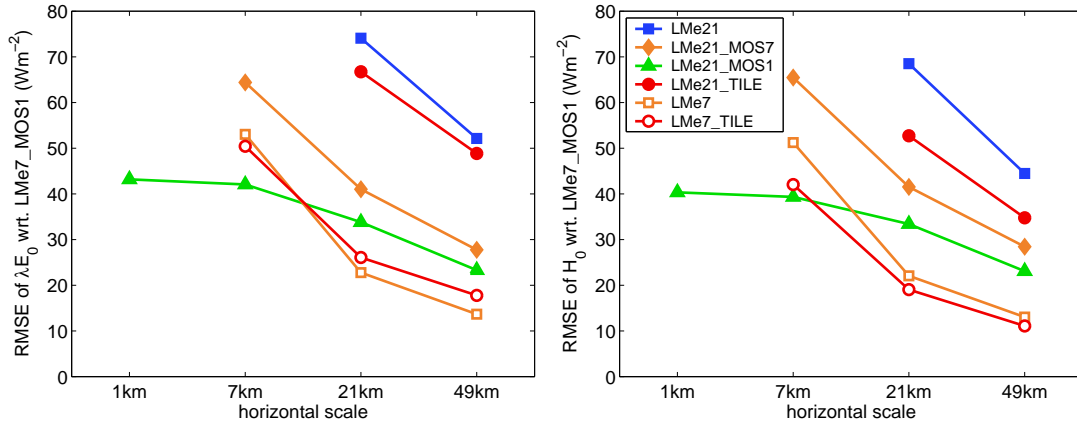
Figure 4.14: Same as Fig. 4.10, but for runs on the Extended-LM domain.

effective parameter approach) is confirmed (see also Tab. 4.4). It is remarkable that LMe21_MOS7 and LMe21_TILE utilise almost the same number of sub-pixels, i.e. require similar computational resources, but LMe21_MOS7 gives significantly better results. Consequently, under the investigated conditions (central European heterogeneities, 21 km resolution) a coarse mosaic should be preferred compared to a tile scheme. Again, land-use seems not to be the dominant parameter to explain small scale flux variability.

4.3.3 Analysis of high resolution simulation

High resolution simulations (LM1) are analysed in order to verify the assumptions underlying the mosaic and the tile approach, and to elucidate why LM7_MOS1 and LM1 agree so well: Surface values of potential temperature and specific humidity vary much more than the corresponding atmospheric values at scales smaller than 7 km (Fig. 4.15): The standard deviation of T_s and q_s are by a factor 9 and 5, respectively, greater than the standard deviation of T_{atm} and q_{atm}. Consequently, the variability in surface quantities has a much larger impact on surface fluxes than the variability of the atmospheric reference values. Additionally the correlation between small scale anomalies in surface quantities and atmospheric variables decreases quite rapidly with increasing height. This means that the modelled atmosphere is very diffusive and very efficient in diminishing small scale inhomogeneities introduced by the surface. In other words, the blending height for the considered cases and scales is very low. The dominant variability of the surface and the low blending height support the basis of the approximation underlying mosaic and tile approach, namely to neglect subgrid-scale atmospheric variability. Experimental data analysed by Mahrt and Sun (1995) supports this approximation. Extensions of the mosaic or the tile approach by introducing blending height concepts (Claussen, 1991) or by considering the vertical propagation of surface anomalies (Seth et al., 1994; Molod et al., 2003) seems to be of minor importance. Integrations with only refined surface (LM7_MOS1) and fully refined runs (LM1) give very similar results because both have exactly the same representation of surface charateristics.
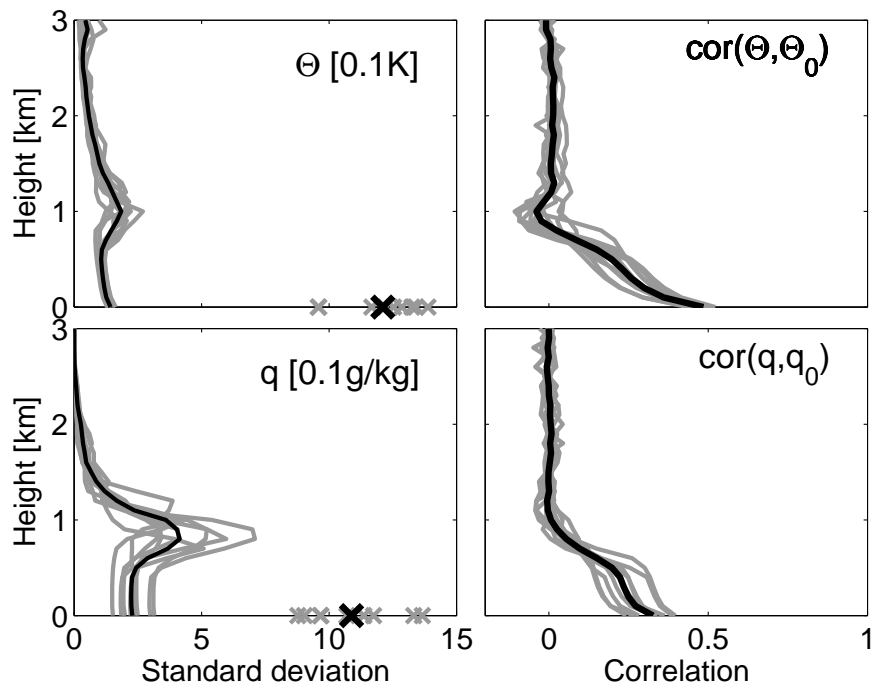
Figure 4.15: Left: Standard deviation of potential temperature and specific humidity in the atmosphere and at the surface (crosses). Right: Correlation of atmospheric variables at different heights with surface values. Grey lines and crosses indicate results for individual LM1 simulations at 12 UTC; black lines and crosses give the overall mean. All fields have been high-pass filtered with 7 km resolution to analyse only small scale variability.
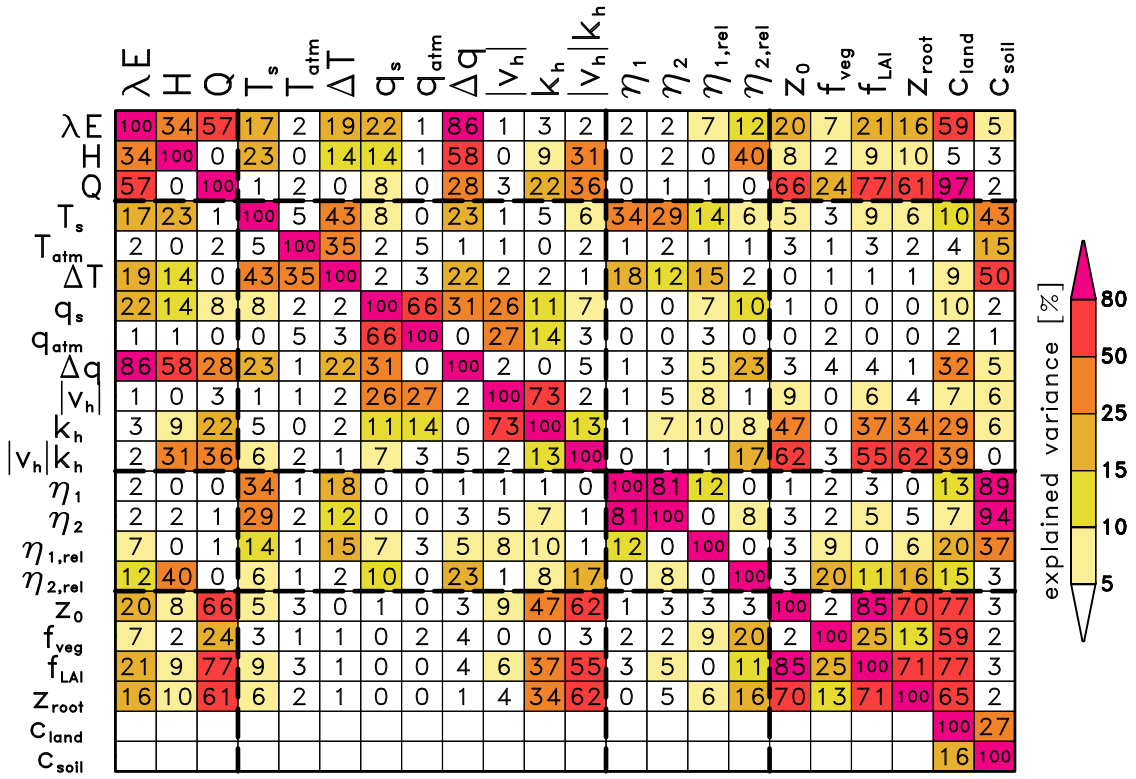
Figure 4.16: Spatial explained variance among surface flux patterns and corresponding influencing variable patterns predicted by LM1 within the Extended-LITFASS domain at 30 May 2003, 12 UTC (homogeneously dry conditions). Dashed lines group the variables into fluxes, fast varying variables, slow varying variables and time constant quantities. $\Delta T := T_{atm} - T_s$; $\Delta q := q_{atm} - q_s$; $\eta_{rel} = \eta/\eta_{PV}$; for definition of other variables, see Appendix A.

The importance of considering the variability of surface variables is also revealed by analysing the influence of various variables on the pattern of predicted fluxes by LM1. Figures 4.16 and 4.17 present the explained spatial variance among all variables which may influence the surface fluxes. The analysis was confined to the Extended-LITFASS domain to ensure the best quality of all input fields, especially of soil moisture. Note that this analysis can only identify linear relations. Consequently, low values of explained variance indicate only a small linear impact. The most important aspects concerning heterogeneity of surface fluxes to be drawn from Figures 4.16 and 4.17 are:

- For both cases, the atmospheric reference values of temperature T_{atm} and humidity q_{atm} obviously have a much smaller impact on the predicted fluxes than the corresponding surface values T_s and q_s. This finding justifies the approximation of mosaic and tile approach to maintain variability of surface variables and to neglect the corresponding atmospheric variability.

- Concerning λE_0, a large part of the variability is explained by surface variables,

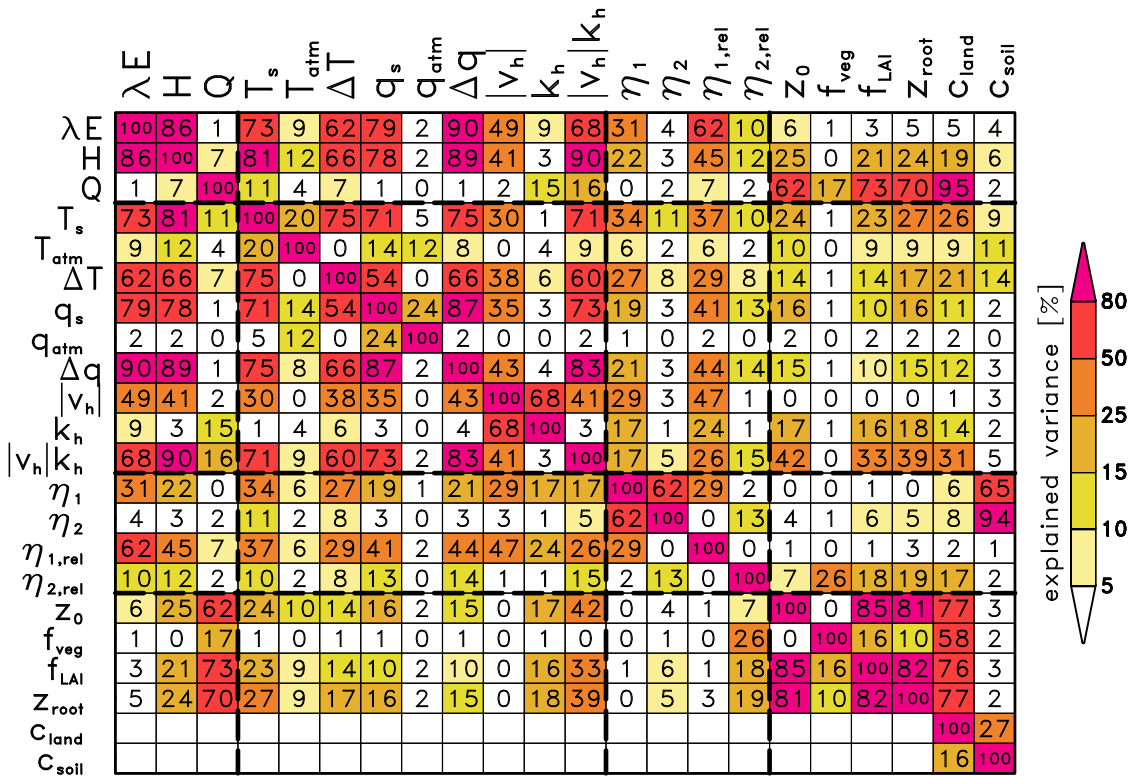|	λE	H	Q	Ts	Tatm	ΔT	qs	qatm	Δq	|vh|	Kh	|vh|Kh	η1	η2	η1,rel	η2,rel	Z0	fveg	fLAI	Zroot	Cland	Csoil
λE	100	86	1	73	9	62	79	2	90	49	9	68	31	4	62	10	6	1	3	5	5	4
H	86	100	7	81	12	66	78	2	89	41	3	90	22	3	45	12	25	0	21	24	19	6
Q	1	7	100	11	4	7	1	0	1	2	15	16	0	2	7	2	62	17	73	70	95	2
Ts	73	81	11	100	20	75	71	5	75	30	1	71	34	11	37	10	24	1	23	27	26	9
Tatm	9	12	4	20	100	0	14	12	8	0	4	9	6	2	6	2	10	0	9	9	9	11
ΔT	62	66	7	75	0	100	54	0	66	38	6	60	27	8	29	8	14	1	14	17	21	14
qs	79	78	1	71	14	54	100	24	87	35	3	73	19	3	41	13	16	1	10	16	11	2
qatm	2	2	0	5	12	0	24	100	2	0	0	2	1	0	2	0	2	0	2	2	2	0
Δq	90	89	1	75	8	66	87	2	100	43	4	83	21	3	44	14	15	1	10	15	12	3
|vh|	49	41	2	30	0	38	35	0	43	100	68	41	29	3	47	1	0	0	0	0	1	3
Kh	9	3	15	1	4	6	3	0	4	68	100	3	17	1	24	1	17	1	16	18	14	2
|vh|Kh	68	90	16	71	9	60	73	2	83	41	3	100	17	5	26	15	42	0	33	39	31	5
η1	31	22	0	34	6	27	19	1	21	29	17	17	100	62	29	2	0	0	1	0	6	65
η2	4	3	2	11	2	8	3	0	3	3	1	5	62	100	0	13	4	1	6	5	8	94
η1,rel	62	45	7	37	6	29	41	2	44	47	24	26	29	0	100	0	1	0	1	3	2	1
η2,rel	10	12	2	10	2	8	13	0	14	1	1	15	2	13	0	100	7	26	18	19	17	2
Z0	6	25	62	24	10	14	16	2	15	0	17	42	0	4	1	7	100	0	85	81	77	3
fveg	1	0	17	1	0	1	1	0	1	0	1	0	0	1	0	26	0	100	16	10	58	2
fLAI	3	21	73	23	9	14	10	2	10	0	16	33	1	6	1	18	85	16	100	82	76	3
Zroot	5	24	70	27	9	17	16	2	15	0	18	39	0	5	3	19	81	10	82	100	77	2
Cland																					100	27
Csoil																					16	100

explained variance [%]

Figure 4.17: Same as Fig. 4.16, but for 7 June 2003, 12 UTC (heterogeneous soil moisture conditions after convective rainfall).

in particular the type of land-use c_{land} and soil moisture η. Under rather homogeneous soil moisture conditions like at 30 May 2005, the influence of c_{land} via stomatal resistance parameters dominates, while under inhomogeneous conditions (7 June 2005) soil moisture becomes more important. For the second case the wind speed is relevant too, but strongly correlated with the soil moisture pattern (explained variance of 47%). Regarding H_0, surface quantities are not dominating, but the dynamic exchange coefficient $|v_h|K_h$ has a considerable impact. Since H_0 is less determined by surface variables, mosaic and tile approach tend to give slightly larger errors in terms of H_0 than of λE_0. The variability of Q is almost completely induced by the type of land-use via the differences in surface albedo.

- Absolute soil moisture contents (η_1, η_2) have much less skill to explain the variability of surface fluxes than the corresponding relative soil moisture contents ($\eta_{1,rel}$, $\eta_{2,rel}$) as defined by (3.3). Relative soil moisture is only partly correlated to the type of land-use (explained variance less than 20%). Consequently, the tile approach cannot represent a considerable part of the soil moisture variability and therefore leads to less accurate results than the mosaic approach.

4.4 Main results

This chapter addressed the central point of this study - the evaluation of surface fluxes predicted by various parameterisation schemes. The most important conclusions, which can be drawn from this evaluation, are summarised in the following:

- The model improvements apart from heterogeneity parameterisations (e.g. using MSMA soil moisture data, removal of coding errors, land-use dependency of stomatal resistance) have a clear positive impact: The enhanced model version (LM7) is able to represent the overall temporal evolution of surface fluxes (characterised by dry out phases interrupted by rain events) as well as their spatial distribution (forest-farmland contrast) accurately during the LITFASS-2003 experiment - unlike the operational version (LM_OP). Most of the improvement can be attributed to MSMA soil moisture data.

- Two model deficiencies have been identified common for all model versions: At first, the mean daily cycles of surface fluxes exhibit phase shifts; the maximum of sensible heat flux is reached too early and the peak of latent heat flux too late. This effect is most pronounced over forest areas. Secondly, the heat flux over lake areas is overestimated, although the lake surface temperature is prescribed by observations. The explanation of both effects must be postponed to future studies.

- The differences in predicted fluxes of runs with various heterogeneity parameterisations is in general small (less than $50\,(70)\,\mathrm{Wm^{-2}}$ with $7\,(21)\,\mathrm{km}$ grid spacing at $12\,\mathrm{UTC}$) - much smaller than the difference induced by the aforementioned model improvements (more than $100\,\mathrm{Wm^{-2}}$). Within the range of uncertainty of the measurements, all model simulations except the operational run (LM_OP) agree well with the observations. However, fluxes predicted by the standard method of effective parameters at $21\,\mathrm{km}$ resolution (LMe21) is at the limits of the error margins; most likely, an advanced parameterisation scheme (mosaic or tile approach) is beneficial at these scales. Any further assessment of parameterisation methods based on observations is not possible.

- The mosaic approach has the highest skill to reproduce the fluxes predicted by high resolution simulations (LM1), followed by the tile approach. Worst results are given by the effective parameter and dominant land-use approaches, which are equivalent in quality. Errors with respect to LM1 runs are large on small scales, but strongly decrease if averages on larger scales are considered. Model domain averaged fluxes are reproduced by all simulation (except LM_OP) very well (deviations smaller than $10\,\mathrm{Wm^{-2}}$). An analysis of simulations with varying atmospheric (7-21 km) and varying surface resolution (1-21 km) revealed that the partitioning into latent and sensible heat flux is largely determined by the surface representation, whereas the atmospheric resolution affects the net radiation at the surface via non-scale-invariant cloud parameterisations.

- At 21 km atmospheric resolution, a coarse mosaic approach with nine subgrid-boxes gives better results than a tile approach with almost the same number of classes and similar computational costs. The tile approach can only consider heterogeneity effects due to land-use variablity, but other surface parameters, in particular soil moisture, also have a significant impact. Heterogeneity effects caused by more than one parameter can only be taken into account by the mosaic method.

- For high resolution LM runs (LM1), the standard deviations in temperature and humidity are much larger at the surface than at the lowest model. Additionally, anomalies in surface state variables are not highly correlated with corresponding atmospheric values. Both findings show that the atmosphere is quite diffusive on small scales and support the approximations underlying the mosaic and the tile method to neglect subgrid-scale atmospheric variability. Consequently, the patterns of atmospheric state variables explain almost no spatial variability of surface fluxes.

- Inhomogeneous rainfall at 05 June 2003 induced soil moisture variations which affect the surface fluxes at the following days. This memory effect due to soil moisture storage is detectable in LITFASS-2003 observation and is realistically simulated by the LM using mosaic approach in combination with the MSMA data.

5 Impact of surface fluxes on the atmosphere

Near surface fluxes have been evaluated extensively in the last chapter. Users of numerical weather forecasts are, however, mostly interested in near surface weather conditions, profiles of atmospheric state variables and aspects of the hydrological cycle like clouds or precipitation. It can be expected that simulations with better representation of surface fluxes describe the atmospheric state more accurately. This hypothesis is only partly true as demonstrated in the first section of this chapter: Improved flux predictions reduce existing model deficiencies in forecasting the state of the atmosphere, but not completely. An analysis of the atmospheric moisture budget in the second section reveals that horizontal advection is often of the same or even larger importance than surface fluxes. Vertical turbulent fluxes in the boundary layer are investigated in the last section. It will be demonstrated that the entrainment fluxes at the top of the atmospheric boundary layer have a considerable impact.

5.1 Verification of the atmospheric state

The standard method to verify predicted profiles of temperature and humidity is to compare them with radiosonde measurements. Fig. 5.1 shows the systematic (BIAS) and stochastic (standard deviation, STD) errors estimated by this method. Interestingly, LM analysis data (LM7_ana), which is utilised as initial and boundary data, exhibits the smallest errors. This evaluation is not independent as the information from the radiosonde ascents at Lindenberg are used both to generate the analysis and to verify it. However, this result is an indication that prescribing analysis data at initial time and at the boundaries nudges the model towards reality and does not introduce additional errors. Consequently, the simulations LM_OP and LM7 are in closest agreement to the observations at 05 UTC, which is the first ascent after the reinitialisation at midnight. During daytime, typical error pattern evolve, which can be clearly seen in the BIAS profiles at 11 UTC and 17 UTC: The boundary layer simulated by LM_OP (up to 1 - 1.5 km height) is too cold and too wet. Regarding the sign, these errors agree to the observed errors in simulated surface fluxes, namely overestimation of the latent heat flux and too small sensible heat fluxes. Above the atmospheric boundary layer (ABL) at approximately 1.5 - 2.5 km height, similar systematic deviations occur too, but with opposite sign. This effect is likely due to an
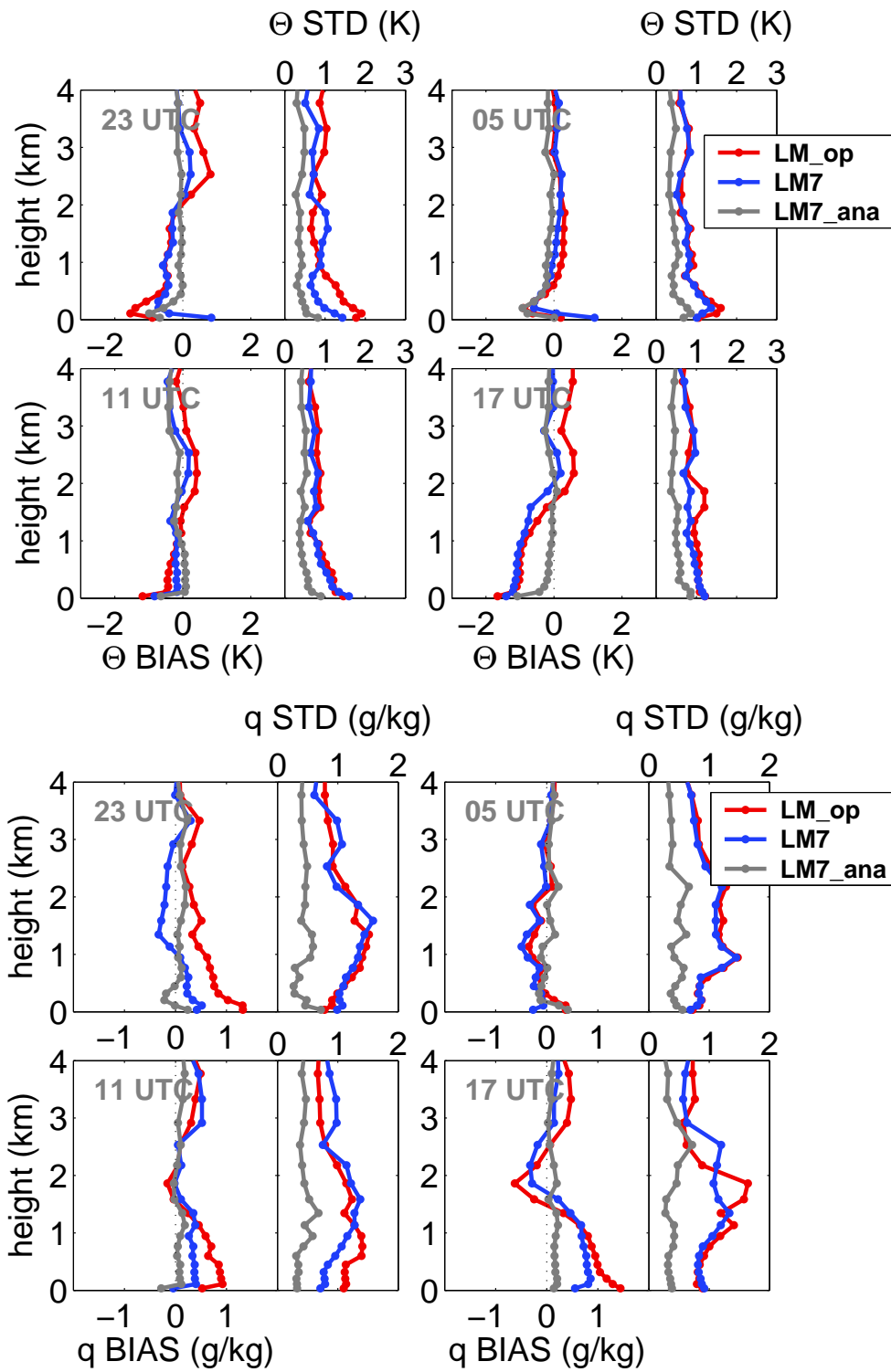
Figure 5.1: Bias and standard deviation of potential temperature profile (top) and specific humidity profile (bottom) with respect to radiosonde observations at Lindenberg during LITFASS-2003. Model data is obtained as averaged profiles for the LITFASS domain.
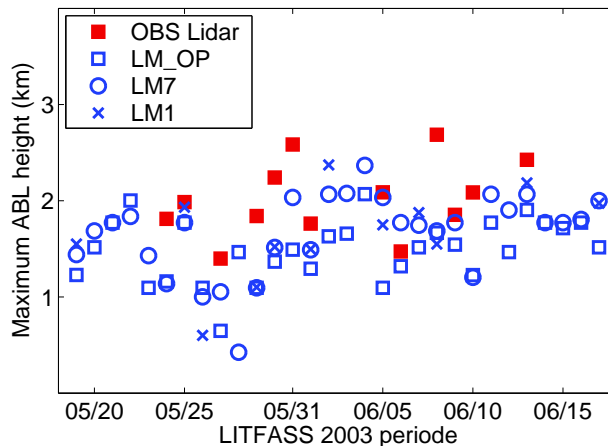
Figure 5.2: Daily maximum of ABL height derived form DIAL Lidar observations and given by various model simulations as mean over the LITFASS domain.

underestimation of ABL height. In this case, the model assumes free atmosphere air (warm and dry) at heights at which ABL air (cold and wet) is observed. The error characteristics of a too cold and too wet ABL have also been detected by operational verifications of several weather services (Pflüger, 2005; Arpagaus, 2005; Kaufmann, 2005). Thus this deficiency is not only related to the LITFASS-2003 period, but of general validity.

The performance of LM7 to predict atmospheric profiles (Fig. 5.1) is representative for all model simulations with improved model formulations and improved soil moisture data; the differences to runs with enhanced heterogeneity parameterisation (e.g. LM7_MOS1 or LM7_TILE) are marginal (not shown), which again indicates that the atmosphere is quite diffusive and rapidly smoothes small scale variability.

Comparing LM7 with LM_OP (Fig. 5.1), the aforementioned model problems are reduced, but not totally removed: The cold bias in the ABL is smaller at 11 UTC, but reaches nearly the same magnitude at 17 UTC. Concerning the humidity profile, the model improvements reduce the bias by more than 50 % at 11 UTC, and a smaller, but still significant error reduction prevails at 17 UTC. In general, the bias errors in the opposite direction at the top of ABL are smaller and shifted towards greater altitudes. This is an indication that the ABL height is increased, but still too low. The random errors (STD, Fig. 5.1) are hardly affected by the improved surface fluxes; LM7 and LM_OP give almost the same results. Probably a considerable portion of these random errors is caused by unpredictable small scale fluctuations measured by the radiosonde.

The comparison with radiosonde data demonstrated indirectly that the ABL height might be underestimated. This assumption can be substantiated by a direct evaluation of the ABL height prediction. During LITFASS-2003, a differential absorption lidar (DIAL) system of MPI-Hamburg (Lammert and Bösenberg, 2006) was operated at Lindenberg and provided profiles of absolute humidity with very high accuracy. Lammert and Bösenberg (2006) developed an algorithm to derive
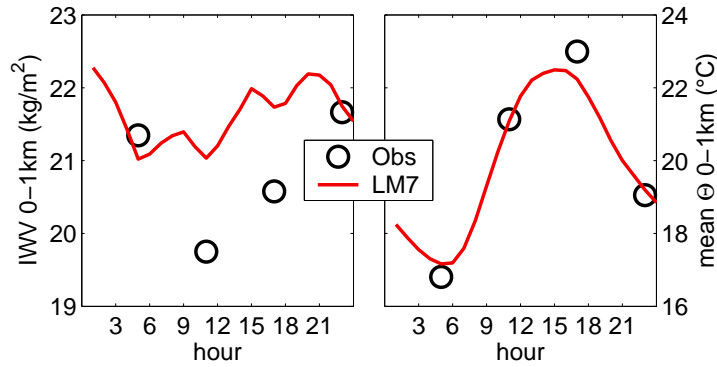
Figure 5.3: Mean daily cycle of vertically integrated vapour content (IWV, left) and of average potential temperature (right) from the surface up to 1 km altitude. Observational values are derived from radiosonde ascents.

time series of ABL height from these measurements. These observations are compared to modelled heights of the potential temperature inversion in Fig. 5.2. All model simulations tend to underestimate the ABL height. The mean measured maximum ABL height is 2020 m, whereas the operational model (LM_OP) and the improved LM (LM7) predict only a mean height of 1350 m and 1600 m, respectively (analysis restricted to days at which measurements are available). The improved surface flux predictions (LM7) result in higher ABL heights, which are, however, still too low. It is remarkable that also the high resolution runs (LM1) do not lead to substantial different results than LM7. Thus the problem of too low ABL heights cannot be simply solved by enhancing the horizontal resolution.

Although the evaluation in the last chapter revealed that almost all errors in predicted surface fluxes at the LITFASS domain can be corrected by improving the model, the errors in atmospheric profiles are only partly removed. These apparently contradicting results can only be explained if other processes than surface fluxes, which influence the ABL evaluation, are represented poorly in the model. Potential explanations are:

- The temperature and humidity profile are also altered by *horizontal advection.* Outside the LITFASS domain the model improvement are much less effective, because of worse information about surface characteristic and no MSMA data. Errors may be accumulated there and can be advected inside the LITFASS domain.

- ABL evolution is also influenced by vertical *entrainment fluxes* at the top of the ABL. If the entrainment fluxes are underestimated, the ABL height will rise too slowly during daytime because not enough dry and warm air from the free atmosphere will be mixed into the ABL supporting in the observed wet and cold bias.

Further inspection of the mean daily cycles of averaged ABL humidity and temperature (see Fig. 5.3) give some evidence of the second hypothesis: The radiosonde
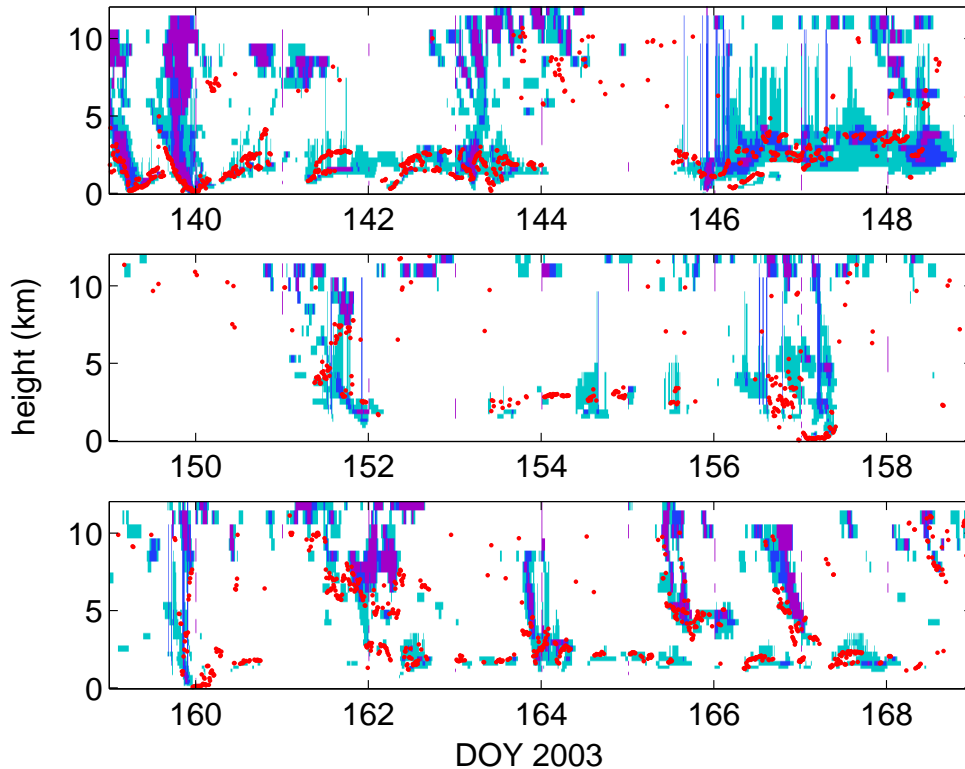
Figure 5.4: Time series of cloud fraction profiles modelled at the grid point Lindenberg by LM7 (cyan: 1-50 %, blue 50-99 %, purple: >99%). Cloud base heights observed by a ceilometer at Lindenberg are indicated by red dots.

observations indicate a reduction of ABL humidity during daytime, although the surface fluxes enhance the humidity content in the ABL. Assuming that advective effects cancel each other for long term averages, this behaviour can only be explained by an entrainment flux of dry air from the free atmosphere. The LM simulations are obviously not able to simulate this pronounced humidity depression during daytime. Regarding the mean potential temperature, the same effect can be observed, but less distinctive: LM7 underestimates the temperature at 17 UTC; this might be caused by a too small entrainment flux of warm air from above the ABL.

Model improvements and more sophisticated heterogeneity parameterisations have only little impact on 2 m-temperature predictions (not shown here, but Fig. C.2 in the Appendix gives some impressions). The differences between various model runs are too small to decide based on LITFASS-2003 observations whether one configuration is superior. Longer time series and in particular larger domains would be needed.

Another interesting aspect of model forecasts is the performance to predict cloud fractions (Fig. 5.4): The existence of clouds and even the temporal evolution of cloud base height are forecasted surprisingly well. There is not one day at which the model fails to represent the overall cloud conditions.
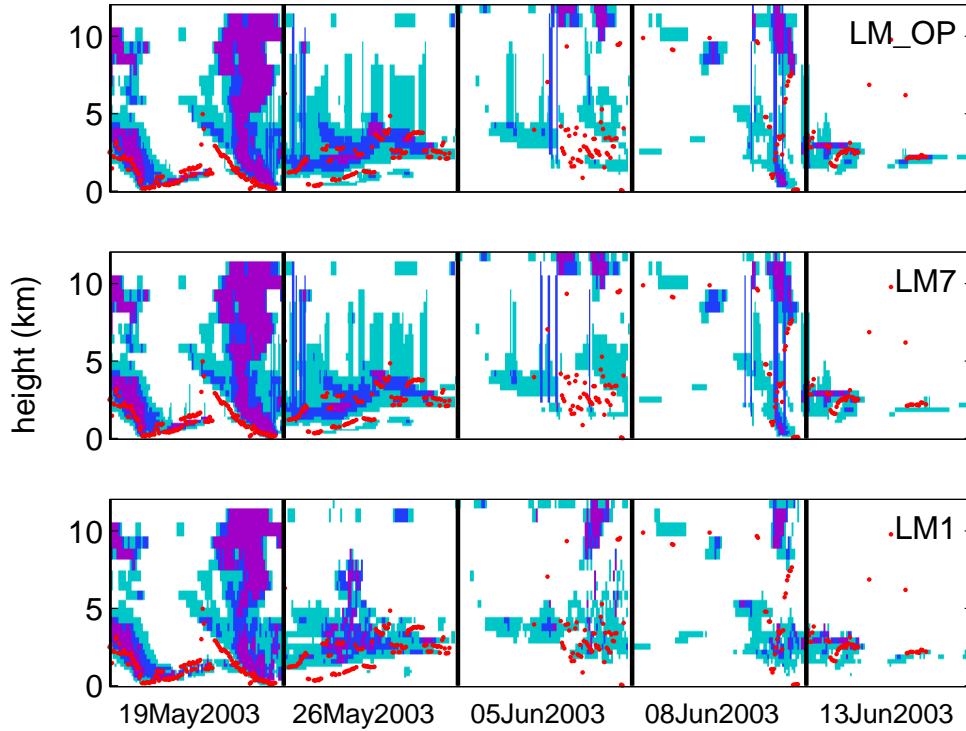
Figure 5.5: Same as Fig. 5.4, but focusing on five cloudy days for three different model versions: operational LM (LM_OP), LM with model improvements (LM7) and high resolution LM run (LM1) with 1 km grid spacing.

The results of LM_OP and LM7 are almost identical (Fig. 5.5), only subgrid-scale clouds produced by the convection scheme (short living, tall clouds, which appear in Fig. 5.5 as thin vertical lines) differ. Convective clouds are triggered depending on low-level moisture convergence and consequently these clouds are most sensitive to changes in surface latent heat fluxes. Results of LM7_MOS1 and LM7_TILE deviate only marginally from LM7 simulations (not shown). Obviously, the differences of surface fluxes are too small (see e.g. Fig. 4.2) to modify cloud evolution significantly. However, refining the grid and switching off the convection scheme (LM1) influence the simulation of clouds much more than changes in the surface fluxes. In particular, resolved convection occurs not as often as parameterised one. Based on ceilometer measurements, it is impossible to judge which representation is more realistic. Note, that even at 1 km horizontal resolution a large portion of cloud cover is still due to subgrid-scale clouds (i.e. cloud fraction below 100%). This subgrid-scale cloud scheme of non-convective clouds in the LM (Schrodin, 1995) is based on a simple relative humidity dependent parameterisation, which was designed for coarse scale hydrostatic models. The scheme is very robust, but probably too insensitive for small scale applications and may underestimate the influence of altered surface fluxes on cloud formation.

During nine days of the 30-day LITFASS-2003 period, rain occurred in the LM domain. All model versions predict similar precipitation fields at these days except
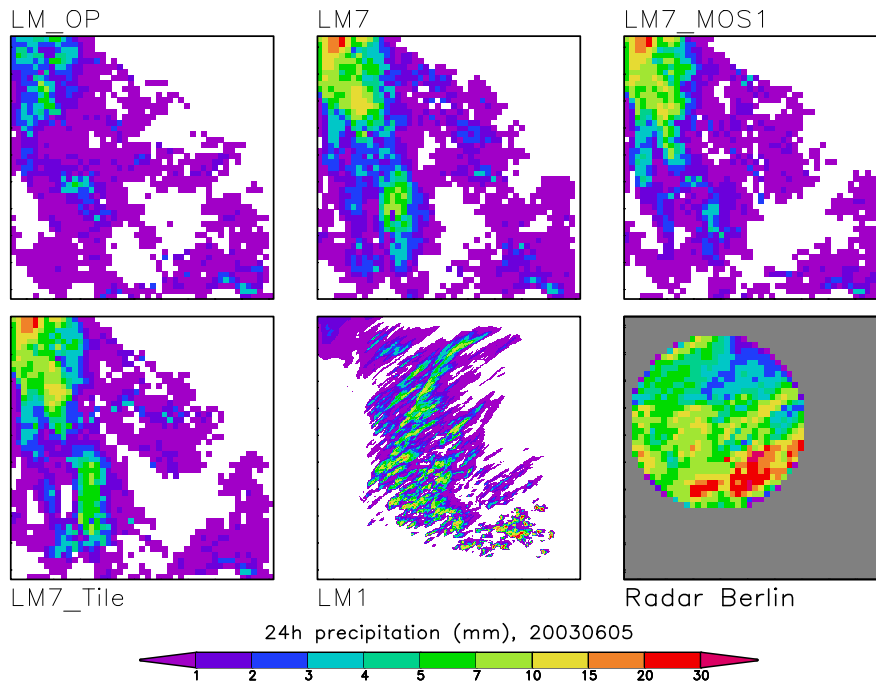
Figure 5.6: Accumulated precipitation during 5 June 2003 in the LM domain predicted by various LM versions (operational LM (LM_OP); improved model version LM7; with mosaic scheme (LM7_MOS1); with tile scheme (LM7_TILE); high resolution LM1 with 1 km grid spacing) and observed by the radar Berlin.

at 5 July 2003 (see Fig. 5.6). It is not possible to give a clear explanation for the differences between the model results at that day. Rainfall occurred late in the evening, when surface fluxes do not longer have a direct effect on cloud processes. It is most likely that differences in the ABL structure interacted nonlinearly with parameterised convection. Similar to cloud formation, refinement and switching off parameterised convection have a larger impact than altering the forcings from the surface. Comparing model results to observations of the radar at Berlin, it becomes obvious that neither general model improvements (LM7) nor heterogeneity parameterisations (LM7_MOS1 and LM7_TILE) cause any improvement in precipitation forecast. High resolution integrations (LM1) also fail to predict the location and amount of rainfall, but at least the band structure of rainfall is in closer agreement to observations than the fields of all coarse scale LM simulations.

5.2 Humidity Budget

One result of the previous chapter is that simulations with improved flux representation correct systematic errors of the boundary layer evolution only partly. A possible explanation is that surface fluxes are not the only processes which influence atmospheric state variables and that other effects like e.g. horizontal advection may have a considerable impact. The relevance of the surface fluxes compared to other

processes can be assessed by a budget analysis. Each flux variable can be associated with a state variable which is altered by the divergence of the flux. Sensible and latent heat fluxes correspond to dry static energy $h := \rho c_p \Theta$ and absolute humidity $a = \rho q$, respectively. The following budget equation relates state variables and fluxes:

$$\frac{\partial}{\partial t} \int_V \rho \Psi \, dV = \int_{\partial V} \rho \Psi \vec{v} \vec{n_a} \, dA + S \tag{5.1}$$

with Ψ equal to $c_p \Theta$ or q. The change of the state variable in a volume V is equal to the integral of fluxes over the surface of the volume ∂V plus an internal source function S. The internal source term S represents all diabatic processes like e.g. radiative heating or heat and moisture release due to phase changes. If the flux integral in (5.1) is calculated by grid-scale variables, all subgrid-scale processes like parameterised turbulence and moist convection are added to the source function S. Assuming the volume V to be an atmospheric grid-box connected to the surface, the flux integral can be subdivided into contributions from surface fluxes F_0^Ψ, from lateral fluxes and from fluxes through the upper boundary:

$$\frac{\partial}{\partial t} \int_V \rho \Psi \, dV = \int_{\partial V_{sur}} F_0^\Psi \, dA + \int_{\partial V_{lat}} \rho \Psi \vec{v_h} \vec{n_a} \, dA + \int_{\partial V_{top}} \rho \Psi w \, dA + S \tag{5.2}$$

By calculating all four contributions on the right hand side of (5.2), it is possible to evaluate the relevance of surface fluxes.

Although the model state provides all data needed to integrate the fluxes over all boundaries, this diagnosis is complicated by numerical problems: In general, horizontal fluxes are rather homogeneous and the contributions to the flux integral at the inflow side of the box and at the outflow side nearly cancel each other. The net divergence of the atmospheric flow (second and third term of (5.2)) is essentially a small difference of big values. Consequently, it is necessary to use exactly the same formulas concerning temporal and spatial discretisation as implemented in the dynamical core of the LM to calculate these terms. Unfortunately, most non-hydrostatic mesoscale models like the LM use advective formulations instead of flux formulations. This has two implications: At first, the flux divergence is splitted by the product rule into a advective and mass convergent term, which are treated separately. Secondly, the air density is not a prognostic variable and mass conservation is in general not perfectly assured.

These difficulties must be considered if changes in mass have a significant impact on the budget. The variance of any budget quantity can be subdivided into three components (neglecting third order moments):

$$\text{Var}\,(\rho\Psi) = \overline{\rho}^2 \, \text{Var}\,(\Psi) + \overline{\Psi}^2 \, \text{Var}\,(\rho) + 2\overline{\rho}\,\overline{\Psi} \, \text{Cov}\,(\rho, \Psi) \tag{5.3}$$

(with Ψ equal to $c_p \Theta$ or q). Setting e.g. Ψ equal to $c_p \Theta$, (5.3) states that the variability of the dry static energy can be explained by fluctuation of potential temperature Θ or mass ρ. The third term takes correlations of both fluctuations into account.
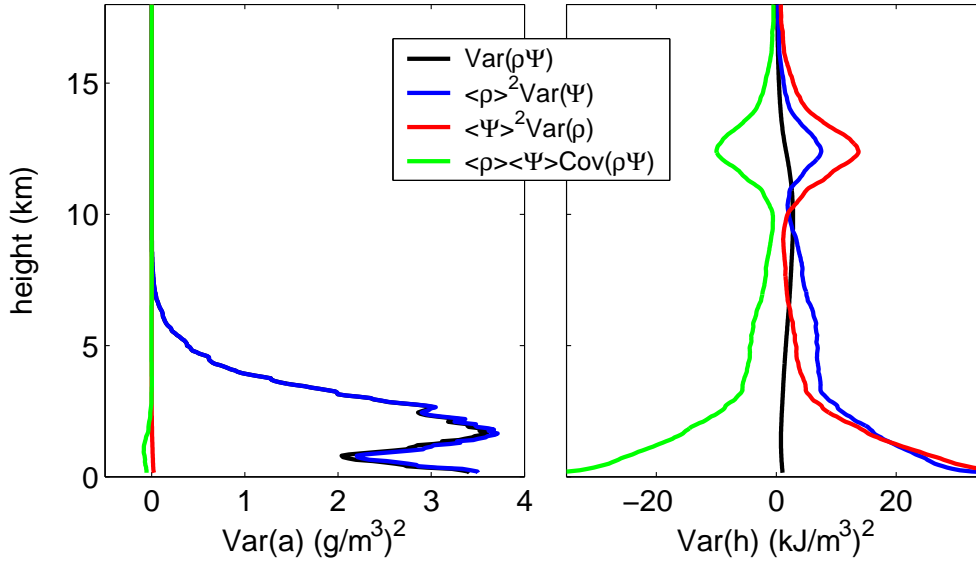
Figure 5.7: Left: Separation of standard deviation of absolute humidity a into components induced by variations in air density (blue), by humidity fluctuations (red) and by their correlation (green). Right: same as left, but for the dry static energy h and with respect to potential temperature fluctuations. Both analyses are based on all radiosonde ascents at Lindenberg during LITFASS-2003.

It is straightforward to estimate all three components from the time series of all radiosonde ascents during LITFASS-2003, as presented by Fig. 5.7. Regarding the humidity budget, almost all variability is caused by variations in specific humidity. Changes in the absolute humidity due to variations of air mass and correlations between specific humidity are negligible. In contrast, the contributions of temperature and density variations to the dry static energy budget are of the same magnitude. It is remarkable that these contributions are almost completely compensated by the covariance term, which indicates that potential temperature and air density are highly anticorrelated. This relation is a direct consequence of the gas equation under isobaric conditions.

In essence, mass and humidity budget are in practice (at least during LITFASS-2003) almost independent, whereas the development of the energy and mass budget are tightly connected. Any budget diagnosis method can easily be checked by calculating the left and right hand side of (5.2) separately and analysing the residuum. Applying this test to the humidity budget gives very good results, but fails with respect to the energy budget due to the aforementioned numerical problems. This result does not necessarily imply that LM predictions violate energy conservation significantly, but it shows that it is not possible to diagnose energy fluxes through atmospheric boundaries with an accuracy that is required for a budget analysis. Consequently, the following analysis will be restricted to the humidity budget.

The impact of evapotranspiration fluxes on humidity is expected to increase with the size of the box that is considered, because small scale humidity fluctuations
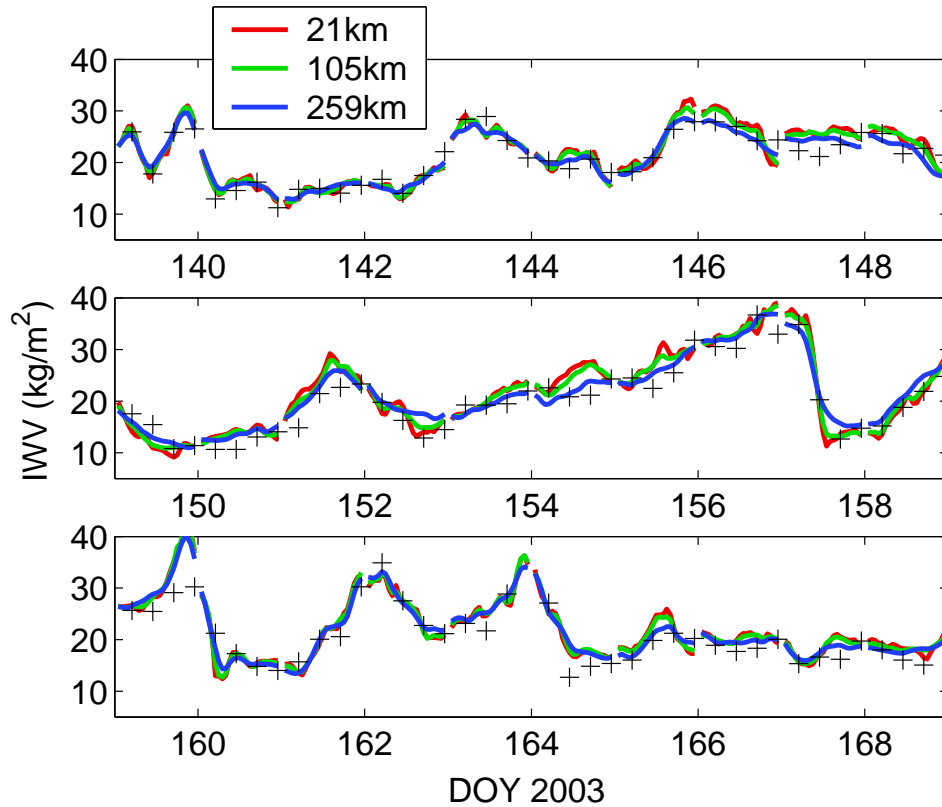
Figure 5.8: Model predicted (LM7) time series of mean vertical integrated water vapour path (IWV) for boxes centred over Lindenberg with different edge sizes. Radiosonde measurements at Lindenberg are displayed by black crosses.

which are advected through the box cancel each other. Therefore, the budget analysis is performed using boxes with edge sizes of 21, 105 and 259 km; all centred over Lindenberg. The smallest box closely represents the LITFASS domain. Vertically, all boxes reach to the top of the model (~23 km height). At heights above the troposphere, it is not necessary to choose the position of the upper boundary carefully, because atmospheric moisture is confined to the lower part of the troposphere and the upper parts of the atmosphere do not contribute to the humidity budget at all (see also Fig. 5.7).

Fig. 5.8 shows the box mean of vertically integrated water vapour (IWV) content diagnosed from LM7 predictions and observed by radiosondes at Lindenberg. Observations and model results agree remarkably well. The mean IWV of the smallest box shows the largest variability, which is likely due to advection of small scale humidity fluctuations. Nevertheless, it is worthwhile to mention, that the IWV of all boxes agree very well, although the size of boxes differs by one order of magnitude. This is an indication that large changes in IWV are caused by large scale phenomena like synoptical forcings and are not generated locally.
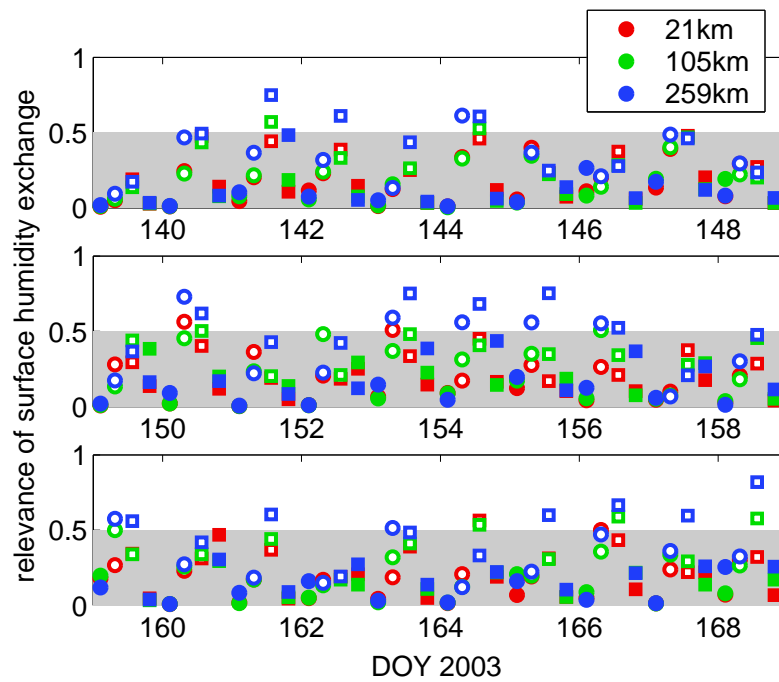
Figure 5.9: Relevance of the surface humidity exchange r_{eva} diagnosed for boxes of different size and averaged over 6 hours: filled circle (0-6 UTC), circle (6-12 UTC), square (12-18 UTC), filled square (18-24 UTC). Analysis based on LM7 integrations.
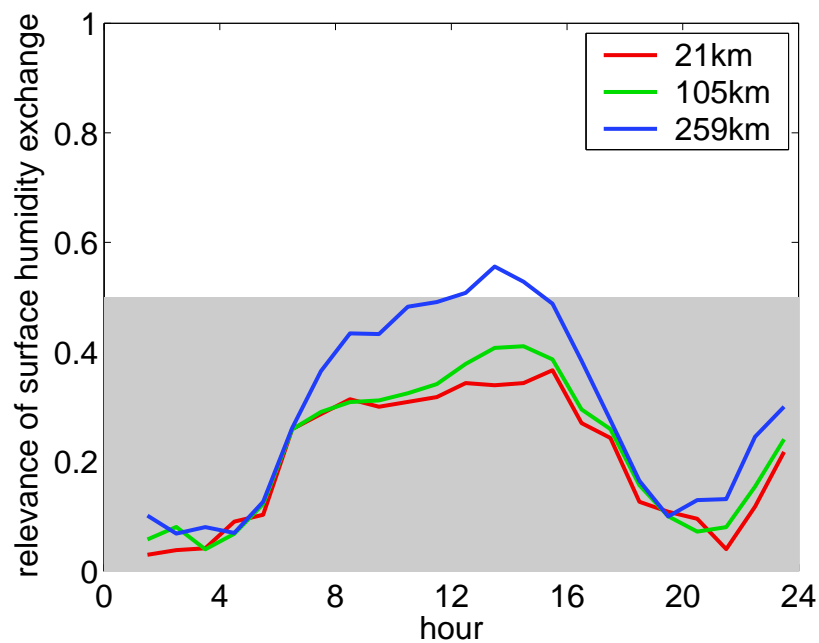

Figure 5.10: Mean daily cycle of relevance of surface humidity exchange estimated similarly to Fig. 5.9

In order to quantify the impact of evapotranspiration in comparison to other processes, the relevance of surface humidity exchange r_{eva} is defined as ratio of the fraction of IWV tendency that is attributed to evapotranspiration:

$$r_{eva} = \frac{|\Delta \text{IWV}_{\lambda E_0}|}{|\Delta \text{IWV}_{\lambda E_0}| + |\Delta \text{IWV}_{v_h q}| + |\Delta \text{IWV}_{S_q}|} \tag{5.4}$$

with the IWV tendencies initiated by surface fluxes $\Delta \text{IWV}_{\lambda E_0}$, by lateral fluxes $\Delta \text{IWV}_{v_h q}$ and by internal sources ΔIWV_{S_q}.

Fig. 5.9 shows the times series of r_{eva} derived from LM7 integrations and Fig. 5.10 summarises these results as mean daily cycle. The relevance is low during nighttime due to the shut down of plant transpiration. The relevance is higher for larger domains since advection of small scale humidity fluctuation is less important. There are only two situation during LITFASS-2003 when the surface fluxes have the dominant impact ($r_{eva} > 0.5$) on the development of the moisture budget in the LITFASS domain. This finding has important implications for both model configurations and experimental setups: The LITFASS domain is too small to investigate the effect of surface fluxes on the evolution of atmospheric profiles and budget without severe perturbations due to advection. At least a domain covering more than $\sim 250 \times 250 \, \text{km}^2$, like the LM domain, is needed to capture surface fluxes and atmospheric evolution as a closed cycle on suitable days with low wind speed conditions.

5.3 Atmospheric flux profiles

The main source of turbulent sensible and latent heat fluxes in the atmosphere are the near surface fluxes H_0 and λE_0, respectively. The divergence of the atmospheric fluxes affects the profiles and budgets of atmospheric state variables directly. Atmospheric fluxes are consequently linking the exchange between surface and atmosphere, discussed in the last chapter, to the evolution of the atmosphere and in particular of the ABL, which was the focus of the previous sections. Therefore, it is worthwhile to evaluate the models performance to predict atmospheric fluxes directly.

5.3.1 Verification of flux profiles

Only vertical turbulent fluxes will be considered in the following. Horizontal turbulent fluxes are in general small and become important only at the edges of convective up- and downdrafts. They are hardly measurable and models with a horizontal grid spacing that is significantly larger than the height of the ABL (e.g. LM7) neglect these fluxes because they are not relevant on the resolved scales. Models with 1km

grid spacing, like LM1, should, however, take these fluxes into account, but unfortunately the required three dimensional parameterisation of turbulence had still been under development at the time this study was created. This model deficiency will likely result in an overestimation of the horizontal variablity at small scales.

Fig. 5.11 shows three examples of model predicted and observed atmospheric flux profiles. The integrations LM7_MOS1 and LM1 have been selected to represent simulations with a coarse and a fine atmospheric resolution, respectively, but with very similar forcings from the surface. The atmospheric grid of LM7_MOS1 is too coarse to resolve any turbulent eddies within the LITFASS domain. It implies that the total turbulent exchange is parameterised by the subgrid-scale turbulence scheme. Regarding LM1, the total turbulent flux is the sum of the parameterised component and the resolved grid-scale contribution. The resolved part can be estimated by a eddy covariance (EC) method. The ensemble mean, required by this EC technique, is approximated by averaging in space and time over the LITFASS domain and one hour:

$$
\begin{aligned}
H_{scal}(z, t_0) &= c_p \overline{\rho w' \Theta'} && (5.5) \\
\lambda E_{scal}(z, t_0) &= L_h \overline{\rho w' q'} && (5.6) \\
\text{with} \ \ \overline{x}(z, t_0) &:= \frac{1}{1\,\mathrm{h}} \frac{1}{A_{Lit}} \int_{t_0}^{t_0+1h} \int_{A_{Lit}} x(\vec{r_h}, z, t')\, d\vec{r_h}\, dt' \\
\text{and} \ \ x'(\vec{r_h}, z, t) &:= x(\vec{r_h}, z, t) - \overline{x}(z, t_0) \ \forall\, t \in [t_0, t_0 + 1h]
\end{aligned}
$$

The LM results are compared to large-eddy simulations (LES) of the model PALM (Raasch and Schröter, 2001) and HELIPOD measurements (Bange et al., 2006). PALM was operated with a grid spacing of $50\,\mathrm{m}$, which allows to resolve almost all eddies that are relevant for the transport of energy and moisture (for details see Uhlenbrock et al., 2004). Since the model equations that determine the resolved dynamics are based on first principle, it is expected that a LES can represent the turbulent state of the atmosphere very accurately. The surface fluxes are prescribed externally based on the land-use map and the flux composites that have been derived for each land-use type. Due to this measurement forced integration mode, the LES can be considered as a surface flux extrapolation tool, which derives atmospheric flux profiles and the subsequent development of the ABL on the basis of physical principles.

Nevertheless, it is unavoidable to make some model assumptions that limit the accuracy of the LES results: At first, PALM uses periodic lateral boundary conditions. Advective effects, which turned out to be important by the budget analysis, cannot be taken into account. Secondly, the dynamical equations of PALM make use of the Boussinesq approximation, which assumes a constant density except for the buoyancy term. PALM calculates only kinematic fluxes and the transformation to energetic fluxes requires an assumption about the value of the constant air density, which cannot be related to any model assumption. At last, the forcing at the upper boundary, especially the wind stress, is time constant. Changes in the large scale dynamics, like turning of wind direction, are not represented.
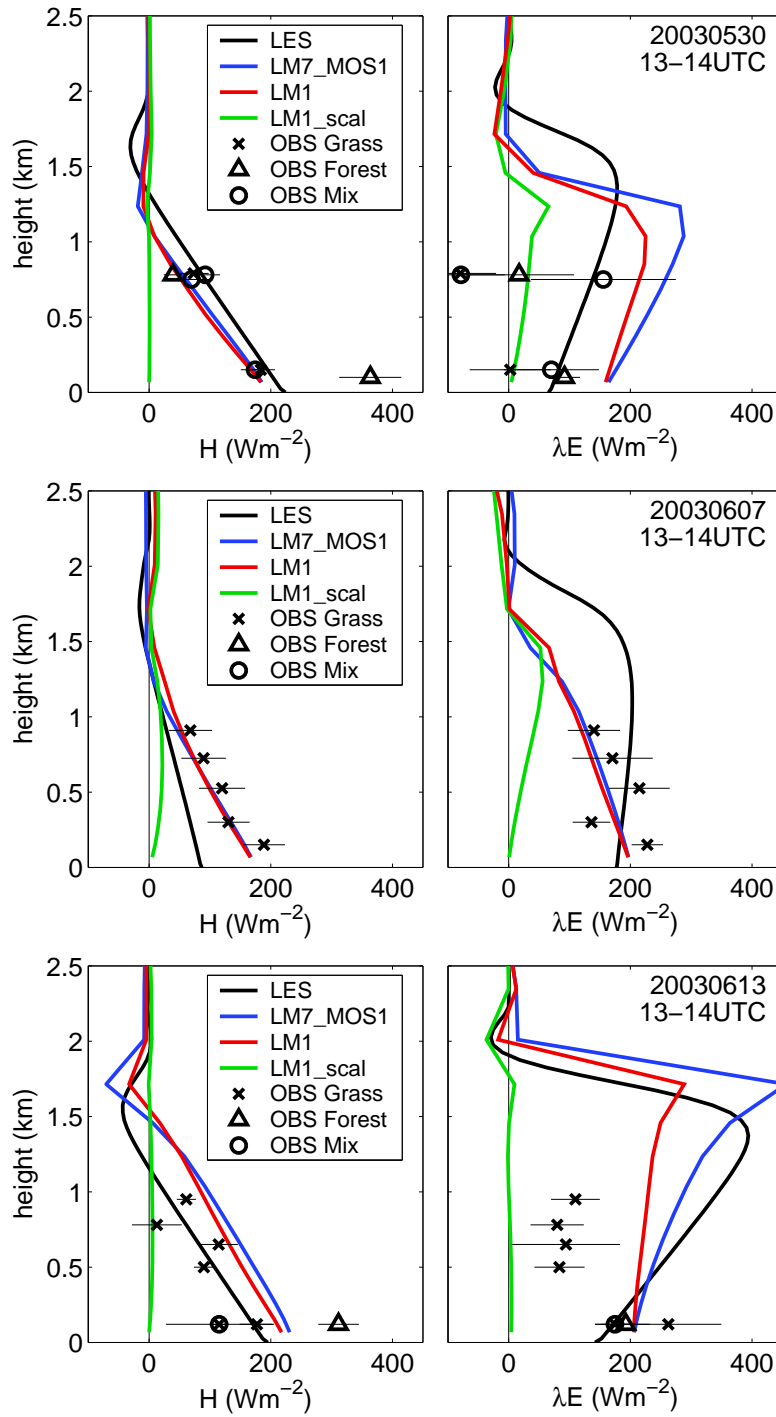
Figure 5.11: Vertical profiles of sensible (right) and latent (left) heat fluxes at three different days. Model results are averages over the LITFASS domain. For LM1, the resolved grid-scale contribution (LM1_scal) is displayed additionally. Observations (OBS) are derived from HELIPOD flight legs in north-south direction over forest and over grassland and an east-west flight leg over various types of land-use (MIX).

The airborne system HELIPOD is measuring temperature, humidity and wind vector along the helicopter flight leg with a very high sampling rate. The EC technique is applied to estimate mean fluxes averaged over each leg. The statistical uncertainty due to the limited sample size is indicated by error bars (Fig. 5.11). A comparison of HELIPOD observations and model results in terms of direct matches is not possible because the HELIPOD observations are only representative for the flight leg over a certain type of land-use, but not for the whole LITFASS domain. Nevertheless, the HELIPOD measurements give valuable information about the magnitude of the true average flux.

Inspecting Fig. 5.11, all results resemble the following general features of a convective boundary layer (see standard textbooks, e.g. Stull, 1988): The sensible heat flux H decreases linearly with height. Close to the top of the ABL H becomes negative due to the entrainment of warm air from the free atmosphere aloft. In contrast, the latent heat flux may increase with height and often reaches its maximum at the top of the ABL. This effect is due to dry air that is entrained downwards from the free atmosphere.

Concerning the sensible heat flux, model results and observations agree quite well; deviations are larger for the latent heat flux. Turbulent motion during LITFASS-2003 is mainly driven by temperature anomalies and not by humidity anomalies. Humidity can be considered almost as passive tracer. Consequently, moisture transport is less organised and less predictable than heat transport.

The examples displayed by Fig. 5.11 are not necessarily representative for all situation during LITFASS and can only give indications on interesting issues, that need further analysis. Looking at the examples in detail, three aspects are worth a more careful analysis, which will be presented in the next two subsections:

- The LM tends to underestimate the entrainment flux of sensible heat at the top of the ABL.

- Although the atmospheric resolution differs and a high resolution simulation can resolve a larger part of the eddy spectrum, LM7_MOS1 and LM1 give quite similar results.

- The grid scale contribution to the total fluxes (see LM1 results), especially to the sensible heat flux, is very small.

Investigations are extended to more cases and to the full model domain by a statistical comparison of atmospheric fluxes predicted by LM7 and LM7_MOS1 with respect to fluxes forecasted by high resolution LM1 integrations (Fig. 5.12). There are no great systematic deviations between the simulations with different atmospheric resolution; biases are small for both H and λE. Obviously, dynamical heterogeneity effects, which alter the turbulent transport systematically, are not detectable. The random fluctuations (RMSE in Fig. 5.12) are bigger, in particular with respect to the latent heat flux. Again, this supports the hypothesis that latent heat flux
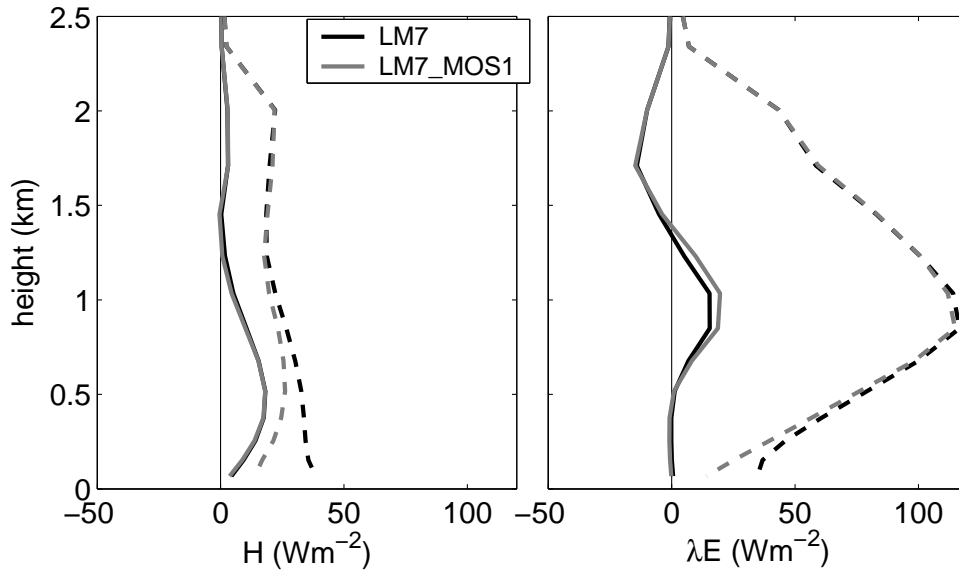
Figure 5.12: Mean systematic deviation (BIAS, solid line) and root mean square error (RMSE, dashed) of flux profiles with respect to LM1 simulations estimated from 12 UTC predictions at nine golden days and averaged for the whole LM domain.

is less predictable since humidity acts like a passive tracer. The surface fluxes of LM7_MOS1 are in closer agreement to LM1 than the surface fluxes LM7, which is indicated by a smaller RMSE of LM7_MOS1 close to the surface. This advantage of LM7_MOS1 vanishes rapidly with increasing height, in particular with respect to the latent heat flux. This means that most of the uncertainty in predicted fluxes in the upper part of the ABL are not due to surface fluxes, but due to entrainment processes from above.

5.3.2 Entrainment fluxes

Experimental data (e.g. Caughey and Palmer, 1979) as well as LES results (e.g. Kim et al., 2003) indicate that the entrainment flux of sensible heat H_e is approximately proportional to the corresponding surface flux H_0. This is not a direct physical, but a statistical relation, which describes the average behaviour of nature. The observed constant of proportionality is usually in the order of -0.1 to -0.2. Fig. 5.13 shows that the LES results of PALM resemble this relation quite well. Entrainment fluxes of LM7 are in contrast independent from the current magnitude of the surface flux and always very low.

This behaviour is a direct consequence of the turbulence scheme: In reality, large eddies are generated by instabilities close to surface, rise and finally penetrate the capping inversion due to inertia. Such processes are called non-local, since the mixing and the triggering of eddies are located at different places. The turbulence closure in the LM is, however, completely local. This means that mixing will only
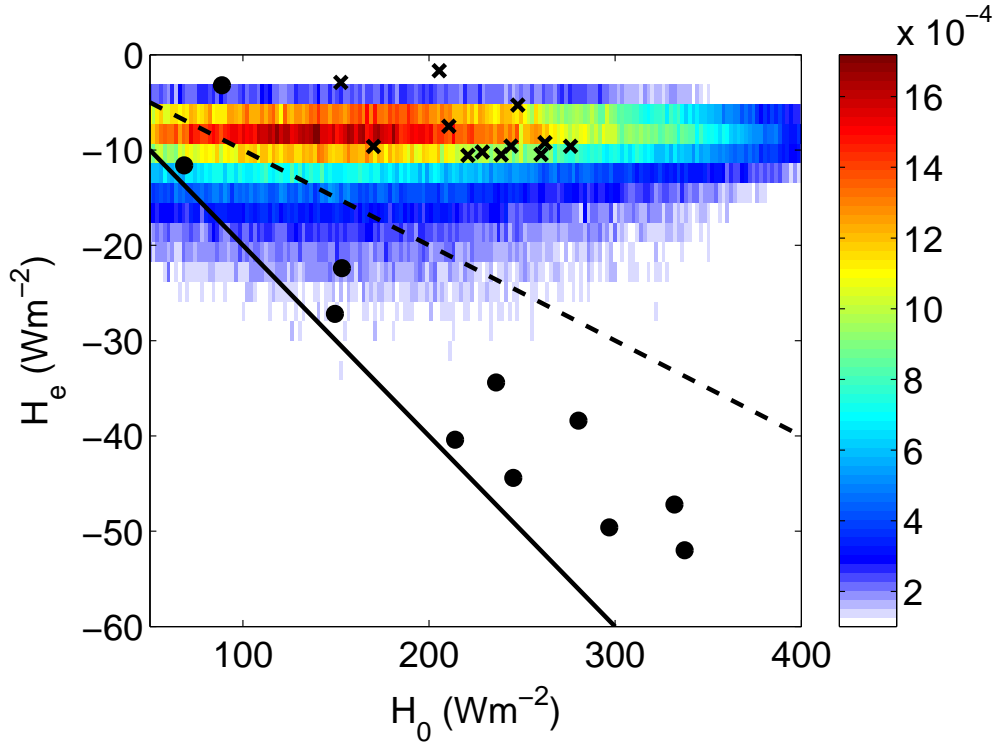
Figure 5.13: Shaded colours: Joint frequency distribution (arbitrary units) of surface heat flux H_0 and entrainment flux H_e at the top of ABL estimated from LM7 simulation (sample: LITFASS-2003 period, 9-14 UTC, LM domain). Crosses indicate single value combination predicted by LM1 (sample: 30 May 2003, 7 June 2003; averages over 1 h and LITFASS domain) and the dots mark values obtained by LES simulation (sample: 30 May 2003; averages over 15 min and LITFASS domain). The solid and dashed lines indicate the relations $H_e = -0.2H_0$ and $H_e = -0.1H_0$ as a guide to the eye, respectively.

be switched on if instability occurs at the same position. The high resolution simulations LM1 does not give better results (see crosses at Fig. 5.13) because the turbulent transport is still almost completely parameterised, as mentioned before. It can be expected that if more of the turbulent transport becomes resolved by grid-scale dynamics, non-local processes in terms of large eddies will automatically be taken into account and will enhance the prediction of entrainment fluxes. However, the following paragraphs will demonstrate that resolving more eddies alone is not sufficient to solve the problem. It is most likely that the vertical model resolution at the top of the ABL is too coarse to resolve penetrating eddies sufficiently.

In summary, the representation of entrainment at the top of the ABL can be identified as serious model deficiency of LM. Concerning coarse grid simulation, which must parameterise the turbulent transport, it is mandatory to enhance the turbulence scheme by non-local components (e.g. Holtslag and Moeng, 1991). Regarding high resolution simulation which partly resolve turbulent mixing, the sensitivity with respect to vertical resolution should be tested.
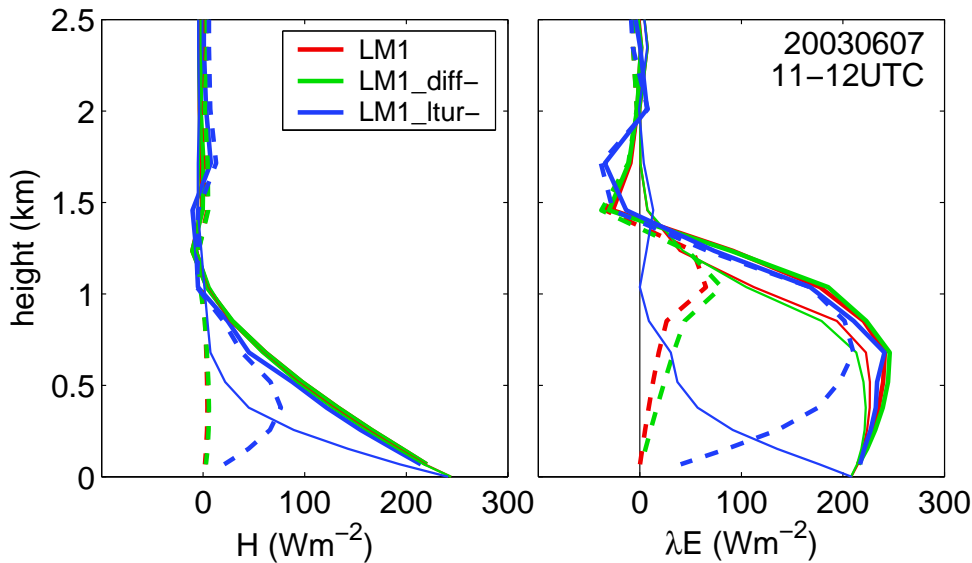
Figure 5.14: Mean flux profiles averaged over the LITFASS domain predicted by LM1, LM1_diff- (decreased horizontal mixing) and LM1_ltur- (smaller asymptotic turbulent length scale). Thick solid lines show the total flux, thin lines the parameterised component and dashed lines the resolved part.

5.3.3 Resolved versus parameterised fluxes

The high resolution LM1 simulations predict remarkably low resolved turbulent fluxes. Before addressing the question whether this behaviour is realistic, it is necessary to identify the mechanisms that partitions parameterised and resolved fluxes. Two hypothesis are tested: At first, the horizontal mixing, which is implemented to damp very short waves and to ensure numerical stability, might be too strong and suppresses horizontal inhomogeneities which are needed to excite resolved circulations. The sensitivity with respect to this effect is tested by a simulation similar to LM1, but with the horizontal diffusivity constant reduced by 50% (LM1_diff-). Secondly, the subgrid-scale turbulence might be too dominant and suppresses resolved circulations by removing instabilities too quickly. One of the most important constants of this parameterisation is the asymptotic turbulent length scale l_{tur}^*, which is set to 500 m by default in the LM. Reducing this value to 100 m (LM1_ltur-) makes the subgrid-scale scheme less effective.

The reduction of the horizontal diffusion slightly enhances the resolved component (see Fig. 5.14), but has only a very small overall impact. In contrast, the reduction of the turbulent length scale, has a very strong effect: In the upper part of the ABL, the parameterised fluxes are reduced and nearly all turbulent transport becomes resolved. Remarkably, the total turbulent flux remains nearly unchanged for all simulations. This means, that changing the asymptotic turbulent length scale alters the partitioning of the turbulent transport into the parameterised and resolved part, but the total flux seems to be determined by an attractor.
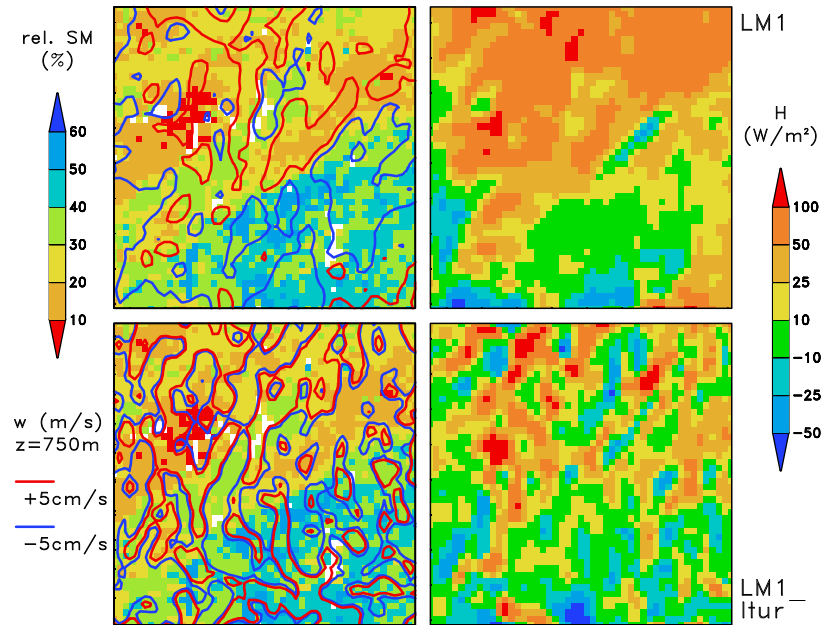
Figure 5.15: Left: Relative soil moisture of the upper layer shaded by colours and contours of vertical velocity at 750 m above ground at 7 June 2003, 12 UTC simulated by LM1 (top) and LM1_ltur- (bottom, smaller asymptotic turbulent length scale). Right: Total sensible heat flux 750 m above ground.

It is possible to give a physical explanation for such an attractor as far as H is concerned: A heat flux profile, which decreases not linearly with height, will result in differential heating of the ABL, which will be immediately counteracted by compensating heat fluxes. The linear shape of the profile is the only quasi-stationary solution. As long as the boundary values given by the surface flux, the entrainment flux and ABL height are not altered, the whole profile is fixed and cannot be modified by a parameterisation scheme.

Although mean flux profiles remain unchanged, the spatial structure of the fluxes is affected. The total heat flux structure at the middle of the ABL is displayed in Fig. 5.15. Compared to LM1, LM7_ltur- exhibits much more small scale variability, which nicely corresponds to the structure of the average vertical velocity field. Most of the turbulent transport in LM1 is simulated by the subgrid-scale turbulence scheme in terms of non-resolved eddies. Reducing the turbulent length scale results in shifting the wavelength of these eddies towards the resolved scale and they become visible as fluctuation with a wavelength in the order of the grid spacing. Although these variations cancel out each other if averages over a few grid points are considered, they can significantly affect the model simulation by the interaction of nonlinear parameterisation (e.g. the moist convection scheme or microphysics), which utilise forcing data at the grid point scale. Additionally, Fig. 5.15 illustrates, that the soil moisture inhomogeneities induced by the convective rain event at 5 June 2003 (see Section 3.3, Figures 3.10 and 3.12) affects not only surface fluxes, but excites circulations throughout the whole ABL.
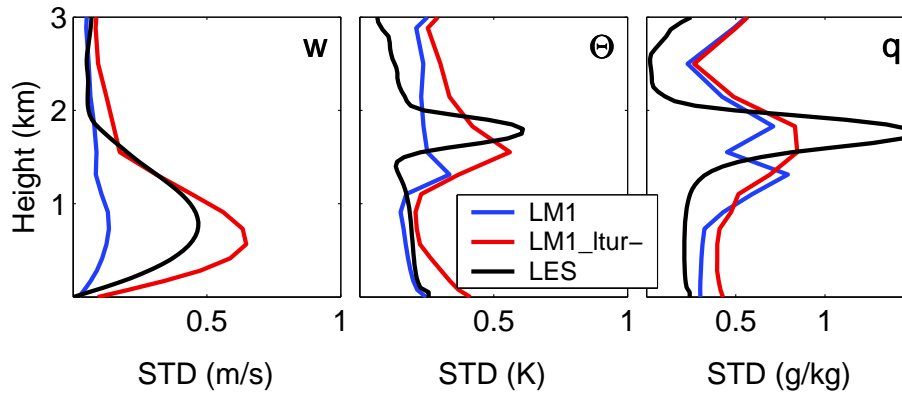
Figure 5.16: Profiles of standard deviation estimated from model simulated fields at 7 June 2003, 12 UTC, which cover the Extended-LITFASS domain. LES results are aggregated on the LM grid in order to analyse data with the same resolution.

In order to decide whether LM1 with almost no resolved turbulent mixing or LM1_ltur- are closer to reality information about the spatial structure of flux patterns are needed. Unfortunately neither direct measurements nor data about the spatial flux structure from LES are available. A somewhat indirect assessment can be provided by comparing the variance profiles of state variables predicted from the two LM version to LES results (see Fig. 5.16). LES data has been aggregated on the 1 km grid of the LM to ensure that the same portion of the variability spectrum is analysed. The variability of Θ and q given by LM1 in the lower part of the ABL agrees quite well with the LES results, but the variability of w and of all variables in the entrainment zone is significantly underestimated. In contrast, the variability of w predicted by LM1_ltur- is slightly larger than given by LES, but still in quite good agreement. Additionally, LM1_ltur- yields a higher variability of Θ and q in the entrainment zone, which is, however, still smaller and less pronounced compared to the LES. On the other hand, LM1_ltur- tends to overestimate the variability of temperature and humidity in the lower part of the ABL. In essence, this comparison indicates that the settings of l_{tur}^* should be reconsidered, because LM1 seems to generate too few resolved eddies. But recalibrating l_{tur}^* will not solve all problems. Again, the representation of the entrainment turned out to be a serious model deficiency and must be improved in order to adequately simulate the right ratio of variablity in the ABL versus variability in the entrainment zone.

5.3.4 Small scale variability of fluxes

The last chapter demonstrated that the approximation of the mosaic and the tile approach (neglecting small scale variability at the lowest model level while diagnosing surface fluxes) does not introduce significant errors. But this is not the only simplification of these approaches: Using a coarse atmospheric grid additionally implies
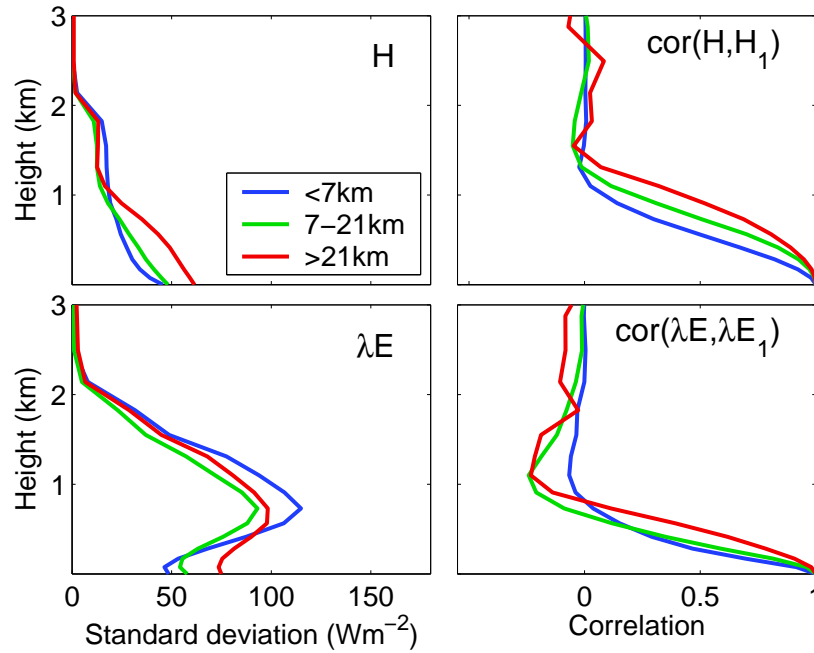
Figure 5.17: Left: Mean standard deviation of parameterised turbulent atmospheric fluxes estimated as average from LM1 integration results at 12 UTC at nine golden days. Right: Correlation of fluxes at different height with respect to the flux at the top of the lowest atmospheric layer. The analysis considers various horizontal scales by an appropriate spatial high- and low-pass filtering.

neglect of small scale variability, especially of fluxes and of the ABL height. The relevance of these two aspects will be investigated in order to confirm the validity of both approaches.

The variability of fluxes can be analysed by inspecting the mean standard deviation profiles of turbulent fluxes shown by Fig. 5.17. The effect of variablity at different horizontal scales is separated by an appropriate spatial high- and low-pass filtering of the corresponding fields. A high correlation to the near surface fluxes indicates that the variablity is induced by the surface, whereas the variablity in regions with small correlation is most likely generated by random and non-surface dependent processes.

In the lower part of the ABL the small scale standard deviation is rather small. In the entrainment zone the small scale contribution is considerably larger, but the correlation with surface fluxes is close to zero. This means that these fluctuations are not controlled by the surface. Inspecting the correlation profiles it is evident that the correlation to surface flux anomalies decays most rapidly with height for small scale flux fluctuations. It follows that these fluctuations have a small vertical extent and are probably modified quite effectively by horizontal diffusion. Accordingly, large scale anomalies in sensible heat fluxes have the highest correlation with the boundary layer height (see Fig. 5.18) and small scale variations are of minor importance. These
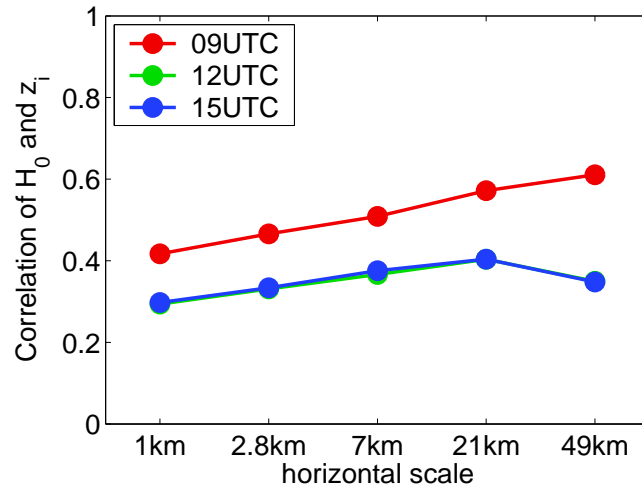
Figure 5.18: Correlation of boundary layer height z_i with surface sensible heat flux H_0. The fields have been low-pass filtered to exclude variability that is smaller than the values indicated on the x-axis. Sample: LM1 simulation for the whole LM domain for nine golden days.

findings indicate that the relevance of small scale flux variations that are initiated at the surface are low. This substantiates the validity of the mosaic and the tile approach.

5.4 Main results

From the point of view of NWP applications, accurate predictions of surface fluxes itself are of minor interest, but they might be beneficial for the forecast of atmospheric state variables. The evaluation of atmospheric state variables and fluxes presented in this chapter confirmed this impact, but also revealed other model problems which are independent from surface fluxes:

- The ABL predicted by the operational model (LM_OP) at Lindenberg is too cold, too wet and too thin. These errors are reduced in forecasts using model improvements (LM7) because of more accurate surface fluxes. Simulations with enhanced parameterisation of surface heterogeneity give similar results to LM7 as far as atmospheric profiles are considered.

- An analysis of the humidity budget revealed that most of the time advective effects explain more of the changes in the water vapour content over the LIT-FASS domain than the surface fluxes. Only if larger domains (approximately 250 km by 250 km) are considered the influence of surface fluxes tend to prevail in the afternoon. The errors in predicted ABL characteristics thus may partly be due to advective effects.

- The LM in all variants predicts systematically too low entrainment rates at the top of ABL. This underestimation also contributes to the aforementioned systematic errors of ABL profiles at Lindenberg. The LM exhibits no statistical dependency between the magnitude of surface sensible heat flux and entrainment unlike e.g. the LES results and findings of other studies.

- Almost all vertical turbulent transport of high resolution LM runs (LM1) is parameterised. If the asymptotic turbulent length scale is reduced, resolved grid-scale circulations take over a considerable part of the transport. Nevertheless, the sum of parameterised and resolved flux remains constant. Although the mean transport averaged over e.g. the LITFASS domain is unaffected, the spatial flux distribution is changed and the variance of the vertical wind velocity is increased.

6 Conclusions

The work presented before is mainly based on model integrations over the 30-day period of the LITFASS-2003 experiment. Consequently, the findings are more representative than results derived from a single case study, but they should only be applied in situations with similar environmental conditions. It should be considered that the landscape of the LITFASS domain and its surrounding area is intensively used by mankind for forestry and agriculture. Therefore, it is characterised by fine scale land-use contrasts on scales of a few kilometres, and the surface is densely covered by vegetation. Weather conditions in spring and summer 2003 including the LITFASS-2003 experiment were extraordinarily dry (Schär and Jendritzky, 2004) and soil moisture availability was limited.

The following paragraphs will summarise the main findings as answers to fundamental questions concerning surface-atmosphere exchange processes. The conclusions will be discussed in comparison to previous studies published in literature.

What is essential to model exchange processes over homogeneous land-surfaces successfully as a prerequisite to modelling efforts over heterogeneous surfaces?

A mesoscale model with a SVAT scheme of moderate complexity (e.g. without detailed biochemical description of photosynthesis) can simulate the most important characteristics of land-surface fluxes. In particular, the LM in combination with the SVAT scheme TERRA is able to reproduce most flux measurements during LITFASS-2003 within the accuracy of the observations. This good performance can only be achieved, if accurate input parameters are provided (Section 4.1; Mölders, 2001). A sensitivity study (Section 3.1) and the analysis of high resolution LM simulations (Section 4.3.3) revealed that especially parameters controlling plant transpiration (i.e. leaf area index, stomatal resistance, and soil moisture) are of greatest relevance. It is essential to consider the differences between various types of vegetation in all parameters. The operational LM, for example, fails to simulate the contrast of surface fluxes over forest and grass realistically because it assumes constant stomatal resistance parameters and a constant vegetation albedo for all kind of plants (Section 4.1, Fig. 4.4).

As far as the LM is considered, the following enhancements apart from heterogeneity parameterisations are recommended (see Section 2.3):

- Improvements of the land-surface parameter maps, especially of the soil type and root depth data sets (Section 3.2, Fig. 3.3).

- Land-use dependent values of vegetation albedo, and minimal / maximal stomatal resistance (Section 2.3 and Appendix B).

- Removal of the artifical flux reduction (Section 2.3.1 and Appendix D), which has already been considered in the multi-layer TERRA version.

- Revision of the drainage formulation to avoid a decoupling of soil layers with respect to soil moisture dynamics and of the lower boundary in the soil (Section 3.3, Fig. 3.7).

How can accurate soil moisture analyses be obtained?

Providing accurate soil moisture analyses is a challenging data assimilation task because observations of area averaged soil moisture on scales of some kilometres are not available. This study proposes to use soil moisture fields obtained by integrations of a SVAT scheme, which is completely driven by observational data (Section 3.3). This measurement driven soil moisture analysis (MSMA) will only give good results if the SVAT model itself is able to simulate the soil moisture evolution realistically. TERRA, the SVAT scheme of LM, has a good performance in this respect.

Concerning LITFASS-2003, soil moisture data obtained by MSMA is much closer to reality than the product of the operational variational scheme by DWD and improves the flux predictions of LM clearly (Section 4.1). MSMA captures soil moisture inhomogeneities, which are induced by heterogeneous rainfall, realistically in space and time. Assimilating radar observations is very useful in this respect. MSMA enables a mesoscale model to simulate soil moisture feedback processes, which may influence surface fluxes on time scales of one week (Section 4.2, Fig. 4.8). Additionally, MSMA ensures that soil moisture data and the model are in balance, if the same SVAT scheme is used for MSMA and model integrations. As far as surface flux predictions are concerned, the balance of a soil moisture analysis might even be more important than its accuracy in terms of close agreement to observations (case study in Section 4.1, Fig. 4.5).

Successful applications of MSMA related methods are recently published in literature (e.g. Mitchell et al., 2004; Trier et al., 2004). DWD is currently supporting research activities to extent the MSMA technique towards operational applications (Simmer et al., 2005).

How should a model experiment be designed in order to evaluate the performance of different surface-atmosphere exchange parameterisations?

Effects due to different model configurations, in particular with respect to initial and boundary conditions, likely exceed the impact of modified surface-atmosphere exchange parameterisations (Weaver et al., 2002; Schlünzen et al., 2003). Deviations of simulations can only be attributed to differences in the surface representation, if similar configurations are chosen. Equal boundary conditions are essential. This can be assured most accurately, if the same domains are used (Section 3.4, Fig. 3.13). Concerning initial conditions, it is important to maintain the same balanced soil moisture state with respect to evapotranspiration control if data from different sources is interpolated to the model grid. Keeping volumetric soil moisture constant in case of altered soil type can result in great deviations of surface fluxes (Section 3.4, Fig. 3.17). Appropriately scaled soil moisture contents should be conserved by any interpolation scheme. Alternatively, a balanced soil moisture state may be deduced by applying MSMA with a sufficiently long spin-up time.

In literature, there are two studies, which may be affected by problems due to poor experimental designs. a) Shao et al. (2001) used different model domains since they applied a nesting strategy for atmospheric refinement. They compared a run with high atmospheric and low surface resolution (HIGHATM) and one run with opposite refinement (HIGHSURF) to a reference simulation (REF) with high resolution for both components. Their finding, that HIGHATM was in closer agreement to REF than HIGHSOIL, may simply be caused by the boundary conditions: HIGHATM and REF were integrated on the same domain, HIGHSURF not. b) Mölders et al. (1996) have initialised the soil moisture homogeneously with a constant value. If the refinement affected the soil type distribution, this can easily explain the large change in surface fluxes of a factor three, which is documented by their study.

What kind of errors have to be expected if a model does not explicitly account for subgrid-scale variability?

An answer to this question based on observations is not possible since measurement uncertainties are too large (Section 4.2). The deviation with respect to high resolution simulations (1 km grid spacing) is greatest at the grid-box scale and strongly decreases when fluxes are averaged over larger domains (Section 4.3, Figs. 4.10 and 4.14). Although information on coarser scales than the grid point scale might by sufficient for many practical applications, an accurate representation of fluxes at the pixel scale is vital for any model, because most parameterisations as well as resolved processes use input data at the pixel scale. At single grid-boxes, a mean absolute BIAS of $29\,\mathrm{Wm^{-2}}$ ($35\,\mathrm{Wm^{-2}}$) in predicted latent or sensible heat fluxes has to be expected at noon for the LM at $7\,\mathrm{km}$ ($21\,\mathrm{km}$) resolution with effective parameter approach (BIAS values are obtained as average of errors in H_0 and λE_0 listed by

Tables 4.3 and 4.4). It is worthwhile to note that this error decreases only slightly by a refinement from 21 to 7 km resolution. Consequently, land-surface heterogeneity is an important issue even at resolutions below 10 km. The same magnitude of error is also found by Heinemann and Kerschgens (2005 and 2006b). Averaged over the whole model domains of this study (approximately 300×300 km^2 for 7 km resolution; 1200×900 km^2 for 21 km resolution), there are no significant deviations in predicted surface fluxes. This finding contradicts the results of Mölders and Raabe (1996) and Mölders et al. (1996), who found significant large scale effects, but it is questionable whether these signals can be attributed exclusively to variations of the surface representation (see statement at the end of the previous subsection).

What kind of heterogeneity parameterisation is preferable?

The differences of predicted surface fluxes by integrations with various heterogeneity parameterisations are in general smaller than the uncertainty of measurements. A ranking based on observations is thus not possible (Section 4.2). The performance of various heterogeneity parameterisations can be assessed using high resolution simulations as reference: Integrations using the mosaic approach are by far in closest agreement to high resolution runs (mean absolute BIAS for individual grid-boxes of 4 (8) Wm^{-2} at 7 (21) km grid spacing), followed by the tile approach (15 (28) Wm^{-2}). Worst results are obtained for the effective parameter approach (29 (35) Wm^{-2}) and dominant land-use (25 Wm^{-2}) method (Section 4.2, Tables 4.3 and 4.4). The remarkable finding that the effective parameter method is not significantly better than the dominant land-use technique confirms similar statements of Schlünzen et al. (2003). The ranking of methods agrees with the results of Heinemann and Kerschgens (2005 and 2006b). The mosaic approach is more accurate than the tile approach because it can also consider surface variability, which is not connected to the type of land-use, in particular soil moisture variations (Section 4.3.3). These additional variabilities can be so important that a coarse mosaic approach using only a few subgrid-pixels gives better results than a tile scheme with an equivalent number of sub-classes (Section 4.3, Fig. 4.14). The relevance of a dynamical description of surface heterogeneity, especially due to soil moisture variations, is also stressed by Yates et al. (2003) and Weaver (2004). In this respect, the mosaic approach is more flexible than the tile approach. Nonetheless, the mosaic approach is frequently used with more subgrid-pixels than classes defined by the tile approach. Consequently, the tile approach tends to require less computational costs. Using differentiated soil physics for each subgrid-pixel is preferable for both tile and mosaic approach.

The following recommendations for modelling efforts are concluded from these results: The dominant land-use and effective parameter approach should only be used for applications, which make no use of surface fluxes on the grid-box scale and especially do not utilise this information as input data for other parameterisations (e.g. turbulence or convection schemes). The tile approach may be an appropriate compromise between accuracy and computational costs for operational weather forecasting purposes. Research activities demanding high accuracy, should apply the

mosaic technique because it is most flexible, objective and accurate. Additionally, the mosaic approach offers the opportunities to exploit high resolution soil moisture analyses (e.g. derived by MSMA) and can easily coupled with hydrological models, which simulate lateral exchange of soil water.

What are the effects of neglecting subgrid-scale atmospheric variability in the mosaic and tile approaches?

According to blending height theory, the mosaic and tile approaches, which apply the bulk aerodynamical formula locally with the local roughness length, are only valid as long as blending height (defined as altitude at which surface heterogeneities are no longer detectable) and height of lowest model level are equal; otherwise corrections are needed. The good performance of the mosaic approach demonstrates that these concerns have no great practical relevance. Implicit assumptions about the variability at the atmospheric reference level are not necessary because an analysis of high resolution LM integration revealed that the variance of atmospheric state variables is small and not correlated strongly with surface anomalies (Section 4.2, Fig. 4.15). These statements may have to be revised under different conditions, most likely if large roughness length variations occur.

Changing the atmospheric resolution has a significant effect on cloud representation (Section 4.3.2, e.g. Fig. 4.13). Consequently, the net radiation at the surface is modified and the magnitude of the turbulent fluxes is altered. Since cloud representation shows nearly no sensitivities to changing surface fluxes by using different heterogeneity parameterisations, it is unlikely to attribute this effect to dynamical heterogeneity processes. Obviously, it is a deficiency of the cloud scheme, which accounts insufficiently for subgrid-scale condensation as e.g. outlined by Ament et al. (2004). It is recommended to revise this parameterisation and to account for subgrid-scale humidity fluctuations. Tile and mosaic schemes may give information about this variability.

How do surface fluxes affect the atmosphere?

The impact of surface fluxes on the atmosphere strongly depends on the considered region and climate conditions. Therefore, it is impossible to give a comprehensive assessment based on investigations of a single period at a single location. The following statements should only be regarded as contribution from LITFASS-2003 to the very broad issue of analysing feedback processes from the surface to the atmosphere.

Surface fluxes are only one process among others, like e.g. horizontal advection, which determine the evolution of the atmosphere. A budget analysis (Section 5.2) revealed that evapotranspiration does not explain more than half of the total humidity fluctuations unless domains of at least $250 \times 250\,\mathrm{km}^2$ in size are considered.

Consequently, integrations, which predict surface fluxes accurately within the LIT-FASS domain (e.g. LM7), can correct systematic errors in atmospheric profiles only partly (Section 5.1). Remaining errors are attributed to improper horizontal advection and to small entrainment fluxes (Section 5.3, Fig. 5.13). Typically, LM boundary layers are too thin, too cold and too wet. The differences in simulated surface fluxes induced by heterogeneity parameterisation schemes are too small to affect the evolution of boundary layer profiles.

Unlike many other studies (for a review see Pielke, 2001), this work could not detect a significant direct influence of surface fluxes on cloud formation or precipitation. Two main reason can explain this result: The period of LITFASS-2003 was dominated by high-pressure, fair weather conditions, which are rather insensitive to changes in surface fluxes. Secondly, the modifications in surface fluxes induced by heterogeneity parameterisations are only relevant on small scales. It is unlikely that these small-scale fluctuations have a large impact on processes at higher altitudes since the atmosphere is quite diffusive.

What are interesting aspects of future work?

- This work identified numerous **model deficiencies**, which have not been solved, yet. The phase shift in surface fluxes may be investigated by analysing model simulations and observations during other recent or upcoming experiment campaigns (e.g. LITFASS-98, COPS). Additionally, it might be interesting to couple the LM with a more sophisticated SVAT scheme (e.g. the Common Land Model 'CLM' (Dai et al., 2003)) in order to test whether improved representation of transpiration and of the canopy layer may be beneficial. The lack of entrainment flux should be counteracted by implementing non-local closures into the turbulence scheme of LM and enhancing its vertical resolution. This might help to reduce the systematic errors of the boundary layer predicted by LM (too thin, too cold, too wet). Stand-alone tests with the surface layer transfer scheme of LM should be performed in order to explain the errors in flux predictions over lakes.

- The **measurement driven soil moisture analysis (MSMA)** has turned out to be a promising alternative to the existing variational soil moisture analysis scheme. It is worthwhile to extend this technique towards operational applications. Two prerequisites are essential for any MSMA scheme: Accurate observations and the ability of the SVAT model to reproduce the temporal evolution of soil moisture realistically. These are the two aspects which should be in the focus of future work: Radar observations have a very good spatial coverage and high temporal resolution, but exhibit typical measurement errors like e.g. clutter or shading effects. Appropriate filter and correction procedures are needed. First tests with the multi-layer scheme of TERRA (Simmer et al., 2005) have shown that the model tends to dry out too fast during spring and that the vertical redistribution of soil moisture is erroneous. Correcting these

shortcomings will enhance the accuracy of MSMA and of LM model forecasts itself.

- Efforts to **evaluate the mosaic and tile schemes using observations** should be intensified because most of the results of this study are only based on comparisons to high resolution model integrations. Two-wavelength scintillometer measurements in the infrared and microwave spectral range (e.g. Meijninger et al., 2006) provide line averages of latent and sensible heat fluxes, which are in principle closer related to the area-averaged fluxes diagnosed by a model than the point measurements obtained at eddy-covariance stations. Implementing a forward operator to extract these line averages out of the model fields will offer the opportunity to use these observations for verification purposes. Furthermore, heterogeneity parameterisations should improve forecasts of near surface weather conditions, in particular of temperature and humidity at 2 m height. This hypothesis can be verified by a statistical comparison of integrations with mosaic or tile scheme to standard observations at SYNOP stations over a long time range and a sufficiently large domain.

- Mosaic and tile approach provide **information about the subgrid-scale variability** of surface state variables and surface fluxes. This information is an essential boundary condition for second order turbulence schemes and might be useful for non-local entrainment parameterisations, convection schemes or schemes to parameterise subgrid-scale condensation.

- The relevance of a heterogeneity parameterisation depends on the grid spacing of a model. Therefore, it is worthwhile to extend the investigations of this study to **different scale ranges** - both to coarser and finer scales: Porting the algorithm to the climate version of LM would allow investigations on the benefits of such schemes for regional climate predictions. Concerning fine scales, it is interesting to assess what kind of heterogeneity parameterisation is needed at deep-convection-resolving scales of 2-3 km, which will be grid spacings of limited area NWP models in near future (e.g. the LMK project of DWD (Doms and Förstner, 2004)).

- Up to now, the mosaic and tile schemes, as they are implemented into LM, disaggregate atmospheric variables at the lowest model level homogeneously. Applying more sophisticated **disaggregation** schemes for radiation and precipitation, like statistical methods (Hahmann, 2003) or surrogates (Venema et al., 2006), might be beneficial for regional climate integrations. Deterministic disaggregation schemes can be used to consider effects of subgrid-scale orography: Giorgi et al. (2003) demonstrate that disaggregating temperature and humidity according to the subgrid-scale orography results in improved predictions of near surface weather conditions, in particular of snow cover.

A List of symbols

Symbol	Definition
a	absolute humidity
c_{land}	type of land-use
c_p	isobaric heat capacity of air
c_{soil}	soil type
D	hydraulic diffusivity
e	turbulent kinetic energy (TKE)
E_0	total evapotranspiration
E_{trans}	plant transpiration
E_{bare}	bare soil evaporation
E_I	evaporation from interception store
E_P	potential evaporation
E_s	sublimation from snow
f_I	surface fraction covered by intercepted water
f_{LAI}	leaf area index
f_s	surface fraction covered by snow
f_{veg}	plant cover
g	acceleration of gravity
G_0	soil heat flux at the surface
h	dry static energy
H_0	sensible heat flux at the surface
H	sensible heat flux within the atmosphere
IWV	vertically integrated water vapour content
K	hydraulic conductivity
K_h	transfer coefficient of heat/moisture
K_h^{atm}	atmospheric diffusion coefficient of heat/moisture
K_m	transfer coefficient of momentum
K_m^{atm}	atmospheric diffusion coefficient of momentum
L_{down}	downwelling long wave radiation at the surface
L_{net}	long wave net radiation at the surface
l_{tur}	turbulent length scale
l_{tur}^*	asymptotic turbulent length scale
L_{up}	downwelling long wave radiation at the surface
M	momentum flux
Q	net radiation at the surface
Q_{down}	downwelling radiation
q^*	specific saturation humidity
q_{atm}	specific humidity at the atmospheric reference level
q_s	virtual specific humidity of the surface

Symbol	Definition
PAR	downward, photosynthetic active radiation
P_r	precipitation rate (liquid) at the surface
p_s	surface pressure
P_s	precipitation rate (snow) at the surface
R	Residuum of the energy balance at the surface
r_{ca}	evaporative resistance between canopy air and the atmosphere
r_{eva}	relevance of evapotranspiration
Ri_b	bulk Richardson number
r_{lc}	evaporative resistance between leaves and canopy air
RR	precipitation rate
R_s	surface runoff
r_{stom}	stomatal resistance
R_x	runoff generated at soil layer x
S_{down}	downwelling short wave radiation at the surface
S_h	stability function for heat/moisture flux
S_m	stability function for momentum flux
S_{net}	short wave net radiation at the surface
S_{up}	upwelling short wave radiation at the surface
T	temperature
T_{atm}	temperature at the atmospheric reference level
T_g	effective temperature of the surface
T_s	temperature of the snow-free surface
T_{snow}	snow temperature at the surface
T_{2m}	air temperature at $2\,\mathrm{m}$ height above the surface
$|v_h|$	wind speed at the atmospheric reference level
w	vertical wind component
W_I	water content of the interception store
W_s	water content of the snow store
z_0	roughness length
z_i	height of the atmospheric boundary layer
z_{root}	root depth
α_{bare}	short wave broadband albedo of bare soil
α_{IR}	long wave (infrared) broadband albedo
α_{snow}	short wave broadband albedo of snow
α_{so}	short wave (solar) broadband albedo
α_{veg}	short wave broadband albedo of vegetation
β	Bowen ratio
η	volumetric soil moisture
η_{ADP}	air dryness point
η_{FC}	field capacity
η_{PWP}	permanent wilting point
η_{PV}	pore volume
λ	heat of vaporisation
λE_0	latent heat flux at the surface
λE	latent heat flux within the atmosphere
κ	von-Karman constant
ρ	air density
σ	Stefan-Boltzmann constant
θ	potential temperature

B Surface parameter look-up table

Table B.1: Look-up table of land-use dependent surface parameters adopted from the operational table of DWD with some modifications according to Seuffert (2001). Vegetation albedo is estimated from LITFASS-2003 radiation measurements and stomatal resistance is adopted from Chen and Dudhia (2001).

	town	grass	crop	shrub	Decid. forest	Conif. forest	Mixed forest
Roughness length (m) z_0	1.0	0.03	0.1	0.1	1.0	1.0	1.0
Plant cover f_{veg} min/max	0.05/0.1	1/1	0.5/1	0.1/0.5	1/1	0.5/1	0.5/1
LAI f_{LAI} min/max	0.1/4	0.5/4	0.2/4	0.1/3	0/6	8/8	2.25/7
Root depth (m) z_{root}	0.3	0.15	0.3	0.4	0.8	0.8	0.8
Vegetation albedo α_{veg}	0.18	0.2	0.2	0.15	0.12	0.1	0.12
Stomatal resist. min/max (s/m)	100/ 3000	60/ 2000	100/ 3000	100/ 4000	200/ 5000	200/ 5000	200/ 5000

C Phase shift error of modelled surface fluxes

The phase shift of modelled surface fluxes compared to observations (see Fig. 4.2) can be quantified by defining the half time of the daily flux cycle as time at which half of the total sensible or latent energy input to the atmosphere is released. This half time of sensible and latent heat flux is observed at 11:20 UTC for both components, but modelled at 10:30 UTC and at 11:35 UTC, respectively. It is worthwhile to note, that the daily cycles of net radiation is not shifted at all and matches the observations almost perfectly (see Fig. 4.3).

The problem of phase shifts in H_0 and λE_0 is not completely understood yet, although it is an important issue: Standard verifications of operational LM forecasts (e.g. Damrath, 2005) report a too early maximum of parameterised convective precipitation during day time. Since convection is triggered by moisture convergence in particular due to surface fluxes, phase shifts in surface fluxes likely affect the daily cycle of convective precipitation.

Various simulations with model modifications have been performed in order to reveal model sensitivities: The humidity stress in the parameterisation of plant transpiration (LM7_HUM) has been switched on; the multilayer soil module has been used (LM7_ML) and has additionally been modified by doubling the heat conductivity (LM7_HC+). The results in terms of mean daily cycles are summarised in Fig. C.1. Neither changes in the transpiration parameterisation nor modifications
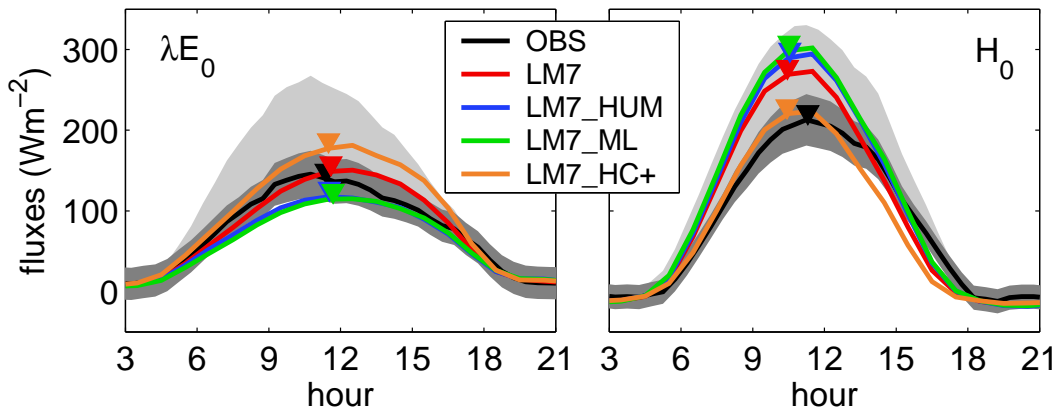

Figure C.1: Mean daily cycles of fluxes calculated by various LM version. Triangles indicate the half time of the daily flux cycle.
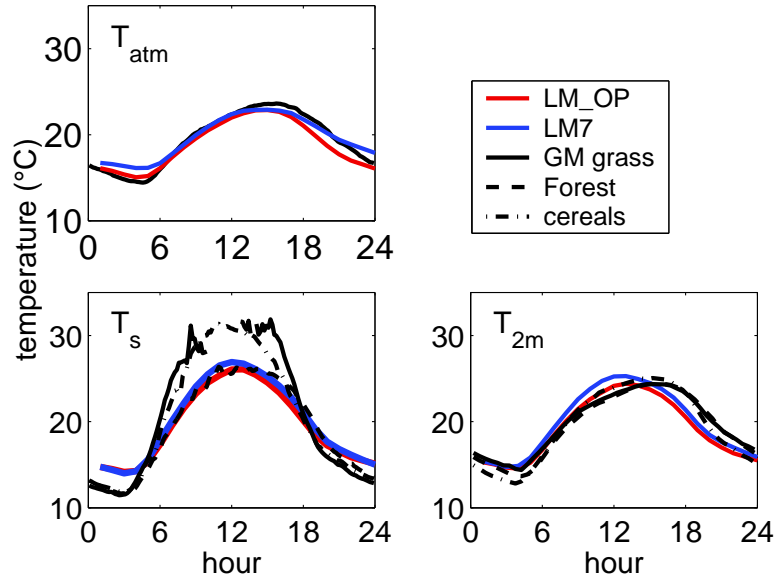
Figure C.2: Mean daily cycle of temperatures at the lowest model level (T_{atm}), the surface (T_s) and 2 m height (T_{2m}). Model data (LM_OP and LM7) represent average values for the LITFASS domain; observations (black) are displayed for the different sites within the LITFASS domain.
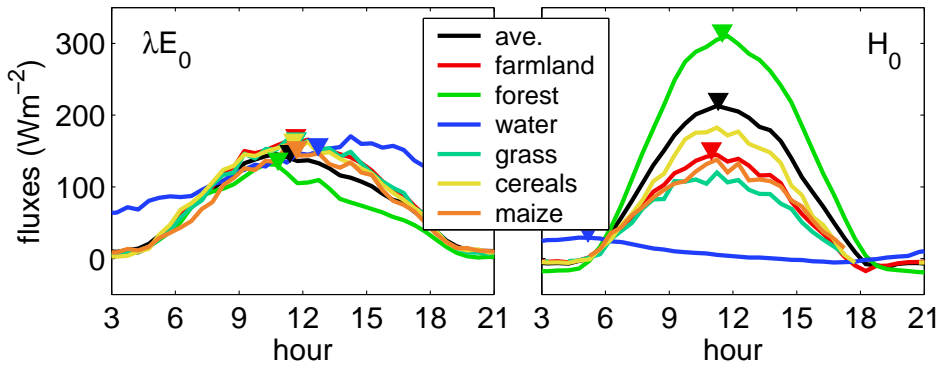

Figure C.3: Mean daily cycles of near surface fluxes measured over various surfaces. Triangles indicate the half time of the daily flux cycle. (Triangles are missing for surfaces with incomplete daily cycle due to measuring gaps at nighttime.)

in the calculation of the ground heat flux have a significant impact on the phase shift problem.

The phase shift in predicted fluxes can be caused by phase shifts in the state variables, which determine the flux according to the bulk equations (equations 2.18 and 2.12). A comparsion of observed and modelled state variables is limited to those variables influencing the sensible heat flux H_0 (Fig. C.2) and cannot be extended to the latent heat flux since near surface humidity is not measured. Deviations concerning the phase of the daily cycle of T_s and T_{atm}, which are both relevant for the diagnosis of H_0, cannot be detected. Only the maximum of T_{2m} is shifted

towards the morning. This phase shift has also been detected by the operational verification (Damrath, 2005). The latter error has, however, no direct influence on the model prediction, since T_{2m} is only a diagnostic output variable. But indirectly this error can partly explain the overestimation of soil moisture by the operational soil moisture analysis: Although the LM predicts the right amplitude of the T_{2m} evolution, it is too warm at the synoptical measuring time 12 UTC due to the phase shift. Consequently the variational soil moisture analysis scheme may correct for this deviation and enhances the soil moisture content artificially.

If state variables are correct, but not the derived fluxes, the parameterisation of the processes in the surface layer may be wrong or just too simple. The observed early maximum of latent and the late maximum of sensible heat flux, which are not reproduced by the model, occur most pronounced above forest (Fig. C.3) - an area of tall vegetation. The transfer scheme of LM does not take effects of tall vegetation into account: The heat capacity of the vegetation layer or differential insolation within the canopy is neglegted. The current parameterisations of LM are not able to reproduce land-use dependent phase shifts, which are indicated by observations (Fig. C.3). Testing of more advanced transfer schemes, which resolve tall vegetation and parameterise plant physiological processes like photosynthesis in more detail, is recommended to further address the phase shift problem.

D LM coding errors

Atmospheric models are very complex programs: The LM for example consists of more than 30 modules and more than 40000 lines of program code in total. Although models are written with much care, it is impossible to avoid coding errors. It is important to bear this fact in mind and to check the code as soon as unexpected effects occur. As a spin-off of this study, numerous coding errors of LM have been discovered and removed.

Aerosol optical depth

During the development phase of LM, the radiation scheme was ported from the global model GME, but by accident a piece of code was not copied. This coding error had two implications: An algorithm to detect the tropopause and to toggle from stratospheric to tropospheric aerosol failed and consequently low absorption coefficients of stratospheric aerosol are assumed throughout the whole atmosphere. Only the lowest model layer is an exception if the surface temperature is considerably larger than the atmospheric temperature (see peak of red curve in Fig. D.1).
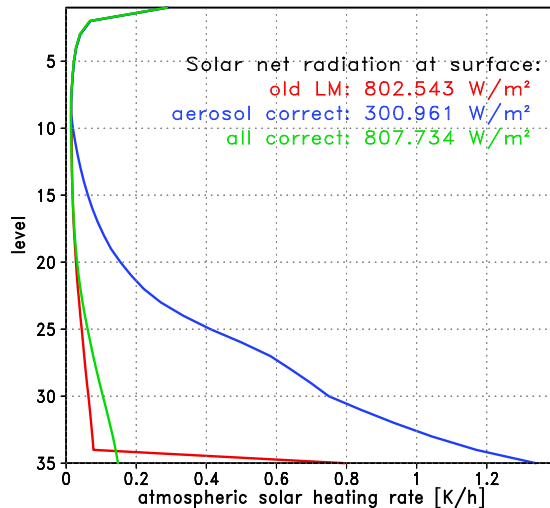

Figure D.1: Heating rates due to solar insolation at all LM model levels (level with the highest number is lowest to the surface) calculated using a dry standard atmosphere. Depicted are the results of the erroneous, operational LM version (red), the version with corrected aerosol distribution, but wrong calculation of optical thickness (blue) and the correct version (green).
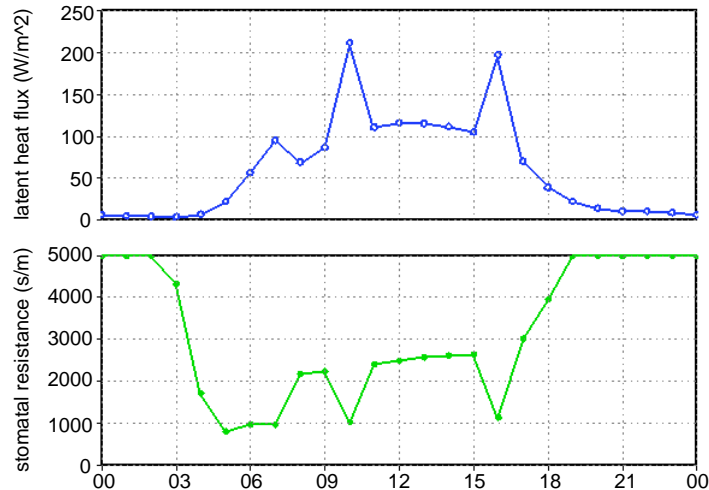
Figure D.2: Top: Time series of latent heat flux at the grid point Falkenberg modelled by TERRA-ML stand-alone with erroneous transpiration at the permanent wilting point. Bottom: Corresponding time series of stomatal resistance.

Secondly, the aerosol optical thickness of each layer is not calculated by integrating the absorption coefficient over a single layer, but as an integral from the top of atmosphere down to the lower layer boundary. By chance, both errors cancel each other: The aerosol absorption is underestimated by using the stratospheric aerosol properties and overestimated by accumulating the optical thickness. Correcting only the first error results in dramatically increased aerosol absorption and unrealistically high heating rates (see blue profile in Fig. D.1). This effect is almost completely compensated by removing the second error. On average the heating profiles of erroneous and corrected LM versions are quite similar and that is why this error has not been discovered throughout five years of intense use of LM for operational forecasts and research purposes. Nonetheless, the error modifies the shape of the heating profile. In particular the lowest model level is heated too much (over land during daytime), which seriously affects the exchange between surface and atmosphere. DWD has immediately corrected this coding error by issuing LM version 3.15.

Transpiration at the permanent wilting point

Stress of plants due to limited soil moisture is diagnosed based on the mean soil moisture content in the root zone, which ranges from the surface down to the root depth. This mean soil moisture content is determined by accumulating the soil moisture in the root zone and dividing it by the root depth. Layers with soil moisture below the permanent wilting point shall not contribute to plant transpiration and therefore the multilayer version of TERRA ignores these layers while accumulating root zone soil moisture. Unintentionally, this procedure is equivalent to setting the soil moisture of these layers to zero. If soil moisture of a certain layer decreases below the permanent wilting point, the mean root soil moisture content will abruptly drop
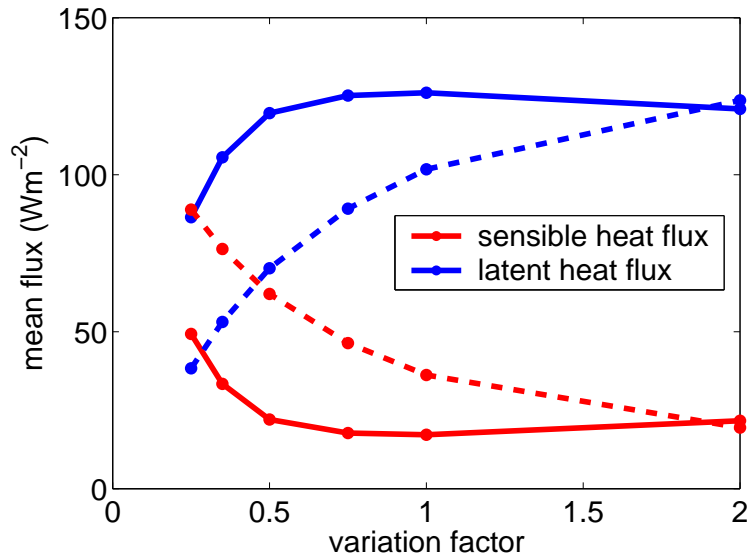
Figure D.3: Mean surface fluxes calculated by a sensitivity study (similar to the study presented in Section 3.1) varying root depth and using TERRA stand-alone with transpiration reduction inversely proportional to root depth (dashed) and without (solid lines). All values are averages over the entire operational LM domain.

to a significantly lower value. These discontinuous changes are directly reflected by the stomatal resistance and finally by the latent heat flux (see Fig. D.2). DWD has revised the calculation of the mean soil moisture content in the root zone.

Reduction of transpiration inversely proportional to root depth

The reduction of transpiration proportional to root depth, which was implemented without documentation as a rescue measure to limit evaporation, has already been discussed in Section 3.2. Fig. D.3 shows the effect of this not scientifically motivated parameterisation on surface fluxes: Using the unmodified parameterisation of Dickinson (1984), root depth has little effect on fluxes. Only if the root depth is more than halved, the roots will no longer penetrate the deep soil layer sufficiently and shortage of water in the thin upper layer causes a reduction of transpiration. The artifical reduction of transpiration proportional to root depth superimpose this effect and results in a sensitivity of surface fluxes to root depth in all root depth ranges. Since there is no scientific reason for such a dependency, the rescue measure is considered to be an error and was removed for all integrations performed in this study. DWD did not modify the operational LM, because they avoided any efforts on improving the two-layer version of TERRA. This version will soon be replaced by the multi-layer version, which operates without any artifical flux reduction.
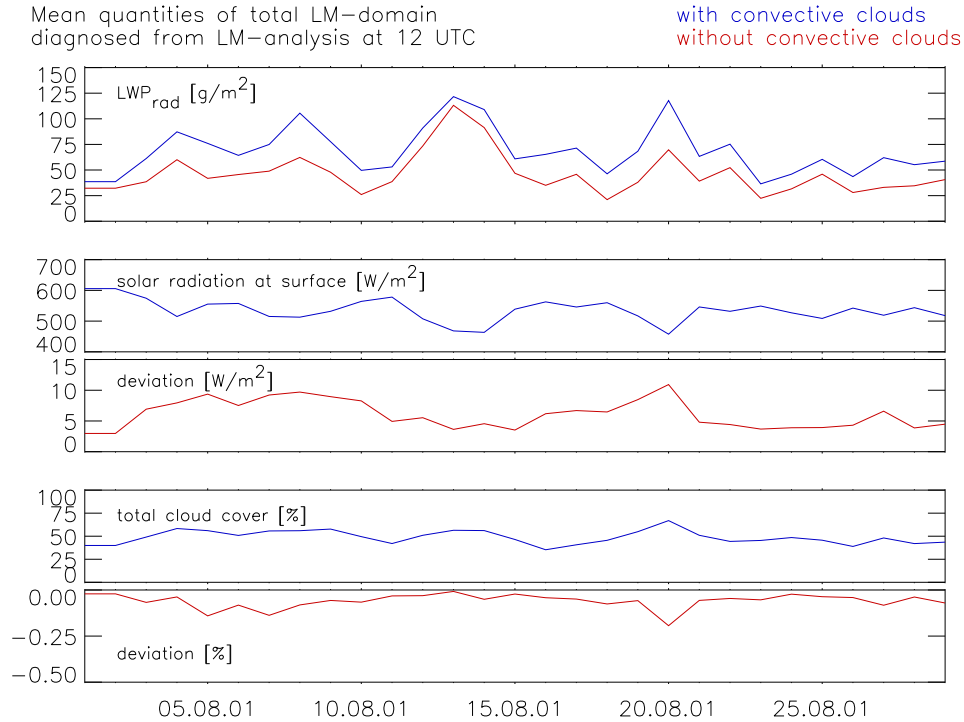
Figure D.4: Time series of liquid water path as used in the radiation scheme (LWP$_{rad}$), net solar radiation at the surface and total cloud cover during August 2001 at 12 UTC, respectively.

Omitting convective cloud cover

The radiation scheme of LM is only called once per hour (to save computational costs) and is executed before the convection scheme. Consequently, convective clouds have not been diagnosed and are ignored when the radiative fluxes are predicted at the first time step. This inaccuracy is not cured before the radiation scheme is invoked for second time after one hour of simulation time. Omitting convective cloud cover in the first hour of an integration may result in biased radiative fluxes, in particular if the runs are started at daytime as indicated by Fig. D.4. In central Europe, an overestimation of radiation in the order of 5-10 Wm^{-2} can be expected. DWD has not corrected this coding error in the LM, as this inaccuracy is considered to be of minor importance. But the error was corrected in the global model GME, because the correction removed considerable spin-up problems in the tropics.

Coding errors of the Tiedtke convection scheme

Two shortcomings in the Tiedtke moist convection scheme have been identified:
a) The fluxes of dry static energy, humidity and liquid water are extrapolated linearly below convective clouds to zero at the surface. This procedure is reasonable with respect to the first two variables as it mimics a height constant extraction of energy and humidity in the sub-cloud layer. But the flux of liquid water is per definition zero below the cloud since there is no liquid water at all. b) Instabilities at a certain level

117

are diagnosed by adding an artificial temperature increment of $0.5\,\mathrm{K}$ to account for subgrid-scale variability before checking the buoyancy of this parcel. This increment is only added to buoyancy calculations, but not to the mass-flux calculations itself. Consequently cold air may rise and may destabilise the stratification. DWD has affirmed the first coding error. As far as the second shortcoming is concerned, they assume that both formulations, adding the temperature increment to the mass-flux calculation or not, are in principle valid. Nonetheless, test cases have shown that the revised formulation gives better results. Up to know, both aspects have not been considered in the operational LM version.

Inaccurate diagnosis of surface fluxes

The dynamical core of LM and TERRA calculates surface fluxes explicitly based on the values of the previous time step. In contrast, the diagnosed fluxes, which are used as output variables and as input variables of the convection scheme, are determined implicitly depending partly on the values of the actual time step. This inconsistency has been removed by DWD in LM version 3.15.

Bibliography

Ament, F., S. Crewell, and C. Simmer, Impact of horizontal model resolution on cloud parameters forecasted by a non-hydrostatic mesoscale model, in *Proceedings of 14th International Conference on Clouds and Precipitation ICCP 2004, Bologna 19-23 July*, pages 1883–1886, 2004.

Arola, A., Parameterization of Turbulent and Mesoscale Fluxes of Heterogeneous Surfaces, *J. Atmos. Sci.*, 56, 584–598, 1999.

Arpagaus, M., Operational Verification of Vertical Profiles at Meteoswiss, *COSMO Newsletter*, 5, 102–105, 2005.

Avissar, R., Conceptual aspects of a statistical-dynamic approach to represent landscape subgrid-scale heterogeneities in atmospheric models, *J. Geophys. Res.*, 97, 2729–2742, 1992.

Avissar, R. and Y. Q. Liu, Three-dimensional numerical study of shallow convective clouds and precipitation induced by land surface forcing, *J. Geophys. Res.*, 101, 7499–7518, 1996.

Avissar, R. and R. A. Pielke, A Parameterization of Heterogeneous Land Surfaces for Atmospheric Models and Its Impact on Regional Meteorology, *Mon. Wea. Rev.*, 117, 2113–2134, 1989.

Avissar, R. and T. Schmidt, An Evaluation of the Scale at which Ground-Surface Heat Flux Patchiness Affects the Convective Boundary Layer Using Large-Eddy Simulations, *J. Atmos. Sci.*, 55, 2666–2689, 1998.

Bange, J., F. Beyrich, and D. A. M. Engelbart, Airborne measurements of turbulent fluxes during LITFASS-98: Comparison with ground measurements and remote sensing in a case study, *Theor. Appl. Climatol.*, 73, 35–51, 2002.

Bange, J., M. Herold, T. Spieß, P. Zittel, and F. Beyrich, Turbulent Fluxes from HELIPOD Flights above the Heterogenous LITFASS Area, *Boundary-Layer Meteor.*, 2006, in revision.

Betts, A. K., J. H. Ball, A. C. M. Beljaars, M. J. Miller, and P. A. Viterbo, The land surface-atmosphere interaction: A review based on observational and global modeling perspectives, *J. Geophys. Res.*, 101, 7209–7225, 1996.

Beyrich, F. *et al.*, Verdunstung über einer heterogenen Landoberfläche - Das LITFASS-2003 Experiment - Ein Bericht, Arbeitsergebnisse Nr. 79, DWD, 2004.

Bibliography

Beyrich, F., H. J. Herzog, and J. Neisser, The LITFASS project of DWD and the LITFASS-98 experiment: The project strategy and the experimental setup, *Theor. Appl. Climatol.*, 73, 3–18, 2002a.

Beyrich, F., J.-P. Leps, U. Weisensee, J. Bange, P. Zittel, S. Huneke, H. Lohse, H.-T. Mengelkamp, T. Foken, M. Mauder, C. Bernhofer, R. Queck, W. M. L. Meijninger, W. Kohsiek, A. Lüdi, G. Peters, and H. Münster, Area averaged surface fluxes over the heterogeneous LITFASS area from measurements, *Boundary-Layer Meteor.*, 2006, in revision.

Beyrich, F. and H.-T. Mengelkamp, Evaporation over a heterogeneous land surface: EVA_GRIPS and the LITFASS-2003 experiment - an overview, *Boundary-Layer Meteor.*, 2006, in revision.

Beyrich, F., S. H. Richter, U. Weisensee, W. Kohsiek, H. Lohse, H. A. R. de Bruin, T. Foken, M. Göckede, F. Berger, R. Vogt, and E. Batchvarova, Experimental determination of turbulent fluxes over the heterogeneous LITFASS area: Selected results from the LITFASS-98 experiment, *Theor. Appl. Climatol.*, 73, 19–34, 2002b.

Blackadar, A. K., The vertical distribution of wind and turbulent exchange in a neutral atmosphere, *J. Geophys. Res.*, 67, 3095–3102, 1962.

Boone, A., F. Habets, J. Noilhan, D. Clark, P. Dirmeyer, S. Fox, Y. Gusev, I. Haddeland, R. Koster, D. Lohmann, S. Mahanama, K. Mitchell, O. Nasonova, G. Y. Niu, A. Pitman, J. Polcher, A. B. Shmakin, K. Tanaka, B. van den Hurk, S. Verant, D. Verseghy, P. Viterbo, and Z. L. Yang, The Rhone-aggregation land surface scheme intercomparison project: An overview, *J. Climate*, 17, 187–208, 2004.

Bryan, G. H., J. C. Wyngaard, and J. M. Fritsch, Resolution Requirements for the Simulation of Deep Moist Convection, *Mon. Wea. Rev.*, 131, 2394–2416, 2003.

Businger, J., J. Wyngaard, Y. Iszumi, and E. Bradley, Flux profile relationships in the atmospheric surface layer, *J. Atmos. Sci.*, 28, 181–189, 1971.

Caughey, S. J. and S. G. Palmer, Some aspects of turbulence structure through the depth of the convective boundary-layer, *Q. J. R. Meteorol. Soc.*, 105, 811–827, 1979.

Chehbouni, A., E. G. Njoku, J. P. Lhomme, and Y. H. Kerr, Approaches for averaging surface parameters and fluxes over heterogeneous terrain, *J. Climate*, 8, 1386–1393, 1995.

Chen, F. and R. Avissar, The impact of land-surface wetness heterogeneity on mesoscale heat fluxes, *J. Appl. Meteorol.*, 33, 1323–1340, 1994.

Chen, F. and J. Dudhia, Coupling an advanced land surface-hydrology model with the Penn State-NCAR MM5 modeling system. Part I: Model implementation and sensitivity, *Mon. Wea. Rev.*, 129, 569–585, 2001.

Clark, D. B., C. M. Taylor, and A. J. Thorpe, Feedback between the land surface and rainfall at convective length scales, *J. Hydrometeorol.*, 5, 625–639, 2004.

Claussen, M., Estimation of Areally-Averaged Surface Fluxes, *Boundary-Layer Meteorol.*, 54, 387–410, 1991.

Culf, A. D., T. Foken, and J. H. C. Gash, The energy balance closure problem, in *Vegetation, Water, Humans and the Climate*, edited by Kabat and Claussen, pages 159–166, Springer, 2004.

Dai, A., K. E. Trenberth, and T. R. Karl, Effects of clouds, soil moisture, precipitation, and water vapor on diurnal temperature range, *J. Climate*, 12, 2451–2473, 1999.

Dai, Y. J., X. B. Zeng, R. E. Dickinson, I. Baker, G. B. Bonan, M. G. Bosilovich, A. S. Denning, P. A. Dirmeyer, P. R. Houser, G. Y. Niu, K. W. Oleson, C. A. Schlosser, and Z. L. Yang, The Common Land Model, *Bull. Am. Meteorol. Soc.*, 84, 1013–1023, 2003.

Daley, R., *Atmospheric Data Analysis*, Cambridge University Press, 1991.

Damrath, U., Verification results at DWD, *COSMO Newsletter*, 5, 72–74, 2005.

Davies, H., A lateral boundary formulation for multi-level prediction models, *Quart. J. R. Met. Soc.*, 102, 405–418, 1976.

Dickinson, R., Modeling evapotranspiration for the three-dimensional global climate models. In Climate Processes and Climate Sensitivity, *Geophysical Monograph 29, Maurice Ewing Volume 5*, pages 58–72, 1984.

Dingman, S. L., *Physical Hydrology - Second Edition*, Prentice Hall, 2002.

Doms, G. and J. Förstner, Development of a kilometer-scale NWP system: LMK, Technical Report 4, COSMO Newsletter, 2004.

Doms, G. and U. Schättler, *The Nonhydrostatic Limited-Area Model LM (Lokal-Modell) of DWD - Part I: Scientific Documentation*, DWD, available at Deutscher Wetterdienst, Postfach 100465, D-63004 Offenbach, 1999.

Doran, J. C., W. J. Shaw, and J. M. Hubbe, Boundary-layer characteristics over areas of inhomogeneous surface fluxes, *J. Appl. Meteorol.*, 34, 559–571, 1995.

EEA, *Corine land cover (CLC90)*, European Environment Agency, Copenhagen, http://dataservice.eea.eu.int/dataservice/, 2000.

Eltahir, E. A. B. and J. S. Pal, Relationship between surface conditions and subsequent rainfall in convective storms, *J. Geophys. Res.*, 101, 26237–26245, 1996.

Engelbart, D. A. M. and J. Bange, Determination of boundary-layer parameters using wind profiler/RASS and sodar/RASS in the frame of the LITFASS project, *Theor. Appl. Climatol.*, 73, 53–65, 2002.

Bibliography

Essery, R., M. Best, and P. Cox, MOSES 2.2 Technical Documentation, Technical Report 30, Hadley Centre, 2001.

Essery, R. L. H., M. J. Best, R. A. Betts, P. M. Cox, and C. M. Taylor, Explicit representation of subgrid heterogeneity in a GCM land surface scheme, *J. Hydrometeorol.*, 4, 530–543, 2003.

Findell, K. L. and E. A. B. Eltahir, Analysis of the pathways relating soil moisture and subsequent rainfall in Illinois, *J. Geophys. Res.*, 104, 31565–31574, 1999.

Findell, K. L. and E. A. B. Eltahir, Atmospheric controls on soil moisture-boundary layer interactions: Three-dimensional wind effects, *J. Geophys. Res.*, 108, 2003.

Foken, T. and S. P. Oncley, Workshop on instrumental and methodical problems of land-surface flux measurements, *Bull. Am. Meteorol. Soc.*, 76, 1191–1193, 1995.

Friedrich, K., N. Mölders, and G. Tetzlaff, On the Influence of Surface Heterogeneity on the Bowen-Ratio: A Theoretical case study, *Theor. Appl. Climatol.*, 65, 181–198, 2000.

Garratt, J. R., Sensitivity of climate simulations to land-surface and atmospheric boundary-layer treatments - a review, *J. Climate*, 6, 419–449, 1993.

Giorgi, F., An Approach for the Representation of Surface Heterogeneity in Land Surface Models. Part I: Theoretical Framework, *Mon. Wea. Rev.*, 125, 1885–1899, 1997.

Giorgi, F. and R. Avissar, Representation of Heterogeneity Effects in Earth System Modeling: Experience from Land Surface Modeling, *Rev. Geophys.*, 4, 413–438, 1997.

Giorgi, F., R. Francisco, and J. Pal, Effects of a subgrid-scale topography and land use scheme on the simulation of surface climate and hydrology. Part I: Effects of temperature and water vapor disaggregation, *J. Hydrometeorol.*, 4, 317–333, 2003.

Görsdorf, U., F. Beyrich, H. Dier, and U. Leiterer, Composite wind and temperature profiles obtained from a complex of in-situ and remote sensing measurement systems for the forcing of a boundary layer model, *Theor. Appl. Climatol.*, 73, 97–105, 2002.

Hahmann, A. N., Representing Spatial Subgrid-scale Precipitation Variability in a GCM, *J. Hydrometeorol.*, 4, 891–900, 2003.

Hahmann, A. N. and R. E. Dickinson, A fine-mesh land approach for general circulation models and its impact on regional climate, *J. Climate*, 14, 1634–1646, 2001.

Heinemann, G. and M. Kerschgens, Comparison of Methods for Area-Averaged Surface Energy Fluxes over Heterogeneous Land Surfaces using High-Resolution Non-Hydrostatic Simulations, *Int. J. Climatol.*, 25, 379–403, 2005.

Heinemann, G. and M. Kerschgens, On the consideration of mesoscale transports in climate modelling, *Theor. Appl. Climatol.*, 2006a, accepted.

Heinemann, G. and M. Kerschgens, Area-averaged surface energy fluxes using high-resolution non-hydrostatic simulations and comparison with measurements for the LITFASS-2003 experiment, *Boundary-Layer Meteor.*, 2006b, in revision.

Heise, E., Parameterisierungen, in *Die neue Modellkette des DWD I*, volume 27 of *promet*, pages 130–141, DWD, 2002.

Hendersonsellers, A., Z. L. Yang, and R. E. Dickinson, The project for intercomparison of land-surface parameterization schemes, *Bull. Am. Meteorol. Soc.*, 74, 1335–1349, 1993.

Hennemuth, B., J. Bange, F. Beyrich, J. Bösenberg, J. Leps, and P. Zittel, Measurements of water vapour transport in the atmospheric boundary layer over heterogenous terrain, *Boundary-Layer Meteor.*, 2006, in revision.

Herzog, H. J., G. Vogel, and U. Schubert, LLM - a nonhydrostatic model applied to high-resolving simulations of turbulent fluxes over heterogeneous terrain, *Theor. Appl. Climatol.*, 73, 67–86, 2002.

Hess, R., Assimilation of screen level observations by variational soil moisture analysis, *Meteor. Atmos. Phys.*, 77, 145–154, 2001.

Holtslag, A. A. M. and C. H. Moeng, Eddy Diffusivity and Countergradient Transport in the Convective Atmospheric Boundary Layer, *J. Atmos. Sci.*, 48, 1690–1698, 1991.

Hu, Z., S. Islam, and L. Jiang, Approaches for Aggregating Heterogeneous Surface Parameters and Fluxes for Mesoscale and Climate Models, *Boundary-Layer Meteorol.*, 93, 313–336, 1999.

Jackson, T. J. and A. Y. Hsu, Soil moisture and TRMM microwave imager relationships in the Southern Great Plains 1999 (SGP99) Experiment, *IEEE Trans. Geosci. Remote Sensing*, 39, 1632–1642, 2001.

Jacobsen, I. and E. Heise, A new economic method for the computation of the surface temperature in numerical models, *Contr. Atmos. Phys.*, 55, 128–141, 1982.

Kaufmann, P., M. Arpagaus, P. Emiliani, E. Veccia, A. Galliani, and U. Pflüger, Vertical Pofiles - A Comparision between German, Italian and Swiss Verification, *COSMO Newsletter*, 5, 118–122, 2005.

Bibliography

Kim, S. W., S. U. Park, and C. H. Moeng, Entrainment processes in the convective boundary layer with varying wind shear, *Boundary-Layer Meteorol.*, 108, 221–245, 2003.

Klemp, J. and R. Wilhemson, The simulation of three-dimensional convective storm dynamics, *J. Atmos. Sci.*, 35, 1070–1096, 1978.

Koster, R. D. and M. J. Suarez, A Comparative Analysis of Two land Surface Heterogeneity Representations, *J. Climate*, pages 1379–1390, 1992.

Lammert, A. and J. Bösenberg, Determination of the convective boundary layer height with laser remote sensing, *Boundary-Layer Meteorol.*, 2006, accepted.

Laubach, J. and U. Teichmann, Surface energy budget variability: A case study over grass with special regard to minor inhomogeneities in the source area, *Theor. Appl. Climatol.*, 62, 1999.

Lhomme, J. P., A. Chehbouni, and B. Monteny, Effective parameters of surface-energy balance in heterogeneous landscape, *Boundary-Layer Meteorol.*, 71, 297–309, 1994.

Li, B. and R. Avissar, The Impact of Spatial Variability of Land-Surface Characteristics on Land-Surface Heat Fluxes, *J. Climate*, pages 527–537, 1994.

Lipton, A. E., Cloud Shading Retrieval and Assimilation in a Satellite-Model Coupled Mesoscale Analysis System, *Mon. Wea. Rev.*, pages 3062–3081, 1993.

Liu, Y. Q., C. P. Weaver, and R. Avissar, Toward a parameterization of mesoscale fluxes and moist convection induced by landscape heterogeneity, *J. Geophys. Res.*, 104, 19515–19533, 1999.

Louis, J.-F., A parametric model of vertical eddy fluxes in the atmosphere, *Boundary-Layer Meteorol.*, 17, 187–202, 1979.

Lynn, B. H., F. Abramopoulus, and R. Avissar, Using Similarity Theory to Parameterize Mesoscale Heat Fluxes Generated by Subgrid-Scale Landscape Discontinuities in GCMs, *J. Climate*, pages 932–951, 1995b.

Lynn, B. H., D. Rind, and R. Avissar, The importance of mesoscale circulations generated by subgrid-scale landscape heterogeneities in general-circulation models, *J. Climate*, 8, 191–205, 1995a.

Lynn, B. H., W. K. Tao, and P. J. Wetzel, A study of landscape-generated deep moist convection, *Mon. Wea. Rev.*, 126, 928–942, 1998.

Mahfouf, J.-F., Analysis of Soil Moisture from Near-Surface Parameters: A Feasibility Study, *J. Appl. Meteorol.*, 30, 1534–1547, 1991.

Mahfouf, J.-F., E. Richard, and P. Mascart, The influence of soil and vegetation on the development of mesoscale circulations, *J. Clim. Appl. Meteorol.*, 26, 1483–1495, 1987.

Mahrt, L., The Bulk Aerodynamic Formulation over Heterogeneous Surfaces, *Boundary-Layer Meteor.*, 78, 87–119, 1996.

Mahrt, L., Surface Heterogeneity and Vertical Structure of the Atmosphere, *Boundary-Layer Meteor.*, 96, 33–62, 2000.

Mahrt, L. and J. Sun., Dependence of surface exchange coefficients on averaging scale and grid size, *Q. J. R. Meteorol. Soc.*, 121, 1835–1852, 1995.

Margulis, S. A. and D. Entekhabi, Feedback between the land surface energy balance and atmospheric boundary layer diagnosed through a model and its adjoint, *J. Hydrometeorol.*, 2, 599–620, 2001.

Mason, P. J., The formation of areally-averaged roughness lengths, *Q. J. R. Meteorol. Soc.*, 114, 399–420, 1988.

Mauder, M., C. Liebethal, M. Göckede, J.-P. Leps, F. Beyrich, and T. Foken, Processing and quality control of eddy covariance data during LITFASS-2003, *Boundary-Layer Meteor.*, 2006, in revision.

Meijninger, W. M. L., F. Beyrich, A. Lüdi, W. Kohsiek, and H. A. R. de Bruin, Scintillometer-based Turbulent Fluxes of Sensible and Latent Heat over a Heterogenous Land Surface - A Contribution to LITFASS-2003, *Boundary-Layer Meteor.*, 2006, to be printed.

Mellor, G. and T. Yamada, Development of a turbulence closure model for geophysical fluid problems, *Rev. Geophys. Space Phys.*, 20, 851–875, 1982.

Mironov, D. and M. Raschendorfer, Evaluation of Empirical Constants in the New LM Surface Layer Parameterization Scheme, *COSMO Technical Report, http://www.cosmo-model.org*, 1, 2001.

Mitchell, K. E. *et al.*, The multi-institution North American Land Data Assimilation System (NLDAS): Utilizing multiple GCIP products and partners in a continental distributed hydrological modeling system, *J. Geophys. Res.*, 109, doi:10.1029/2003JD003823, 2004.

Mölders, N., On the uncertainty in mesoscale modeling caused by surface parameters, *Meteorol. Atmos. Phys.*, 76, 119–141, 2001.

Mölders, N. and A. Raabe, Numerical Investigation on the Influence of Subgrid-Scale Surface Heterogeneity on Evaporation and Cloud Processes, *J. Appl. Meteorol.*, 35, 782–795, 1996.

Bibliography

Mölders, N., A. Raabe, and G. Tetzlaff, A comparison of two strategies on land surface heterogeneity used in a mesoscale β meteorological model, *Tellus*, 48A, 733–749, 1996.

Molod, A., S. Hadyee, and D. Waugh, A New Look at Modelling Surface Heterogeneity: Extending Its Influence in the Vertical, *J. Hydrometeorol.*, pages 811–825, 2003.

Noilhan, J. and S. Planton, A simple parameterization of land surface processes for meteorological models., *Mon. Wea. Rev.*, 117, 536–549, 1989.

Petch, J. C., A. R. Brown, and M. E. B. Gray, The impact of horizontal resolution on the simulation of convective development over land, *Q. J. R. Meteorol. Soc.*, 128, 2031–2044, 2002.

Pflüger, U., Operational Verification of Vertical Profiles at DWD, *COSMO Newsletter*, 5, 106–112, 2005.

Pielke, R. A., Influence of the spatial distribution of vegetation and soils on the prediction of cumulus convective rainfall, *Rev. Geophys.*, 39, 151–177, 2001.

Pinty, J. P., P. Mascart, E. Richard, and R. Rosset, An investigation of mesoscale flows induced by vegetation inhomogeneities using an evapotranspiration model calibrated against hapex-mobilhy data, *J. Appl. Meteorol.*, 28, 976–992, 1989.

Raasch, S. and M. Schröter, PALM - A large-eddy simulation model performing on massively parallel computers, *Meteorol. Zeitschrift*, 10, 363–372, 2001.

Rijtema, P. E., Soil moisture forecasting, Technical Report Nota 513, Instituut voor Cultuurtechniek en Waterhuishouding, Wageningen, 1969.

Ritter, B. and J.-F. Geleyen, A Comprehensive Radiation Scheme for Numerical Weather Prediction Models with Potential Applications in Climate Simulation, *Mon. Wea. Rev.*, pages 303–325, 1992.

Ronda, R. J. and H. A. R. de Bruin, A note on the concept of 'effective' bulk exchange coefficients for determination of surface flux densities, *Boundary-Layer Meteorol.*, 93, 155–162, 1999.

Ronda, R. J., B. J. J. M. van den Hurk, and A. A. M. Holtslag, Spatial heterogeneity of the soil moisture content and its impact on surface flux densities and near-surface meteorology, *J. Hydrometeorol.*, 3, 556–570, 2002.

Roy, S. B., C. P. Weaver, D. S. Nolan, and R. Avissar, A preferred scale for landscape forced mesoscale circulations?, *J. Geophys. Res.*, 108, doi:10.1029/2002JD003097, 2003.

Schär, C. and G. Jendritzky, Climate change: Hot news from summer 2003, *Nature*, 432, 559–560, 2004.

Schlünzen, K. H. and J. J. Katzfey, Relevance of sub-grid-scale land use effects for mesoscale models, *Tellus*, 55A, 232–246, 2003.

Schraff, C. and R. Hess, *A Description of the Nonhydrostatic Regional Model LM. Part III: Data Assimilation*, http://www.cosmo-model.org, 2003.

Schrodin, R. and E. Heise, The Multi-Layer Version of the DWD Soil Model TERRA_LM, Technical Report 2, Consortium for Small-Scale Modelling (COSMO), Technical Report, available at http://www.cosmo-model.org, 2001.

Schrodin (ed.), *Dokumentation des EM/DM-Systems*, DWD, available at Deutscher Wetterdienst, Postfach 100465, D-63004 Offenbach, 1995.

Seth, A. and F. Giorgi, Three-dimensional model study of organized mesoscale circulations induced by vegetation, *J. Geophys. Res.*, 101, 7371–7391, 1996.

Seth, A., F. Giorgi, and R. E. Dickinson, Simulating fluxes from heterogeneous land surface: Explicit subgrid method employing the biosphere-atmosphere transfer scheme (BATS), *J. Geophys. Res*, 99, 18651–18667, 1994.

Seuffert, G., Two approaches to improve the simulation of near surface processes in numerical weather prediction models, *Bonner Meteorologische Abhandlungen*, 55, 2001.

Seuffert, G., P. Gross, C. Simmer, and E. F. Wood, The influence of hydrologic modeling on predicted local weather: Two-way coupling of a mesoscale weather prediction model and a land surface hydrology model, *J. Hydrometerol.*, 3, 505–523, 2002.

Seuffert, G., H. Wilker, P. Viterbo, M. Drusch, and J.-F. Mahfouf, The usage of screen level parameters and microwave brightness temperature for soil moisture analysis, *J. Hydrometeorol.*, 5, 516–531, 2004.

Shao, Y., M. Sogalla, M. Kerschgens, and W. Brucher, Effects of land-surface heterogeneity upon surface fluxes and turbulent conditions, *Meteorol. Atmos. Phys.*, 78, 157–181, 2001.

Simmer, C., F. Ament, R. Grasselt, and R. Girmes, *Abschlussbericht zum Forschungsprojekt 'Von Messdaten angetriebenes Wasserbilanzmodell'*, 2005.

Steppeler, J., S. U. Doms, G., H. W. Bitzer, A. Gassmann, U. Damrath, and G. Gregoric, Meso-gamma scale forecast using the non-hydrostatic model LM, *Met. and Atm. Phys.*, 82, 75–96, 2003.

Stull, R. B., *An Introduction to Boundary Layer Meteorology*, Kluwer Academic Publisher, 1988.

Tiedtke, M., A comprehensive massflux scheme for cumulus parameterization in large-scale models, *Mon. Wea. Rev.*, pages 1779–1800, 1989.

Bibliography

Tittebrand, A., A. Schwiebus, and F. H. Berger, The influence of land surface parameters on energy flux densities derived from remote sensing data, *Meteorol. Zeitschrift*, 14, 227–236, 2005.

Trier, S., F. Chen, and K. Manning, A study of convection initiation in a mesoscale model using high-resolution land surface initial conditions, *Mon. Wea. Rev.*, 132, 2954–2976, 2004.

Uhlenbrock, J., S. Raasch, B. Hennemuth, P. Zittel, and W. M. L. Meijninger, Effects of land surface heterogeneities on the boundary structure and turbulence during LITFASS-2003: large-eddy simulations in comparison with turbulence measurements., in *16th Symposium on Boundary Layers and Turbulence, American Meteorological Society, Portland/Maine, USA*, 2004.

Unden, P. *et al.*, *HIRLAM-5 Scientific Documentation*, Hirlam-5 project, c/o Per Unden SMHI, S-601 Norrköpping, Sweden, 2002.

USGS, *GTOPO30 Digital elevation model*, EROS Data Center, US Geological Survey, Sioux Falls, SD, http://edcaac.usgs.gov/gtopo30.asp, 1997.

van Lipzig, N., M. Schröder, S. Crewell, F. Ament, J.-P. Chaboureau, U. Löhnert, V. Matthias, E. van Meijgaard, M. Quante, U. Willen, and W. Yen, Model predicted low-level cloud parameters. Part I: Comparison with observations from the BALTEX Bridge Campaigns, *Atmos. Res.*, 2006, accepted.

Venema, V., S. Meyer, S. G. Garcia, A. Kniffka, C. Simmer, S. Crewell, U. Löhnert, T. Trautmann, and A. Macke, Surrogate cloud fields generated with the iterative amplitude adapted fourier transform algorithm, *Tellus*, 58A, 104–120, 2006.

Weaver, C. P., Coupling between large-scale atmospheric processes and mesoscale land-atmosphere interactions in the US Southern Great Plains during summer. Part I: Case studies, *J. Hydrometeorol.*, 5, 1223–1246, 2004.

Weaver, C. P., S. B. Roy, and R. Avissar, Sensitivity of simulated mesoscale atmospheric circulations resulting from landscape heterogeneity to aspects of model configurations, *J. Geophys. Res.*, 107, doit.: 10.1029/2001JD000376, 2002.

Wen, L., W. Yu, C. A. Lin, M. Beland, R. Benoit, and Y. Delage, The role of land surface schemes in short-range, high spatial resolution forecasts, *Mon. Wea. Rev.*, 128, 3605–3617, 2000.

Yates, D. N., F. Chen, and H. Nagai, Land surface heterogeneity in the cooperative atmosphere surface exchange study (CASES-97). Part II: Analysis of spatial heterogeneity and its scaling, *J. Hydrometeorol.*, 4, 219–234, 2003.

Zeng, X. M., M. Zhao, B. K. Su, J. P. Tang, Y. Q. Zheng, Y. J. Zhang, and J. Chen, The effects of land-surface heterogeneities on regional climate: A sensitivity study, *Meteorol. Atmos. Phys.*, 81, 67–83, 2002.

Danksagung